



**ORGANIC BINDER MEDIATED $\text{Co}_3\text{O}_4/\text{TiO}_2$ HETEROJUNCTION FORMATION FOR
HETEROGENEOUS ACTIVATION OF PEROXYMONOSULFATE**

By

SARAH KASANGANA KAPINGA

**Thesis submitted in fulfilment of the requirements for the degree
Master of Engineering: Chemical Engineering**

In the

Faculty of Engineering

At the

CAPE PENINSULA UNIVERSITY OF TECHNOLOGY

Cape Town Campus

Supervisors:

Dr Mahabubur Chowdhury &

Prof Veruscha Fester

March 2019

DECLARATION

I, Sarah Kasangana Kapinga, hereby declare that the contents of this thesis represent my own work, and that this thesis has not previously been submitted for academic examination towards any qualification. Furthermore, it represents my own opinions, not necessarily those of the Cape Peninsula University of Technology.

Signature

Signed in Cape Town this day _____

ABSTRACT

A shortage of water has resulted in the need to enhance the quality of wastewater that is released into the environment. The advanced oxidation process (AOP) using heterogeneous catalysis is a promising treatment process for the management of wastewater containing recalcitrant pollutants as compared to conventional processes.

As AOP is a reliable wastewater treatment process, it is expected to be a sustainable answer to the shortage of clean water. AOP using heterogeneous catalysis based on Co_3O_4 particles and PMS, in particular has been found to be a powerful procedure for the degradation and mineralization of recalcitrant organic contaminants. In addition, due to the growing application of Co_3O_4 in lithium batteries, large quantities of these particles will be recovered as waste from spent lithium batteries, so there is a need to find a use for them.

Although this method has received some promising feedback, challenges still need to be addressed, such as the toxicity of cobalt particles, the poor chemical and thermal stability and particle aggregation, and the prompting of lower catalytic efficiency in long haul application. Furthermore, the removal of the catalyst after the treatment of pollutants is also an issue.

In order to be applicable, a novel catalyst must be produced requiring the combination of Co_3O_4 with a support material in order to inhibit cobalt leaching and generate better particle stability. From the available literature, TiO_2 was found to be the best support material because it not only provides a large surface area for well dispersed Co_3O_4 , but it also forms strong Co-O-Ti bonds which greatly reduced cobalt leaching as compared to other support materials. Moreover, it also greatly encourages the formation of surface Co-OH complexes, which is considered a crucial step for PMS activation. Therefore, the issues cited above could be avoided by producing a $\text{Co}_3\text{O}_4/\text{TiO}_2$ heterojunction catalyst.

The techniques used to evaluate the optical and morphological characteristics of the $\text{Co}_3\text{O}_4/\text{TiO}_2$ were ultraviolet and visible (UV-Vis) spectra, X-ray diffraction (XRD), Fourier transform infrared (FTIR) analysis and transmission electron microscope (TEM). The catalytic performance of

$\text{Co}_3\text{O}_4/\text{TiO}_2$ heterojunction catalyst was evaluated by the degradation of different dyes (methyl orange, commercial dyes in a synthetic dye bath).

From the results obtained, it can be seen that Co_3O_4 and TiO_2 have a strong interaction. The produced $\text{Co}_3\text{O}_4/\text{TiO}_2$ heterojunction structure had a rod-like structure, showing a good catalytic efficiency while inhibiting cobalt leaching, reducing it by up to 97% less than that of the pristine Co_3O_4 . The organic binder mediated route is a more economical and greener technique to produce this sort of catalyst as compared to the other methods from the literature.

The 70:30 $\text{Co}_3\text{O}_4/\text{TiO}_2$ had the lowest cobalt leaching while maintaining a good catalytic activity: 97% of 40mg/l of MO was degraded under 15 minutes while using a 0.18g/L of PMS. The catalyst was determined to be effective for the treatment of commercial metal-complex dye, taking less than 20 minutes of reaction time to achieve a colourless solution from dark colour solutions. In addition, the catalytic efficiency of the $\text{Co}_3\text{O}_4/\text{TiO}_2$ produced materials that are repeatable so its reusability showed no significant loss in catalytic activity over four recycling stages. The quenching experiments showed that the sulphate radicals are the main active species.

ACKNOWLEDGEMENTS

First, I would like to thank God Almighty for giving me the strength, knowledge, ability and opportunity to undertake this research study and to persevere and complete it satisfactorily. Without His blessings, this achievement would not have been possible.

Secondly, I would like to thank my supervisors:

Dr. Mahabubur Raman Chowdhury: thank you for giving me a second chance when I needed it. In addition, thank you for the patient guidance, encouragement and advice provided throughout my time as a student. I have been extremely lucky to have a supervisor who cared so much about my work. In addition, Prof. Veruscha Fester, thank you for your advice and understanding throughout my work.

Dr. Franscious Cummings, Dr Oputu Ogheneochuko Utieyin and Dr Chamier: thank you for the assistance with the various tests needed all through my work.

Thirdly, I would like to thank all the staff and students who helped me in the Flow Process and Rheology Centre (FPRC) at the Cape Peninsula University of Technology (CPUT).

Finally, I must express my gratitude to Julien, my fiancé, for his continued support and encouragement, and my dearest mother: you raised me to believe that I could achieve anything I set my mind to. Completing this work would have been all the more difficult were it not for your support.

DEDICATION

To my dearest and loving mother

Helene Kapinga Tumba

I would not be the woman I am today if it was not for you.

To my loving fiancé

Julien Bourgeois

I would not have chosen to share this journey with anyone else but you.

To my beautiful daughters

Abigail and Amber

Although you made this journey difficult, you made the achievement even sweeter.

In loving memory of my father

Emmanuel Kasangana

I hope you are proud of me wherever you are.

PUBLICATION

Mahabubur Chowdhury, Sarah Kapinga, Franscious Cummings, Veruscha Fester;
Co₃O₄/TiO₂hetero-structure for methyl orange dye degradation. *Water Sci
Technol* wst2018383. doi: <https://doi.org/10.2166/wst.2018.383>

TABLE OF CONTENTS

DECLARATION	ii
ABSTRACT	iii
ACKNOWLEDGEMENTS	v
DEDICATION	vi
PUBLICATION	vii
TABLE OF CONTENTS	viii
LIST OF TABLES	xi
LIST OF FIGURES	xii
LIST OF SYMBOLS	xiv
LIST OF ABBREVIATIONS	xv
GLOSSARY: TERMS AND CONCEPTS	xvi
CHAPTER 1: INTRODUCTION	1
CHAPTER 2: LITERATURE REVIEW AND THEORY	6
2.1 Introduction	6
2.2 Conventional treatment processes	6
2.3 Advanced oxidation process	7
2.3.1 Azo dyes treatment-using AOP	14
2.4 Heterogeneous catalysis using cobalt oxide and TiO ₂ as support material	15
2.5 Cobalt oxides	17
2.5.1 Application of cobalt oxide in lithium ion batteries	18
2.5.2 Recovery of lithium cobalt oxide from the cathode of spent lithium-ion batteries	18
2.6 Titanium dioxide	19
2.7 Importance of heterogeneous catalyst	20
2.7.1 Importance of heterogeneous catalyst support	21
2.7.2 TiO ₂ : as support in heterogeneous catalysis	22
2.7.3 TiO ₂ : as support in metal heterogeneous catalysis	24
2.8 Hydrothermal process	24
2.9 Effect of experimental conditions on heterogeneous catalytic degradation of organic pollutant	28
2.9.1 Effect of pH	28

2.9.2 Effect of concentration (pollutants)	30
2.9.3 Effect of catalyst loading.....	31
2.9.4 Effect of operating temperature	32
2.9.5 Effect of PMS concentration.....	32
2.10 Mode of application: suspended vs. immobilized system	33
2.11 Material characterization techniques.....	34
2.11.1 Transmission electron microscopy.....	34
2.11.2 X-ray diffractometry	35
2.11.3 Fourier Transform-Infrared Spectroscopy (FTIR).....	37
2.11.4 Energy Dispersive X-ray Spectrometry (EDS).....	38
2.11.5 Electron energy loss spectroscopy	39
2.12 Conclusion	40
CHAPTER 3: EXPERIMENTAL PROCEDURE	42
3.1 Introduction	42
3.2 Materials and methodology	42
3.2.1 Materials.....	42
3.2.2 Hydrothermal preparation of cobalt oxide	42
3.2.3 Preparation of $\text{Co}_3\text{O}_4/\text{TiO}_2$ heterojunction catalyst.....	42
3.3 Catalyst performance	44
3.4 Experimental techniques	47
3.4.1 Batch synthesis	47
3.4.2 Metal oxide catalyst preparation.....	48
3.5 Characterization of $\text{Co}_3\text{O}_4/\text{TiO}_2$ heterojunction catalysts	49
CHAPTER 4: RESULTS AND DISCUSSION.....	50
4.1 Introduction	50
4.2 Structural characterization of $\text{Co}_3\text{O}_4/\text{TiO}_2$ heterojunction structure	50
4.2.1 X-ray diffraction analysis.....	50
4.2.2 TEM results of TiO_2 , Co_3O_4 and $\text{Co}_3\text{O}_4/\text{TiO}_2$ heterojunction structure.....	51
4.2.3 FTIR results for structural analysis of TiO_2 , Co_3O_4 and $\text{Co}_3\text{O}_4/\text{TiO}_2$ heterojunction structures	62
4.3 Evaluation of catalytic activity and cobalt leaching of the $\text{Co}_3\text{O}_4/\text{TiO}_2$ heterojunction.....	63
4.3.1 Effect of Co_3O_4 loading in the $\text{Co}_3\text{O}_4/\text{TiO}_2$ heterojunction structure	63
4.3.2 Effect of calcinations temperature	67
4.4 The effect of operational parameters on catalytic performance	69

4.4.1 Effects of catalyst loading on MO.....	69
4.4.2 Effects of PMS loading on MO degradation	70
4.4.3 Effect of reaction temperature on the catalytic performance	71
4.4.4 Effect of dye concentration on the degradation rate	72
4.4.5 Comparison between $\text{Co}_3\text{O}_4/\text{TiO}_2$ heterojunction and various studies.....	73
4.5 Comparison between homogeneous and heterogeneous catalytic oxidation.....	76
4.6 Determination of reactive species (radical)	77
4.7 Application of $\text{Co}_3\text{O}_4/\text{TiO}_2$ heterojunction for the treatment of commercial dyes...	78
4.8 Catalyst recyclability and efficiency after four runs	79
4.9 Conclusion	80
CHAPTER 5: SUMMARY OF RESULTS AND CONCLUSION.....	82
5.1 Introduction	82
5.2 Summary	82
5.3 Conclusion	84
5.4 Contribution.....	84
5.5 Recommendations.....	84
REFERENCES	85
APPENDICES.....	101
Appendix A	101

LIST OF TABLES

Table 2.1: Key advantages and disadvantages of different Advanced Oxidation processes	11
Table 2.2: Oxidation potential of commonly used oxidants	12
Table 2.3: Kinetic rates of HR and SR on different targeted compounds	13
Table 2.4: Advanced powder process comparison.....	25
Table 3.1: Process variable for the synthesis of $\text{Co}_3\text{O}_4/\text{TiO}_2$ heterojunction.....	44
Table 3.2: Optimization of the performance parameters	45
Table 4.1: Previous studies conducted on combined Co_3O_4 with various catalyst supports	73
Table A.1: Experimental conditions for catalytic performance on MO.....	101
Table A.2: Raw data and real concentration calculation for catalytic performance of Co_3O_4 using various ratios on methyl orange	102
Table A.3: raw data of the catalytic performance of 70% at various calcinations temperatures.....	104
Table A.4 : raw data cobalt leaching for various cobalt loading and effect of calcinations temperatures on cobalt ions leaching	106
Table A.5: Raw data and real concentration calculation for the effect of dye concentration on the degradation of MO of 70% $\text{Co}_3\text{O}_4/\text{TiO}_2$	106
Table A.6: data and real concentration calculation for the effect of catalyst load on the degradation of MO of 70% $\text{Co}_3\text{O}_4/\text{TiO}_2$	107
Table A.7: data and real concentration calculation for the effect of PMS load on the degradation of MO of 70% $\text{Co}_3\text{O}_4/\text{TiO}_2$	108

LIST OF FIGURES

Figure 2.1: Sulphate based radical oxidation diagram.....	16
Figure 2.2: Crystal structures of rutile, anatase and brookite titanium dioxide	19
Figure 2.3: Pressure dependence on temperature for different processing routes.....	27
Figure 3.1: Materials and methodology of the synthesis of $\text{Co}_3\text{O}_4/\text{TiO}_2$ heterojunction .	44
Figure 3.2: Catalyst performance in the degradation of MO	45
Figure 4.1: XRD patterns of different materials at different calcinations temperature ...	51
Figure 4.2: (a) and (b) TEM bright-field micrographs of $\text{TiO}_2:\text{Co}_3\text{O}_4$ at 350 °C showing the presence of both TiO_2 and Co_3O_4 nanostructures; (c) EDS spectrum; and (d) SAED pattern	53
Figure 4.3: (a) HAADF STEM micrograph of the composite $\text{Co}_3\text{O}_4/\text{TiO}_2$ material at 350 °C; (b) STEM-EDS spectral image of the area indicated in (a); (c) overlaid EDS map, (d – f), Co, Ti and O maps, respectively, extracted from the STEM-EDS spectral image of (b).....	54
Figure 4.4: (a) and (b) TEM bright-field micrographs of sample (c) EDS spectrum and (d) SAED pattern.....	57
Figure 4.5: (a) HAADF STEM micrograph of the composite $\text{Co}_3\text{O}_4\text{-TiO}_2$ material; (b) STEM-EDS spectral image of the area indicated in (a); (c) overlaid EDS map, (d – f), Co, Ti and oxygen maps extracted from the STEM-EDS spectral image of (b).....	58
Figure 4.6: Electron energy loss spectra comparing the energy loss near edge fine structures (ELNEFS) of the Co- $L_{3,2}$ ionization edge of the structures grown at 350 and 600 °C to that of pure Co_3O_4 nanoparticles at 350 °C	59
Figure 4.7: Electron energy loss spectra comparing the energy loss near edge fine structures (ELNEFS) of the Ti- $L_{3,2}$ and O-K ionisation edges of the structures grown at 350 and 600 °C to that of pure TiO_2 nanoparticles	60
Figure 4.8: FTIR results for structural analysis of TiO_2 , Co_3O_4 and $\text{Co}_3\text{O}_4 / \text{TiO}_2$ heterojunction structures	62
Figure 4.9: Effect of $\text{Co}_3\text{O}_4/\text{TiO}_2$ ratio on a) degradation kinetics of MO, b) Co leaching	64
Figure 4.10: Cobalt leaching vs time during PMS activation reaction.....	65

Figure 4.11: Comparison between pristine Co_3O_4 and the prepared composite catalyst cobalt leaching	65
Figure 4.12: (a) MO degradation kinetics; (b) COD removal via catalysis and PMS self-oxidation; (c) MO degradation via various routes; (d) PMS self-oxidation VS catalytic activity kinetics	67
Figure 4.13: Comparison of a) degradation kinetics and b) co leaching for 70:30 $\text{Co}_3\text{O}_4/\text{TiO}_2$ catalysts synthesized at various temperatures (0.03 g/l catalyst load, 0.03 g/l oxone, 40 mg/l MO and 298 K).....	68
Figure 4.14: Effect of catalyst loading on MO degradation.....	70
Figure 4.15: Effect of PMS loading on MO degradation	71
Figure 4.16: Activation energy from reaction temperature study	72
Figure 4.17: Effect of dye concentration on the rate constant	73
Figure 4.18: Comparison between homogeneous and heterogeneous PMS activation	77
Figure 4.19: Effects of quenching reagents on MO degradation rate constants.....	78
Figure 4.20: Mixed dyes study and degradation rate constant of each individual dye...	79
Figure 4.21: Visible degradation of the mixed dyes batch over time	79
Figure 4.22: Catalyst recyclability and efficiency after four runs.....	80

LIST OF SYMBOLS

Symbol	Description	Units
r	Radius	m^2
k	Rate constant	sec^{-1}
A	Frequency factor	sec^{-1}
Ea	Activation energy	kJ mol^{-1}
R	Gas constant	$\text{kJ mol}^{-1} \text{K}^{-1}$
T	Temperature	Kelvin
λ	Wavelength	nm

LIST OF ABBREVIATIONS

AOP	Advanced Oxidation Process
AAS	Atomic Absorption Spectroscopy
BOD	Biochemical Oxygen Demand
DOM	Dissolved Organic Matter
EDS	Energy Dispersive x-ray Spectroscopy
FTIR	Fourier Transform-Infrared Spectroscopy
GY	Golden Yellow
HR	Hydroxyl Radical
L-H law	Langmuire-Hinshelwood law
MO	Methyl Orange
MR	Methyl Red
NP	Nano-Particle
PMS	Peroxymonosulfate
PAC	Polyaluminum Chloride
PS	Potassium persulfate
SR	Sulphate Radical
TBA	Tert-butyl Alcohol
TEM	Transmission Electron Microscopy
TSS	Total Suspended Solids
UV	Ultra violet
XRD	X-Ray Diffractometry

GLOSSARY: TERMS AND CONCEPTS

Advanced oxidation processes (AOP): in a wide sense, AOP is an arrangement of synthetic treatment methodology intended to expel natural (and in some cases inorganic) materials in water and wastewater by oxidation through responses with hydroxyl radicals or sulphate radicals.

Azo dyes: any synthetic dyes with molecules that contain two adjacent nitrogen atoms between carbon atoms.

Catalyst: a substance that expands the rate of a chemical reaction without itself experiencing any perpetual chemical change.

Heterojunction: the interface that happens between two layers of different crystalline semiconductors. These semiconducting materials have unequal band gap, which differ from a homojunction.

Heterogeneous catalysis: refers to the type of catalysis where the phase of the catalyst is different from that of the reactant. This not only refers to solids and fluids vs gas, but also to immiscible fluids (e.g. oil and water).

Homogenous catalysis: In chemistry, homogeneous catalysis is a chemical reaction where the catalyst and the reactants are in the same phase (e.g. liquid-liquid).

Nanotechnology: an area of technology that covers dimensions and tolerances of less than 100 nanometres, particularly the control of individual molecules and atoms.

Nanoparticles: Nanoparticles are particles somewhere in the range of 1 and 100 nanometres in size with a surrounding interfacial layer.

Support material: In chemistry, a catalyst support is a material, usually a solid, with a high surface area, to which a catalyst is affixed. The support might be inert or take part in the catalytic reactions.

CHAPTER 1: INTRODUCTION

Natural contaminants in water remain an incredible worry to the earth, particularly those unmanageable or non-biodegradable contaminants that cannot be dealt with successfully by traditional processes (Hu & Long, 2016a). Azo dyes, generally utilized as a part of textiles, paper, leather manufacturing, coating and the plastic production, can unequivocally harm the earth due to their non-biodegradability, harmfulness and potential cancer-causing qualities (Cabo *et al.*, 2015; Ma *et al.*, 2015). Methyl Orange, an azo dye with a noteworthy presence in the textile area, is drawing a great deal of consideration and research action (Luo *et al.*, 2015).

Heterogeneous catalytic oxidation of natural contaminants has been used generally for wastewater management, in which the improvement of exceptionally proficient catalysts is of basic significance (Zhou *et al.*, 2015). In recent decades, advanced oxidation processes (AOPs), which include responsive oxygen species like hydroxyl radical ($\bullet\text{OH}$) with standard reduction potential in the range of 1.8–2.7 V (Yang *et al.*, 2009), have received much consideration due to their high efficiency and low-cost characteristics when compared to other chemical, physical and biological strategies for the removal of recalcitrant and harmful organic contaminants (Wei *et al.*, 2015). However, the oxidation of an organic compound by a sulphate oxidant, peroxymonosulfate (PMS) or Oxone, has been utilized on the grounds that it has been determined that sulphate radicals are a promising alternative option to hydroxyl radicals in light of the fact that $\text{SO}_4^{\bullet-}$ is more effective than $\bullet\text{OH}$. $\text{SO}_4^{\bullet-}$, with a redox potential of 2.5 to 3.1 V (Neta *et al.*, 1988). Li and colleagues have determined that it also has a more extended lifetime (Li *et al.*, 2015). Moreover, this sort of oxidant is prompt to be activated by heat (Waldemer *et al.*, 2007), ultraviolet light (Sharma *et al.*, 2015), alkalines (Furman *et al.*, 2010), ultrasound (Cai *et al.*, 2016) and right transitional metal ions (Fe^{2+} , Co^{2+} , Mn^{2+}) (Rastogi *et al.*, 2009; Chan & Chu, 2009; Saputra *et al.*, 2013).

In particular, cobalt oxide (CoOx) particles showed better catalytic activity over other transitional metal oxides, detailed by the most recent literature (De la Peña O'Shea *et al.*, 2009). Regardless of the fact that CoOx NPs could exhibit high catalytic performance, they indicated poor chemical and thermal stability while also showing particle aggregation, leading to lower catalytic efficiency in long haul application (Cheng & Cheng, 2009). The development of dynamic and stable heterogeneous Co-based catalysts for water treatment is vital, and different

methodologies utilizing diverse support material (e.g., carbon materials, clays, zeolites) have been reported (Duarte *et al.*, 2012; Yunjin Yao *et al.*, 2013).

In any case, the heterogeneous catalytic oxidation process using PMS and cobalt particles has another issue too. The real concern is that cobalt particles are lethal and consequently will prompt genuine medical problems (Shukla *et al.*, 2010a). In spite of the fact that the composed Co-based heterogeneous catalysts possess enhanced stability, the leaching of cobalt metal ions is inescapable. In this manner, other successful and ecologically amicable catalysts and methods are as yet required (Agustina *et al.*, 2005). Along these lines, new sorts of heterogeneous cobalt-based catalysts are strongly requested to stay away from cobalt being released in water, and to enhance the oxidation effectiveness by means of support materials (Bezemer *et al.*, 2006; (Den Breejen *et al.*, 2009).

Many efforts have gone into the investigations concerning heterogeneous catalysts for PMS enactment. Anipsitakis and colleagues (2005) have reported heterogeneous activation of PMS by using Co_3O_4 micro-scale particles. Chen *et al.* (2008) proposed Co_3O_4 nanoparticles by means of a precipitation strategy and Yang *et al.* (2008) immobilized Co_3O_4 nano-crystallites onto different support materials. Wang *et al.* (2014) discovered that $\text{Fe}_3\text{O}_4/\text{CS}$ -supported Co_3O_4 nanomaterials display a high activity of PMS activation. Liang *et al.* (2012a) utilized $\alpha\text{-MnO}_2$ as a support for Co_3O_4 nanoparticles, with the end goal that the compound creates a synergistic effect in PMS activation. Muhammad *et al.* (2012), utilized coal fly-supported Co_3O_4 catalysts for phenol degradation and found that the catalyst showed higher activity.

In view of every one of these reviews, regardless of some encouraging results on enhancing the catalytic activity and decreasing cobalt leaching, it remains an incredible challenge to make the heterogeneous PMS activation industrially practical (Hu *et al.*, 2013). Thus in this study, with a specific end goal of minimizing cobalt leaching and expanding the catalytic surface area of Co_3O_4 , Co_3O_4 particles were dispersed onto TiO_2 support. TiO_2 served not only as a support material for achieving well-dispersed Co_3O_4 , which reduces cobalt leaching, but additionally it significantly encouraged the development of surface Co-OH complexes considered the rate-limiting step for PMS activation.

1.2 Research problem

The expanding number of contaminants and their huge chemical diversity require a constant improvement in oxidative water treatment. Cobalt metal ions leaching have been a standout amongst the most imperative issues in the Co_3O_4 based heterogeneous peroxymonosulfate (PMS) activation reaction.

1.3 Research questions

1. What is the effect of having Co_3O_4 in a heterojunction structure with TiO_2 on the catalytic activity?
2. What are the effects of different process parameters, such as different cobalt to TiO_2 ratio and calcination temperatures, on the catalyst performance?
3. Which process parameters give the lowest amount of cobalt leaching?

1.4 Objectives

The aim and objectives of this research project will be as follows:

1. to synthesize a cobalt composite catalyst using cobalt oxide and titanium dioxide (as support material) to decrease cobalt leaching in a heterogeneous PMS activation reaction;
2. to investigate the effects of cobalt loading and calcination temperatures on the $\text{Co}_3\text{O}_4/\text{TiO}_2$ catalytic effectiveness for the degradation of dyes in water; and
3. To evaluate the catalytic properties of the synthesized $\text{Co}_3\text{O}_4/\text{TiO}_2$ heterojunction catalyst.

1.5 Significance

This study will improve the catalytic activities of Co_3O_4 in PMS activation processes, while reducing cobalt leaching. This is significant advancement in wastewater treatment since cobalt ions released in the water result in detrimental health and environmental issues.

1.6 Delineation

1. The degradation pathway of the dyes during the reaction will not be studied in this research.
2. A scale up of the reactor to larger volumes will not be investigated.

1.7 Organisation of dissertation

This work is subdivided into five chapters:

Chapter 1: Introduction

This chapter presents an overview of this study starting with an introduction, a research problem and the different research questions, the significance of the research, the aims the objectives, and finally, the delineation.

Chapter 2: Literature review

This chapter's focal point is on the detailed theoretical background of AOP using sulphate radicals and cobalt based catalyst. Different types of cobalt based catalyst in the application of AOP as well as heterojunction structures are accounted in the literature.

Chapter 3: Experimental procedure

This chapter presents details about the research facility, experiments and the trial setup, experimental conditions, the materials, including chemicals and equipment utilized. The experimental methods utilized, data collection and examination technique utilized through this research study are also discussed.

Chapter 4: Experimental results and discussion

This chapter covers all structure characterization and a catalytic activity assessment of the $\text{Co}_3\text{O}_4/\text{TiO}_2$ heterojunction catalyst. Furthermore, it explains the analysis of important data and afterward discusses, point-by-point, the results from data interpretation.

Chapter 5: Conclusion and recommendations

This last section of the thesis provides a summary and draws conclusions from the results of the entire research venture. From that standpoint, additional suggestions are presented for consideration in this field.

References

All resources referenced in this dissertation are presented in detail.

Appendices

This concluding section presents the raw experimental data, formulas and calculations used to investigate and discuss the results obtained.

CHAPTER 2: LITERATURE REVIEW AND THEORY

2.1 Introduction

This part introduces a brief literature review on the synthesis of $\text{Co}_3\text{O}_4/\text{TiO}_2$ heterojunction structure via an organic binder mediated route for the degradation of organic pollutants (dyes) using an advanced oxidation process utilizing peroxymonosulfate (PMS or Oxone). In view of the accessible studies and relevant literature, heterogeneous catalysis using cobalt oxide is discussed in depth as well as various support materials used to synthesise heterogeneous cobalt based catalysts, TiO_2 in particular. Additionally, this chapter presents the fundamental synthesis and operating parameters in order to maintain a high catalytic performance and achieve low cobalt ion leaching.

2.2 Conventional treatment processes

Wastewater treatment in the dye and textile industry principally includes treatment of wastewater containing an assortment of colours in various concentrations. Preceding release into the environment, the wastewater should be dealt with by efficiently removing traces of dye colour to protect the environment, keeping in mind the end goal of ensuring that the conditions are adhered to according to statutory guidelines (Ashtekar *et al.*, 2013).

Numerous sorts of artificial composite dyes are employed in the textile and dyeing plants, releasing a large amount of extremely coloured wastewater. Prior to release into the environment, these wastes *must* be treated, keeping in mind the end goal of following the ecological protection laws for the receiving waters. Biological treatment processes are regularly used to treat textile effluents. These procedures are, for the most part, productive for biochemical oxygen demand (BOD) and suspended solids expulsion (TSS); however, they are, to a great extent, insufficient for removing colour from the waste (Aziz *et al.*, 2007; Basava Rao & Maohan Rao, 2006).

Thus, treated waste effluents may still contain considerable amounts of colour when released. Presently, the treatment procedures are physio-chemical treatment processes, including adsorption, oxidation, and chemical precipitation. Each one of these methods has its benefits and confinements in application.

Lately, significant research has focussed on the removal of colour from textile effluents. These studies have included utilization of inorganic coagulants, for example, lime, ferric or ferrous sulphate, alum and polyaluminum chloride (PAC) (Klimuik *et al.*, 1999). In the majority of cases, coagulation has been successful in the removal of colour, particularly for wastewater containing dissolvable solids. Nevertheless, high chemical dosages are normally required and large quantities of sludge volume must be disposed of. The cost of sludge disposal is, unfortunately, generally quite high (Kim *et al.*, 2004).

The most well-known water treatment procedures utilized for treatment of wastewater from a surface source are rapid mixing, flocculation, sedimentation/clarification, filtration, disinfection, coagulation distillation, desalination, activated carbon, flotation and skimming (Ashtekar *et al.*, 2013).

It is reported that high operating expenses render conventional wastewater treatment procedures inadequate, as the wastes are transferred from one phase to another without accomplishing complete mineralization (Salari *et al.*, 2005).

2.3 Advanced oxidation process

The shortage of water means that there is a definitive need to enhance the quality of wastewater that is released into the environment. Ordinary wastewater treatment can follow either physical, chemical, or biological processes, or now and again, a combination of these procedures (Slokar & Le Marechal, 1998). The fundamental motivation behind wastewater treatment is to remove supplements, organic compounds and solids from effluents. Existing wastewater treatment technologies are deemed

insufficient for the total removal of toxins, especially organic matters such as azo dyes, for example (Nawaz & Ahsan, 2014).

Most of the time, these organic compounds are resilient to ordinary treatment techniques, thereby rendering tertiary treatment necessary. Advanced oxidation process (AOP) constitutes a promising treatment innovation for the management of wastewater. AOPs are characterized by a common chemical feature whereby the very reactive hydroxyl or sulphate radicals for accomplishing complete mineralization of the natural contaminants into carbon dioxide and water are used (Krishnan *et al.*, 2017).

Lately, advanced oxidation processes (AOPs) such as catalytic wet air oxidation, catalytic wet peroxide oxidation, catalytic ozonation, and photo catalysis by means of various oxidants such as hydrogen peroxide, O₂, O₃, persulfate, and peroxymonosulfate are becoming increasingly imperative advancements for water disinfecting. By activation of different transitional metals in various structures (for example, Co (II) or Co oxides), these oxidants can create free radicals that are all the more capable of destroying natural contaminants in water than the parent oxidants (Yunjin Yao *et al.*, 2013).

In recent times, sulphate radicals as a promising alternative option to hydroxyl radicals have been examined. Numerous metal particles, such as cobalt for example, can initiate peroxymonosulfate (PMS, Oxone) to deliver sulphate radicals for oxidation of natural toxins (Anipsitakis & Dionysiou, 2003; Chan & Chu, 2009). In the field of ecological contamination control, persulfates and peroxymonosulfates (PMS) are optional green oxidizing agents for the oxidative deterioration of natural toxins (Sun *et al.*, 2012).

Sulphate radicals (SO₄^{•-}) are progressively examined as an oxidizing operator for toxin debasement in water treatment. SO₄^{•-} has some unique attributes; for example, it is an exceptionally solid electron acceptor empowering the degradation of stubborn mixes which are obstinate towards the strongest oxidant utilized as a part of wastewater

treatment, the hydroxyl radical ($\bullet\text{OH}$) which is created in advanced oxidation processes (AOPs) (e.g., ozonation or photolysis of hydrogen peroxide (UV/H₂O₂)) (Lutze, 2013).

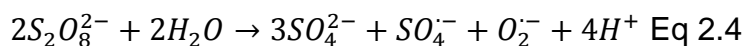
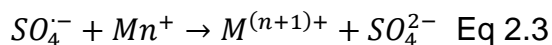
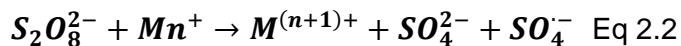
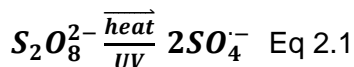
Hence, $\text{SO}_4^{\bullet-}$ based oxidation is oftentimes regarded as a possible substitute oxidative treatment for toxin control in wastewater treatment. Because of the individual nature of $\bullet\text{OH}$ and $\text{SO}_4^{\bullet-}$, $\text{SO}_4^{\bullet-}$ can potentially conquer restrictions of conventional AOPs. It has been found that $\text{SO}_4^{\bullet-}$ is stronger than $\bullet\text{OH}$

Hydroxyl radicals work through unselective multi-step pathways, limiting their effectiveness in complex natural lattices; for instance, waters containing elevated concentration of the fundamental hydroxyl radical scavengers in wastewater, e.g. carbonate/bicarbonate anions and dissolved organic matter (DOM) (Matta *et al.*, 2011), increasing the general scavenging rate of waters needing treatment (Katsoyiannis *et al.*, 2011).

To respond to this limitation, more specific and new strategies delivering responsive radicals were created. The utilization of sulphate radical ($\text{SO}_4^{\bullet-}$) technologies is an ongoing case. For example, Ahmed *et al.* (2012) detailed that sulphate radicals work using the one electron oxidation mechanism, restraining the scavenging effect of inorganic ions and DOM (Monteagudo *et al.*, 2016).

There is a dearth of literature detailing the comparison between hydroxyl radical (HR) and sulphate radical (SR) technologies. Table 2.1 compares the disadvantages and advantages of different AOPs, whereas Table 2.2 compares the reaction rates of SR and HR. Ahmed *et al.* (2014) studied various organic compounds and their kinetic rate using HR and SR oxidation. The SR technology was constantly 10 times faster than HR systems; Sulphate radicals ($\text{SO}_4^{\bullet-}$) are powerful oxidants having a standard redox potential of 2.6 V, which is higher than the standard potential of $\bullet\text{OH}$ (2.8 V) (Gao *et al.*, 2016). $\text{SO}_4^{\bullet-}$ can be produced in situ by the activation of the most common precursors, specifically peroxymonosulfate salt (PMS) or potassium persulfate (PS), by a range of

methods such as thermal activation, photolysis and radiation (Equations 2.1-2.8). Adding transitional metals is acknowledged as a practical way to enact the homogenous activation of peroxymonosulfate/persulfate (PMS/PS) between these methods (Liu *et al.*, 2016).



Normally, peroxymonosulfate is activated to deliver the two radicals – hydroxyl and sulphate – when its peroxide bond (- O-O-) is homilitically severed, as shown in the accompanying equations (Equations 2.6-2.8) (Anipsitakis & Dionysiou, 2004).

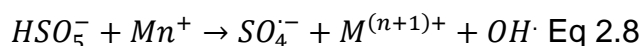
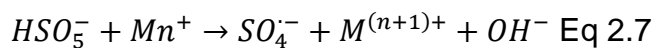
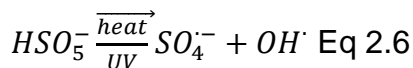


Table 2.1: Key advantages and disadvantages of different Advanced Oxidation processes

AOP	Advantages	Disadvantages
Fenton's Reaction	<ul style="list-style-type: none"> *Able to degrade soluble and insoluble dyes in industrial effluents *No possible formation of bromated by product 	<ul style="list-style-type: none"> *Iron sludge generation due to combined flocculation of the reagent and the organic compounds *Low pH (<2.5) is required to keep iron in solution *pH adjustments will increase operating costs
TiO ₂ catalyzed UV oxidation	<ul style="list-style-type: none"> *No potential formation of bromated by product Recycling of the catalysts *Performance also at higher wavelengths and under solar irradiation 	<ul style="list-style-type: none"> *No full-scale application exists *If the catalyst is added as a slurry, separation step is required *Adapted and optimum concentration of catalyst required a rigorous studies
H ₂ O ₂ /O ₃	<ul style="list-style-type: none"> *Formation of strong non-selective hydroxyl radicals that are able to break down the conjugated double bond *Ozone can be used in its gaseous state and consequently does not raise the volume of wastewater *No sludge generation 	<ul style="list-style-type: none"> *Low rate of degradation as equated to the AOP processes due to less production of hydroxyl radicals *Ozone might produce toxic by-products *High cost *Requires treatment of excess H₂O₂ due to potential for microbial growth
O ₃ /UV	<ul style="list-style-type: none"> *More efficient than O₃ or UV alone *Disinfectant *For equal oxidant concentration, more efficient at generating hydroxyl radical than H₂O₂/UV 	<ul style="list-style-type: none"> *Potential bromated by product *UV light penetration can be obstructed by turbidity *Compounds such as nitrate can interfere with the absorbance of UV light *Energy and cost intensive processes
H ₂ O ₂ /UV	<ul style="list-style-type: none"> *No potential formation of bromated compounds *Full scale drinking water treatment system exists 	<ul style="list-style-type: none"> *Potential bromated by product *UV light penetration can be obstructed by turbidity *Compounds such as nitrate can interfere with absorbance of UV light
Sonication	<ul style="list-style-type: none"> * Less heat transfers relative to UV system *No bromated formation if O₃ is not added 	<ul style="list-style-type: none"> *No full scale application exists *Oxidant may be needed to improve the efficiency of the treatment, thereby increasing cost

Table 2.2: Oxidation potential of commonly used oxidants

Oxidant	Oxidation potential (V)
Fluorine (F)	3.0
Sulphate radical ($SO_4^{\cdot-}$)	2.5-3.01
Hydroxyl radical (OH^{\cdot})	2.8
Ozone (O^3)	2.1
Persulfate ($S_2O_8^{2-}$)	2.1
Peroxymonosulfate (HSO_5^-)	1.82
Hydrogen peroxide (H_2O_2)	1.8

Table 2.3: Kinetic rates of HR and SR on different targeted compounds

Targeted compound	K SR	K HR	
Sulfamethoxazole	$54.12 \pm 0.1 \times 10^{-2} \text{ min}^{-1}$	$3.12 \pm 0.02 \times 10^{-2} \text{ min}^{-1}$	(Ahmed <i>et al.</i> , 2014)
Bifenthrin	$28.65 \pm 0.06 \times 10^{-2} \text{ min}^{-1}$	$1.65 \pm 0.08 \times 10^{-2} \text{ min}^{-1}$	
Mesotrione	$21.32 \pm 0.08 \times 10^{-2} \text{ min}^{-1}$	$1.45 \pm 0.07 \times 10^{-2} \text{ min}^{-1}$	
Carbamazepine	$18.69 \pm 0.03 \times 10^{-2} \text{ min}^{-1}$	$2.96 \pm 0.01 \times 10^{-2} \text{ min}^{-1}$	
Diclofenac	$58.19 \pm 0.4 \times 10^{-2} \text{ min}^{-1}$	$3.65 \pm 0.06 \times 10^{-2} \text{ min}^{-1}$	
Clothianidin	$29.54 \pm 0.1 \times 10^{-2} \text{ min}^{-1}$	$1.20 \pm 0.09 \times 10^{-2} \text{ min}^{-1}$	
Ibuprofen	$1.66 \pm 0.12 \times 10^9 \text{ M}^{-1} \text{ s}^{-1}$	$3.43 \pm 0.06 \times 10^9 \text{ M}^{-1} \text{ s}^{-1}$	(Yang <i>et al.</i> , 2017)
Levofloxacin	$0.93 \pm 0.02 \times 10^{-2} \text{ min}^{-1}$	$20.81 \pm 0.7 \times 10^{-2} \text{ min}^{-1}$	(Epold <i>et al.</i> , 2015)

2.3.1 Azo dyes treatment-using AOP

Removal of toxic organic dyes from textile wastewater is a genuine concern. It is difficult to choose a single method or a combination of treatment methods between the various accessible options (Nawaz & Ahsan, 2014).

Azo colorants can enter the earth from their own manufacturing processes; in any case, the most common ways include their utilization in subsequent industrial sectors, for example, the production of lacquers and paints or plastics, food, textile, paper, and medications colouring (Papić *et al.*, 2006). About 66% of the dyestuff is directed to the textile sector, and it is assessed that around 12% of the utilized dyes are left in wastewaters (Pinheiro *et al.*, 2004).

Because of the growing concern about remaining colour that is connected with harmfulness and aesthetics of discharged effluent, colour removal has become a challenging part of colour wastewater treatment (Arslan-Alaton & Ferry, 2002). Azo colours have been known for some time to resist powerful bio-degradation in aerobic conditions, except for a couple of simple structured dyes (Baughman & Weber, 1994).

The presence of sulfonate groups and azo bonds has been credited with the unmanageability of azo dyes, two features generally considered as xenobiotic. Then again, azo colours have exhibited vulnerability to azo-bond reduction through various mechanisms, bringing about the generation of aromatic amines of rather lethal and cancer-causing substances (Nillson *et al.*, 1993). Along these lines, most of the attention concerning the conceivable dangers emerging from the utilization of azo dyes has been transferred to their reduction products.

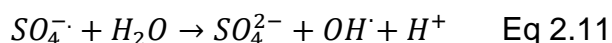
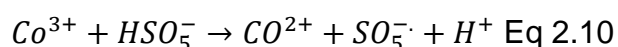
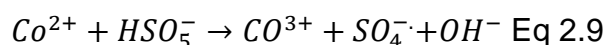
The advantage of advanced oxidation processes (AOPs) in contrast to conventional treatment procedures starts from the reactivity of the free radical species involved, that is, predominantly the hydroxyl radical and sulphate radical species with a high oxidative potential which can quickly and non-selectively oxidize a wide scope of natural toxins

from wastewater (Beltran, 2003; Neamtu *et al.*, 2004) . Furthermore, these procedures are sludge-free (aside from the restricted amount formed in processes including iron salts) because of the total or fractional mineralization of organic carbon. The treatability of azo dyes and dye house effluents by utilizing diverse advanced chemical oxidation processes has been considered (Arslan & Balcioglu, 2001).

2.4 Heterogeneous catalysis using cobalt oxide and TiO₂ as support material

Numerous studies concerning PMS performance have concentrated on cobalt particles and cobalt oxide catalyst because of their best activation effectiveness. On the other hand, Co (II), a profoundly poisonous particle, can draw out a few well-being issues for drinking water. In spite of some encouraging results on enhancing the catalytic action, it is still an incredible test to make the heterogeneous PMS activation innovation monetarily achievable (Yao *et al.*, 2013).

For sulphate radical production, the reaction between Co ions and peroxymonosulphate (PMS, HSO_5^-) has been determined to be an effective method. The radical generation and organic degradation processes can be described as shown below (Anipsitakis & Dionysiou, 2003).



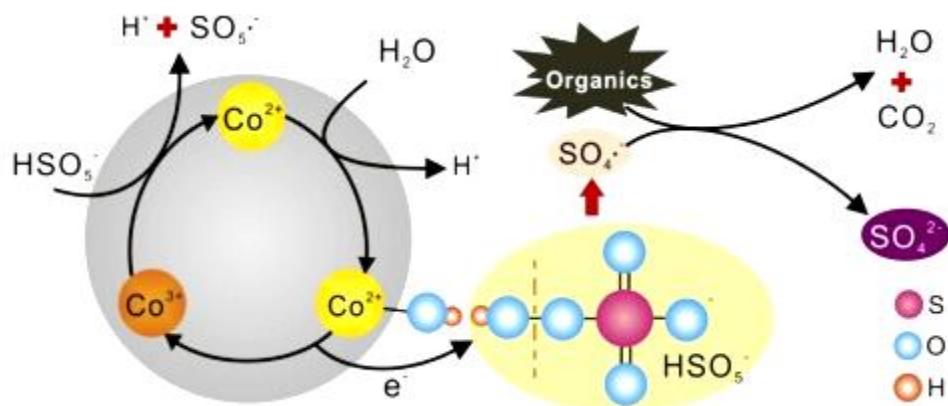


Figure 2.1: Sulphate based radical oxidation diagram

(Hu & Long, 2016b)

Homogeneous catalytic oxidation processes using PMS and cobalt particles have a few other issues. However, the real concern is that cobalt particles are lethal and will prompt genuine well-being issues (Shukla *et al.*, 2010b). As a result, new sorts of heterogeneous cobalt based catalysts are requested to keep away from cobalt being released in water and to enhance the oxidative productivity through support materials.

Even though Co nanoparticles could introduce high catalytic performance, they indicated poor chemical and thermal dependable qualities while also showing particle accumulation, prompting lower catalytic productivity in long haul application. The improvement of dynamic and stable heterogeneous Co-based catalyst for water treatment is essential, and different methodologies utilizing different supports (e.g., clays, carbon materials, zeolites) have been accounted for (Yao *et al.*, 2013).

In Ding's 2012 study, by using cobalt nitrate and bismuth nitrate as precursor salts and NaOH as a precipitation agent, $\text{Co}_3\text{O}_4\text{-Bi}_2\text{O}_3$ nanocomposite oxides (CBO) were prepared as a heterogeneous catalyst for the activation of peroxymonosulfate (PMS) by a conventional reverse co-precipitation method and post-calcination.

Soofivand and Salavati-Niasari (2015) anchored Co_3O_4 nanostructures on top of graphene sheets and the $\text{Co}_3\text{O}_4/\text{graphene}$ ($\text{Co}_3\text{O}_4/\text{GR}$) nanocomposite was prepared

using an effective pre-graphenization method. Photo oxidation of methyl orange (MO) was performed to study the catalytic properties of $\text{Co}_3\text{O}_4/\text{G}$ nanocomposites.

Ramakrishnan *et al.* (2016) used electrochemical deposition, followed by rapid thermal annealing under air and N_2 , to sensitized Cobalt oxide nanoparticles on hydrothermally grown TiO_2 nanorods on FTO (fluorinedoped tin oxide). Electrodeposition time was found to have a direct association with the nanoparticle size of cobalt oxide formed on TiO_2 . They propose this strategy as a financially savvy, basic approach to create a hetero-junction system with enhanced PEC properties.

Lately, with a specific end goal of minimizing cobalt leaching and expanding the catalytic surface area of Co_3O_4 , scattered 10–15 nm nanocrystalline Co_3O_4 particles were immobilized onto 30–40 nm TiO_2 support. TiO_2 not only served as a decent support material for achieving well-dispersed Co_3O_4 but also significantly encouraged the development of surface Co–OH complexes, considered the rate-limiting step for PMS activation (Yang *et al.*, 2008).

2.5 Cobalt oxides

Cobalt (II) oxide is a result of Co_2O_3 cobalt oxide decomposing at 900 °C. It happens as a natural mineral in ores with nickel, arsenic, sulphur and manganese in deposits in Canada, Morocco and Southern Africa. During the roasting procedure, harmful by-products of arsenic and sulphur are produced (Manigandan *et al.*, 2013). The related minerals may taint the Co_3O_4 to some degree (i.e. with Na_2CO_3). However, it can also be produced synthetically. One-dimensional Co_3O_4 nanomaterials have attracted special attention due to their promising application in rechargeable lithium ion battery materials as anode material (Hui *et al.*, 2008; Tan *et al.*, 2016). With the surge in usage of mobile and hand-held devices, large amounts of Co_3O_4 waste materials will certainly be produced in the future.

2.5.1 Application of cobalt oxide in lithium ion batteries

Rechargeable lithium ion batteries (LIBs) have been turning into the fundamental power source of known customer hardware and up-and-coming electric vehicles (Bruce *et al.*, 2008; Winter *et al.*, 1998). However, the present commercial LIBs with graphite as anode with a hypothetical capacity of 372 mAhg^{-1} cannot meet prerequisites for all the more demanding applications because of constraints in energy capacity and reliable operation. As of late, transitional metal oxides have been broadly contemplated as anode materials: for example, SnO_2 (Guo *et al.*, 2008; Yao *et al.*, 2009), In_2O_3 (Ho *et al.*, 2008; Yang & Li, 2014), Fe_2O_3 (Zhu *et al.*, 2011; Wu *et al.*, 2006), MnxOy (Zhao *et al.*, 2008; Wang *et al.*, 2010) and Co_3O_4 , (Yao *et al.*, 2014; Zhang *et al.*, 2015) in view of their higher capacity and volumetric energy density. Among these metal oxides, Co_3O_4 , a standout amongst the most encouraging materials for the cutting edge LIBs to supplant graphite anode, shows incredible reversible properties and high theoretical capacity (890 mAhg^{-1}) contrasted with other transitional metal oxides.

2.5.2 Recovery of lithium cobalt oxide from the cathode of spent lithium-ion batteries

Lithium-ion batteries are used extensively as electrochemical power sources in personal computers, mobile telephones and other modern-life appliances (Lundblad & Bergman, 1997; Plichta & Salomon, 1987). Billions of wasted batteries will be produced every year. For that reason, the recycling of LIBs is critical: even though spent LIBs in general are not classified as 'dangerous waste', disposing of them safely may become a serious problem because of the presence of various toxic and flammable compounds. Consequently, economic benefits could be achieved by recovering major components from LIBs (Kanamori *et al.*, 2009; Catillo *et al.*, 2002). $\text{Li-Co}_3\text{O}_4$ is a favoured material for LIBs cathodes due to its good performance; yet it needs large amounts of Co to meet the market demand. Recovery of cobalt and lithium is one of the most important objectives in the recycling of spent LIBs, in view of the fact that cobalt is a precious and rare metal and a comparatively expensive material in contrast to the other components

of LIBs. And lithium is extremely important in many industrial applications (Tarascon & Armand, 2001; Zhang *et al.*, 1998).

2.6 Titanium dioxide

TiO₂ occurs in three crystalline structures: *anatase* and *rutile* are the most widely recognized types (as the crystalline size of the rutile is constantly bigger than the anatase phase) and *brookite* as the third structural form (an orthorhombic structure, only occasionally used and of little interest for most applications) (D'Agata *et al.*, 2014; Chen *et al.*, 2014). Among the three stages, the rutile phase is the most thermally stable. Brookite and anatase crystalline, over 600°C, encounter a phase transition and change over into the rutile stage (Guo *et al.*, 2007; Xu *et al.*, 2014). The anatase phase contains crisscross chains of octahedral particles connected to each other, while the rutile is comprised of straight chains of opposite edge-shared octahedral structure (Fujimoto *et al.*, 2006; Grosso *et al.*, 2003). Typically the anatase-to-rutile stage change happens between 600–700°C, but for specific applications, it is necessary that TiO₂ anatase be steady at 900°C. In general, the addition of cations stabilizes the anatase TiO₂ nanoparticles (Grosso *et al.*, 2003).

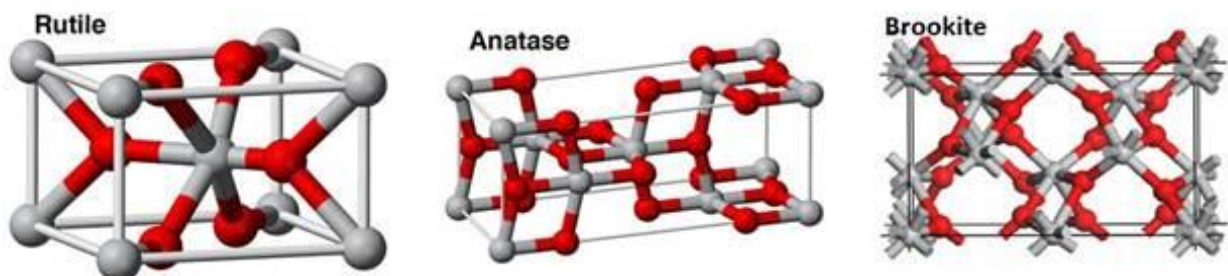


Figure 2.2: Crystal structures of rutile, anatase and brookite titanium dioxide (Woodley & Catlow, 2009; Austin & Lim, 2008)

2.7 Importance of heterogeneous catalyst

Heterogeneous catalysts have emerged as a vital piece of numerous industrial activities, for example, organic synthesis, oil refining and pollution control (Wan & Davis, 1994; Shibasaki-Kitakawa *et al.*, 2007; Uysal & Oksal, 2013). Contemporary heterogeneous catalysts are comprised of several components in precise ratio (Liu *et al.*, 2014). Presently, heterogeneous catalysts are improved for the best reaction rate, which in turn results in optimal selectivity (Leng *et al.*, 2014). It is possible to enhance the heterogeneous catalyst activity by altering the support, by controlling the pore structure or by using approaches such as nanotechnology and nano-science (Cong *et al.*, 1999; Yamaguchi *et al.*, 2005).

For heterogeneous catalysis, the issues of catalyst separation and recuperation from the reaction framework are tended to by utilizing different catalyst supports to immobilize the molecule (Uysal & Oksal, 2013). This then provides a sufficient surface area to the heterogeneous catalyst for it to avoid dissolving into the solution matrix (Yamaguchi *et al.*, 2005). Consequently, heterogeneous catalyst with broad supports – for example, Al_2O_3 , TiO_2 , ZrO_2 , ZnO , and others – is applied in consideration of its accessibility and cost effective manufacturing processes.

Heterogeneous catalysis (gas or liquid phase and solid catalyst) proceeds by means of adsorption of a single or a couple of reactant molecules on the solid surface, improving the reactant fixation on the surface and favouring its activation. The initial step of the reaction is henceforth the reactant adsorption, while the reaction energy includes the activation barrier energies of adsorbed reactants (Aads), or adsorbed intermediates (Iads) and of desorption of products (Pads) (Védrine, 2017).

At the end of the day, the level of catalytic effectiveness gained in a given path is controlled by the 'energetics' of the various intermediates which envelop the adsorbed reactant, the activation energy necessary to convert the bound reactant into an intermediate surface and lastly to a product and its desorption (Bond, 1974).

There is consensus that 85-90% of modern industrial chemical procedures include no less than one catalytic step. The key objective of utilizing a catalyst is to generate high activity (i.e., high conversion of reactants) and in general, high selectivity to a wanted product. The last property is to avoid or limit separation and purification procedures which involve important steps for consideration, particularly economic and general ecological issues (Thomas & Thomas, 2014).

Solid catalysts are classified as (1) conductors, (metals and alloys); (2) semiconductors (oxides and sulphides); and (3) insulators (metal oxides and solid acids or bases, comprising silica–alumina, zeolites, heteropolyacids and natural clays) (Ertl *et al.*, 2008).

The main fields of heterogeneous catalysis, applied industrially, are as follows: oil refining; energy and transport; bulk chemicals; polymers and materials and detergents and textiles; chemicals; pharmaceutical and medical chemicals; food and feed; plant design/engineering and realization; catalyst design; subsequent development of catalysts and of catalytic processes; commercial production of catalysts in sufficient quantities; monitoring and control of chemical reactions; and plant operations and other environmental issues (Védrine, 2017).

2.7.1 Importance of heterogeneous catalyst support

More recently, the significance of a suitable catalyst support material has been of gigantic interest. The thought is that the main catalyst ought to be scattered on an appropriate support to make the catalytic nano-particles stable, acquire optimal performance and minimize the amount of expensive metal used, which in turn will diminish the total catalyst costs (Boudart, 1969; Ziółkowski *et al.*, 1993).

Moreover, with porous qualities, support materials offer a high scattering of nano-particle catalysts and improve electron transfer, both of which add to enhanced catalytic activities (Volta & Portefaix, 1985; Ostrovski, 2012).

In any case, the heterogeneous catalyst support may at some point apply a structural impact, achieved by textural and active phase linked impact (Haber, 1989). Thus, the selected support heterogeneous catalyst must keep its particular properties, for example, dispersion, selectivity, porosity, surface area, and activity (Balandin, 1958; Hinshelwood, 1940). The morphology and pore size of the chosen support materials are an essential part of improving the stability and performance of a heterogeneous catalyst (Ostrovski, 2012).

According to the literature, the support of the heterogeneous catalyst can be zeolites (Hävecker *et al.*, 2012), carbon nanofibers (Balandin, 1958), alumina (Védrine, 2014), active carbon (Volta & Portefaix, 1985), and metal oxides (Grasselli, 2014), such as La_2O_3 , CeO_2 , MnO_2 , TiO_2 , and ZrO_2 . TiO_2 is a renowned heterogeneous catalyst support due to its tuneable porous surface and distribution, high thermal stability and mechanical strength (Thomas, 2012). Being utilized in this way contributes to the ability of TiO_2 to develop redox properties as well as Lewis acidity (Mehlomakulu *et al.*, 2012).

2.7.2 TiO_2 : as support in heterogeneous catalysis

TiO_2 based catalyst support materials are known to have brilliant properties among various material candidates (nitrites, perovskites and carbides, for example) (Bamwenda *et al.*, 1997) because of TiO_2 nano-particle high thermal and chemical stability. TiO_2 based catalyst support has exceptional resistance towards corrosion in various electrolytic media.

TiO_2 can be viewed as a support for heterogeneous catalysts, ensuring stability in electrochemical condition and commercial availability (Tauster *et al.*, 1981). Strong interaction between the catalytic particles and mesoporous TiO_2 has been recorded which has escalated both enhanced catalytic stability and activity. TiO_2 as a catalyst support material additionally demonstrating a certain degree of proton conductivity, which may possibly improve the regime of the triple phase boundary for catalytic reactions (Kim *et al.*, 2003).

The absence of stability is a significant problem for the majority of heterogeneous catalysts. During applications, the agglomeration of particles may obstruct the active sites of the catalyst, believed to add to its instability. As of late, titanium oxide (TiO_2) was presented as an alternative support material for heterogeneous catalysts because of the effects of its high surface area stabilizing the catalyst in its mesoporous structure (Bagheri *et al.*, 2014).

TiO_2 supported metal catalysts have garnered interest because of TiO_2 nano-particle high activity for different reduction and oxidation reactions at low temperatures and pressures. Moreover, TiO_2 was observed as a good metal oxide catalyst support because of the strong metal support interaction, its acid-base and its chemical stability property. The previously mentioned properties demonstrate the high potential in photo catalyst related applications of heterogeneous TiO_2 supported catalysts (Bagheri *et al.*, 2014).

TiO_2 , because of its high efficiency, its non-toxicity and its long-term photo stability, has been used widely in mineralizing dangerous and non-biodegradable environmental contaminants. TiO_2 has substantial mechanical resistance and stability in acidic and oxidative environments. These properties render TiO_2 a primary candidate for heterogeneous catalyst support.

Julkapli and colleagues report the use of the mesoporous TiO_2 of pure anatase phase with large surface area and sharp pore distribution synthesized to increase the degree of dispersion and homogeneity of immobilized catalyst (Nolan, 2013; Luo *et al.*, 2013). Electronic effects and functional mechanisms of the heterogeneous catalysts are influenced by the impact of TiO_2 support (Si *et al.*, 2014). TiO_2 , as a catalyst support, implements an electronic effect where the hypo-electronic Ti^{3+} promotes electro catalytic features of hyper-electronic noble catalyst surface atoms (Julkapli *et al.*, 2014).

This diminishes the adsorption energy of CO intermediates, while simultaneously improving the mobility of CO groups. In the meantime, the adsorption of OH species on TiO₂ has a tendency to encourage the conversion of the chemically poisonous CO intermediates in CO₂, thereby enhancing the durability of the heterogeneous catalyst (Sui *et al.*, 2014).

The two factors indirectly assist with the dispersion and anchor of the heterogeneous catalyst particle (Bamwenda *et al.*, 1997). Additional enhancement in the catalytic stability and activity of the heterogeneous catalysts include altering the TiO₂ support material with semiconductor metal oxides.

2.7.3 TiO₂: as support in metal heterogeneous catalysis

The investigation of metal nanoparticle on TiO₂ support is vital in heterogeneous catalysis because of the size and nature of the interaction of a metal nanoparticle with TiO₂ support (Tauster *et al.*, 1981). The determination of catalytic activity and selectivity of the metal heterogeneous catalyst is strongly influenced by this interaction (Kim *et al.*, 2003). Oxidation and reduction at high temperatures are mandatory steps in the preparation of metal supported TiO₂ heterogeneous catalysts (Lietti *et al.*, 1996; Lin *et al.*, 1993). In any case, the two treatments caused morphological changes to the dispersed metal nano-particles from the sintering of TiO₂. Therefore, it is essential that ideal conditions for the catalyst be maintained.

Moreover, diverse morphological changes will result from metal-TiO₂ support interaction, depending upon the specific metal heterogeneous catalyst (Yan *et al.*, 2005): alloy formation (Park & Seol, 2007) encapsulation and inter-diffusion (Ren *et al.*, 2007), for example.

2.8 Hydrothermal process

Various procedures have been employed to produce nanoparticles, including sol-gel, co precipitation, conventional solid-state reactions and hydrothermal methods (as shown in

Table 2.3) (De Miguel et al., 2002). Solid-state, sol-gel and co precipitation techniques are most frequently utilized and yet have serious disadvantages such as strong state in materials with low purity. Even though sol-gel methods allow for excellent control of composition and morphology, the costs are high.

Extra calcination and processing steps are required in the co precipitation method, and in solid-state and sol-gel procedures. Hydrothermal techniques, on the other hand, allow morphological control and superior composition and do not necessitate calcinations and milling steps. Therefore, hydrothermal synthesis was chosen in this research for the preparation of nano-particles.

Table 2.4: Advanced powder process comparison

	Solid-state reactions	Sol-gel	Co-precipitation	Hydrothermal
Cost	low-moderate	high	moderate	moderate
Composition control	poor	excellent	good	good-excellent
Morphology control	poor	moderate	moderate	good
Purity (%)	< 99.5	>99.99	>99.5	>99.5
Calcination step	yes	yes	yes	no
Milling step	yes	yes	yes	no

Hydrothermal electrochemical techniques, inspired by nature, have the potential to improve the morphology-controlled nanomaterials for an extensive variety of applications. From catalysis and biomaterials for implants to microelectronics and automotive, the main benefits originate from their low energy consumption (low temperatures in one-step process), lessened ecological effect and flexibility underway of numerous new materials in any shape and size (Piticescu *et al.*, 2012).

Riman characterized *hydrothermal synthesis* as a procedure that uses single or heterogeneous phase reactions at elevated pressures > 100 kPa and temperatures $> 25^{\circ}\text{C}$, to crystallize ceramic materials straight from solutions (2002). The pressure is the vapour pressure above the solution at the hydrothermal parameters, namely concentration, composition and temperature of the precursor solutions.

Some benefits of the hydrothermal synthesis are listed below:

- Hydrothermal synthesis is an ecologically friendly method because it happens at lower temperatures and pressures, which are close to the living conditions on Earth. Different procedures necessitate higher temperatures and higher or lower pressures; consequently, they are considered environmentally stressed (see Figure 2.3) (Yoshimura & Suchanek, 1997). Low reactions temperatures reduce issues identified with the volatilization of components and stress induced defects.
- The rate and uniformity of aging, growth and nucleation can be controlled.
- Powders, coatings on metals, polymers, fibres, single crystals, monolithic bodies and ceramics can be prepared.

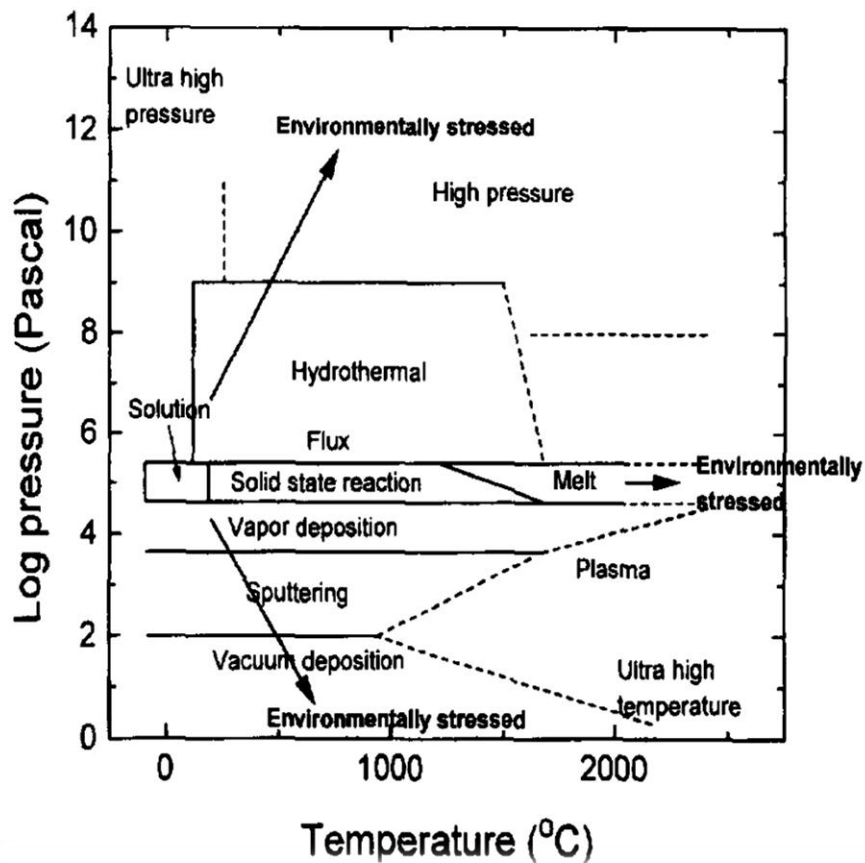
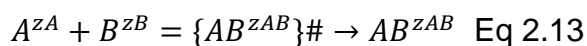


Figure 2.3: Pressure dependence on temperature for different processing routes (Yoshimura & Suchanek, 1997)

The mechanism for the formation of metal oxide particles using metal nitrate solution adheres to the following steps: at first, hydrated metal particles are hydrolyzed to metal hydroxide. Then, metal hydroxides carry on by precipitating as metal oxides through dehydration (Adschiri *et al.*, 2000; Adschiri *et al.*, 2000a).

Hydrolysis is an electrostatic reaction between hydroxyl ions and metal ions. Equation 2.14 expressed the electrostatic contribution to the reaction rate, using ionic species between A^{zA} and B^{zB} in aqueous solution via activated complex $\{AB^{zAB}\}^\ddagger$.



$$\ln k = \ln k_0 + \frac{Ne^2}{2RT} \left(\frac{z_{AB}^2}{r_{AB}} - \left\{ \frac{z_{AB}^2}{r_{AB}} \right\}^\# \right) \left(\frac{1}{\varepsilon} - \frac{1}{\varepsilon_0} \right) \quad \text{Eq 2.14}$$

Where r and z symbolize radius and charge of ionic species; ε expresses the solvent effect with dielectric constant; and ε_0 is the reaction rate in the solvent with dielectric constant (Hayashi & Hakuta, 2010).

Hydrothermal synthesis can be carried out using both batch and continuous systems. The *batch system*, basic and simple, enables control of the oxidation states of the components and allows preparation of systems with a wanted ratio of phases which contain one component in various oxidation states (Galkin *et al.*, 2001). In the *continuous system*, high reaction rate at short residence time is possible. By independently varying the various process parameters, particle size, shape and size, distribution can be controlled to some degree.

2.9 Effect of experimental conditions on heterogeneous catalytic degradation of organic pollutant

2.9.1 Effect of pH

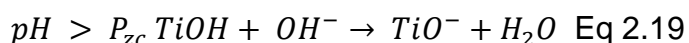
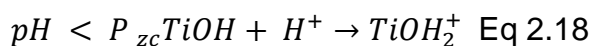
Wastewater pH differs significantly and plays an important part in the catalytic degradation of natural contaminants; the surface charge of the catalyst and the extent of aggregates it forms are controlled by it (Bahnemann *et al.*, 2007).

The ionization and the surface charge of the catalyst (pKa) of a natural toxin can be significantly influenced by the pH.

Electrostatic interaction between the charged radicals, the semiconductor surface, dissolvable particles, and substrate produced during catalytic oxidation strongly relies upon the solution pH. Hence, the pH of the solution plays a key part in the adsorption and catalytic oxidation of contaminants (Haque & Muneer, 2003).

The level of electrostatic attraction or repulsion between the catalyst surface and the ionic forms of organic molecules can fluctuate with a difference in pH, bringing improvement or inhibition of the degradation of natural toxins in the presence of the catalyst (Qamar & Muneer, 2005).

The ionization state of the surface of the catalyst can likewise be protonated and deprotonated under acidic and alkaline conditions individually as appears in the reactions below:



While under acidic conditions, as the pH diminishes, the positive charge of the TiO_2 surface increases (Eq. 2.17); above pH 6.25, with an increase in pH, the negative charge at the surface of the TiO_2 increases. In addition, the pH of the solution influences the formation of hydroxyl radicals by the response between hydroxide ions and induced holes on the TiO_2 surface (Mathews, 1986). The positive holes are considered as the significant oxidation steps at low pH, while at high or neutral pH levels, hydroxyl radicals are considered the predominant species (Shifu & Gengyu, 2005).

It is expected that the generation of both $\bullet\text{OH}$ and $\text{SO}_4^{\bullet-}$ is higher because of the presence of more hydroxyl particles on the TiO_2 surface in the $\text{Co}_3\text{O}_4/\text{TiO}_2$ PMS activation systems. Therefore, the degradation efficiency of the procedure will be logically improved at high pH. To illustrate the impact of pH on the catalytic degradation of organic pollutants and adsorption on the surface of a heterogeneous catalyst, various studies (Singh *et al.*, 2007a; Singh *et al.*, 2007c; Singh *et al.*, 2007b; Rahman & Muneer, 2005a; Rahman & Muneer, 2005b; Qamar & Muneer, 2005; Muneer & Bahnemann, 2002) have been carried out.

2.9.2 Effect of concentration (pollutants)

Effective utilization of heterogeneous catalytic oxidation systems necessitates the study of the dependency of catalytic degradation rate on the substrate concentration (C_0). Lathasree *et al.* (2004), using ZnO as the catalyst, studied the impact of initial concentration (40-100 ppm) on the catalytic degradation of phenol. The initial rates of catalytic degradation were high at the lower concentration range, diminishing as concentration increased. The degradation followed first-order kinetics.

It has been demonstrated in a few studies that as the concentration of the targeted contaminants increases, an increasing number of molecules of the compound are adsorbed on the surface of the catalyst. Thus, the reactive species ($SO_4^{\cdot-}$) required for the degradation of the toxin increases as well (Ahmed *et al.*, 2011).

Nonetheless, the number of $SO_4^{\cdot-}$ radicals formed on the catalyst surface stays steady for a certain catalyst amount and degradation time. The available $SO_4^{\cdot-}$ radicals are insufficient for pollutant degradation at higher concentrations. Subsequently, the rate of degradation diminishes as the concentration of pollutants increases (Bahnemann *et al.*, 2007).

What's more, the generation of intermediates can occur with an increase in substrate concentration. These can also be absorbed on the surface of the catalyst.

Moderate diffusion of the created intermediates from the catalyst surface can result in the deactivation of active sites on the catalyst, which result in a decrease of the reaction rate. Interestingly, at low concentration, the number of catalytic sites will not be the restricting factor and the rate of degradation will correspond to the substrate concentration, as per evident first-order kinetic reaction (Ahmed *et al.*, 2011).

This is in agreement with the Langmuire-Hinshelwood (L-H) law. Several studies have portrayed the dependence of the concentration of different dyes and phenols on catalytic degradation rates utilizing the L-H kinetics model (Mathews, 1988; Mills &

Morris, 1993). The L-H model is used to describe the dependence of the reaction rate on the initial substrate concentrations (Turchi & Ollis, 1990).

2.9.3 Effect of catalyst loading

Various investigations have demonstrated that the catalytic degradation rate firstly increases with catalyst loading and after that, drops at high qualities.

The inclination towards agglomeration (particle-particle interaction) rises at high solids concentration, resulting in a reduction in catalyst surface area accessible for absorption and henceforth a drop in the catalytic degradation rate. Despite the fact that the quantity of active sites in solution will rise with catalyst loading and offer more active sites for adsorption, at a certain point the degradation is compromised because of excessive particle concentration (Selvabharathi *et al.*, 2016).

The trade-off between these two opposing phenomena brings about the need for an optimum catalyst loading for the catalytic reaction (Adesina, 2004). An additional increase in catalyst loading above the optimum value will cause a non-uniform particle distribution; thus the reaction rate would definitely be lower with increased catalyst dosage (Ahmed *et al.*, 2011).

In addition, the aggregation of particles will decrease the interfacial area between the reaction solution and the catalyst at high $\text{Co}_3\text{O}_4/\text{TiO}_2$ concentrations, subsequently decreasing the number of active sites on the catalyst surface (Selvabharathi *et al.*, 2016).

The addition of a larger number of catalysts would increase adsorption sites and give additional catalyst sites to activate PMS, thereby substantially increasing in the reaction rate as long as it is within the optimum amount for catalyst loading. Over all, the high loading of metal will create the aggregation of Co particles, and will not improve Co

dispersion any further; the catalyst surface area will also be reduced with a larger loading of Co on the support material.

2.9.4 Effect of operating temperature

It is acknowledged that the reaction temperature is a basic operating parameter in AOPs, influencing the degradation rate of natural toxins significantly (Sun *et al.*, 2012; Zhang *et al.*, 2016).

Studies demonstrate clearly that the reaction rate increases when the reaction temperature is increased, due to the huge dependence of the kinetic constants on the reaction temperature (Arrhenius law) (Yang *et al.*, 2015). The activation energy (E_a), showing the ease at which a reaction occurs, can be calculated with the Arrhenius Eq (Eq 2.20).

$$k = Ae^{\frac{-E_a}{RT}} \text{ Eq 2.20}$$

In heterogeneous catalytic oxidation, when the E_a value is significantly higher than that of diffusion-controlled reaction ($10\text{--}13 \text{ kJ mol}^{-1}$), it demonstrates that the reaction rate of the oxidation process is more reliant on the rate of intrinsic chemical reactions on the surface of the heterogeneous catalyst as opposed to the rate of mass transfer (Xu & Wang, 2012). When the value of activation energy is higher than that, it indicates that the procedure is in the range of chemical reactions and not adsorption (Fan *et al.*, 2017).

2.9.5 Effect of PMS concentration

Guan *et al.* (2013) studied the effect of PMS concentration on the degradation of BA. BA degradation was enhanced considerably, with an increase in the initial PMS concentration. For instance, the degradation efficiency of BA increased from 47.7% at 0.1mM PMS to 82.5% at 1.0 mM PMS. It is evident that increasing PMS concentration

would make more HSO_5^- attach to the active sites of NiFe_2O_4 , which encourages the generation of radical species.

It has been demonstrated that the degradation efficiency of BA was additionally enhanced by increasing the NiFe_2O_4 dosage. Essentially, increasing the dosage of NiFe_2O_4 provided more active sites on the surface of NiFe_2O_4 for PMS to occupy; in this manner, more species that are reactive could be produced.

Yet, with increasing PMS dosages, certain catalysts had a different catalytic behaviour, where contaminant degradation increased as the catalyst dose was increased from 100 mg/L to 500 mg/L; however, it was ineffective at higher doses (Zhang *et al.*, 2013). As indicated by past literature (Liang *et al.*, 2012a), this phenomenon is likely due to the diffusion limitation in heterogeneous reactions. Especially when the dose of the catalyst surpassed the ideal or optimum value, the unsuccessful oxidant consumption on the surface of the catalyst would be quickened and dominant, prompting a decrease or a constant degradation efficiency (Wang *et al.*, 2013). Similar cases have also been reported in the cases of some oxides and ferrites (Hou *et al.*, 2013; Liang *et al.*, 2012a; Zhang *et al.*, 2013).

PMS without the presence of a metal to activate the $\text{SO}_4^{\cdot-}$ radicals has a slow degradation rate, indicating that the number of radicals released is smaller without the activation.

2.10 Mode of application: suspended vs. immobilized system

The effectiveness of suspended catalysts was observed to be better when contrasted with similar catalysts immobilized on a substrate (Parent *et al.*, 1996). This can be credited to the improved mass transport in suspended form. In any case, the expenses brought about for catalyst recovery makes the slurry system unrealistic.

Interestingly, the immobilized catalyst would be simpler to deal with yet will likely be costlier because of fouling and deactivation of the catalyst.

Deactivation happens, firstly, because the generation of reaction by products cause the loss of active sites on the surface, and fouling block the catalyst pores which change the catalyst surface (Ahmed *et al.*, 2011).

The number of hydroxyl or sulphate groups greatly affects the stability and reactivity of the catalyst. As the reaction proceeds in an immobilized system, the number of hydroxyl/sulphate groups on the catalyst surface decreases and, consequently, the activity of the catalyst drops.

A study by Dutta and Ray (2004) showed that the loss of catalytic activity was due to strongly adsorbed intermediates that occupied the active sites of the catalyst surface. In this manner, more efforts should be centred on eliminating the intermediates that occupy the active sites of the catalyst and regenerate the hydroxyl/sulphate radicals.

2.11 Material characterization techniques

2.11.1 Transmission electron microscopy

The transmission electron microscope is a very important tool for material science. A high-energy beam of electrons is bombed through a very thin sample, and the interactions between the atoms and electrons can be utilized to detect features such as the crystal structure, grain boundaries and dislocations. Moreover, a chemical analysis can be performed. The growth of layers, their composition and defects in semiconductors can be studied using TEM. High resolution can be used to study the shape, size, quality, and density of quantum wells, wires and dots (David & Carter, 1996).

The TEM functions on the same basic principles as the light microscope although it uses electrons instead of light. Because the wavelength light is much bigger than that of

electrons, the optimum resolution achievable for TEM images is much better than from a light microscope. Hence, TEMs are able to show the finest details of internal structure, even as small as individual atoms.

The main application of a transmission electron microscope is to provide high magnification images of the internal structure of a sample. Being able to obtain an internal image of a sample opens new possibilities for what sort of information can be gathered from it.

A TEM operator can investigate the crystalline structure of an object, see the stress or internal fractures of a sample, or even view contamination within a sample through the use of diffraction patterns, to name just a few kinds of studies.

2.11.1.1 Specimen Preparation

A TEM sample must be sufficiently thin to transmit adequate electrons to form a picture with least energy loss. In this manner, sample preparation is an essential part of the TEM analysis. Ultrasonic disk cutting, dimpling and particle milling is a typical sequence of preparation strategies for most electronic materials. *Dimpling* is a preparation technique that produces a specimen with an outer rim of appropriate thickness and a thinned central area that makes handling easier. *Ion milling* is generally the last form of sample preparation. In this procedure, charged argon ions are accelerated to the sample surface by the application of high voltage. The ion impingement upon the sample surface removes material as a result of momentum transfer (Hirsch, 1965).

2.11.2 X-ray diffractometry

X-ray diffraction (XRD analysis or XRPD analysis) is useful for the identification of different phases in poly crystalline aggregate solids, powder specimens and thin-film samples. The unique crystalline structure of materials is the key for identification by this method.

X-rays are high-energy waves and short wavelengths of electromagnetic radiation, characterized by either photon energy or wavelength. Most X-rays have a wavelength in

the range of 0.01 to 10 nanometres; X-ray wavelengths are usually longer than gamma rays and shorter than those of UV rays (Oputu, 2016).

X-rays are produced by high-speed electrons accelerated by a high voltage colliding with a metal target. The kinetic energy of electrons, converted to energy of X-ray radiation, is enabled by the rapid deceleration of electrons on target. The wavelength of x-ray radiation, λ , is linked to the acceleration voltage of electrons (V) as shown in the equation below (Leng, 2013):

$$\lambda = \frac{1.2398 \cdot 10^3}{V} (n) \text{ Eq 2.21}$$

Figure 2.6 illustrates a pair of X-ray incidents on a periodically aligned plane of atoms P_0P_0 , P_1P_1 and P_2P_2 .

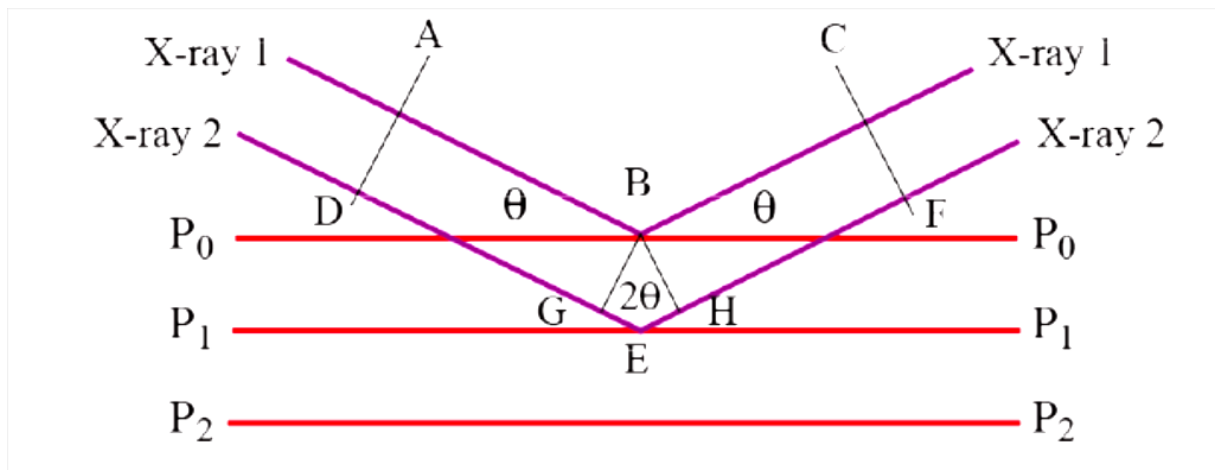


Figure 2.4: X-ray diffracted pair: X-ray 1, reinforced by X-ray 2

For instance, X-ray 1 angle θ symbolizes the angle of diffraction on plane P_0P_0 . An in-phase X-ray 2 produces a diffracted X-ray, which intensifies X-ray 1.

Both rays are connected by the twofold triangle GBHE with an angle 2θ as shown in Figure 2. Bragg and Bragg (1913) suggested that *diffraction* could be viewed as irregular reflectance whose whole number of wavelengths are related to the surface line spacing in Equation 2.43, where n , λ , d and θ are, respectively, integers, X-ray wavelength, distance between parallel atomic planes and angle of incident and diffraction (Atkins & De Paula, 2006).

$$n \lambda = 2d \sin \theta \text{ Eq 2.22}$$

The X-ray mapping of atomic planes is utilized to categorize phases and determine structure in material science. X-ray diffraction patterns of various prepared materials can be matched in the database offered by the Joint Committee on Powder Diffraction Standards (JCPDS) (File, 1967).

2.11.3 Fourier Transform-Infrared Spectroscopy (FTIR)

In order to identify organic (and at times, inorganic) materials, Fourier Transform-Infrared Spectroscopy (FTIR) is the analytical method used as this procedure measures the absorption of infrared radiation by the sample material versus wavelength. The infrared absorption bands detect molecular components and structures (Barth, 2007).

When infrared radiation irradiates a material, absorbed IR radiation more often excites molecules into a higher vibrational state. The wavelength of light adsorbed by a specific molecule is a function of the energy difference between the molecule at rest and excited vibrational states. Molecular structure is characterized by the wavelengths that are absorbed by the sample.

The FTIR spectrometer utilizes an interferometer to control the wavelength from a broadband infrared source. A detector measures the intensity of the reflected light as a function of its wavelength. A computer using Fourier transforms to obtain a single-beam infrared spectrum is used to analyze the signal obtained from the detector: that signal is

call an *interferogram*. The FTIR spectra are typically plots of intensity versus wave number (in cm^{-1}). Wave number is the equal of the wavelength. The intensity is plotted as the absorbance at each wave number or percentage of light transmittance (Berthomieu & Hienerwadel, 2009).

2.11.4 Energy Dispersive X-ray Spectrometry (EDS)

In order to get a localized chemical analysis, EDS utilize the X-ray spectrum produced by a solid sample bombarded with a focused beam of electrons. All components from atomic number 4 (Be) to 92 (U) can be identified on a basic level; however not all instruments are prepared for 'light' components ($Z < 10$).

Qualitative analysis is done by the identification of the lines in the spectrum, straightforward and attributed to the simplicity of X-ray spectra. By measuring the line intensities for each element in the sample and comparing it in the calibration standards of known composition for the same elements, the concentrations of the elements present in a sample (quantitative analysis) can be determined (Goldstein, 2003).

Often Energy Dispersive X-Ray Spectroscopy (EDS or EDX) is a chemical microanalysis technique used in combination with scanning electron microscopy (SEM). The EDS method detects X-rays transmitted from the sample during bombardment by an electron beam to identify the elemental composition of the analyzed volume. Phases or features as small as $1\ \mu\text{m}$ or less can be investigated. The EDS x-ray sensor measures the relative abundance of emitted X-rays versus their energy. The detector is usually lithium-drifted silicon, solid-state device.

When an incident X-ray strikes the detector, a charge pulse proportional to the energy of the X-ray is formed. By using a charge-sensitive preamplifier, the charge pulse is transformed into a voltage pulse (corresponding to the X-ray energy).

The signal is then sent to a multichannel analyzer, which sorts the pulses, by voltage. The energy that is determined from the voltage measurement, for each incident X-ray, is sent to a computer for display and further information assessment. The evaluation of the spectrum of X-ray energy versus counts is needed to identify the elemental composition of the sampled volume.

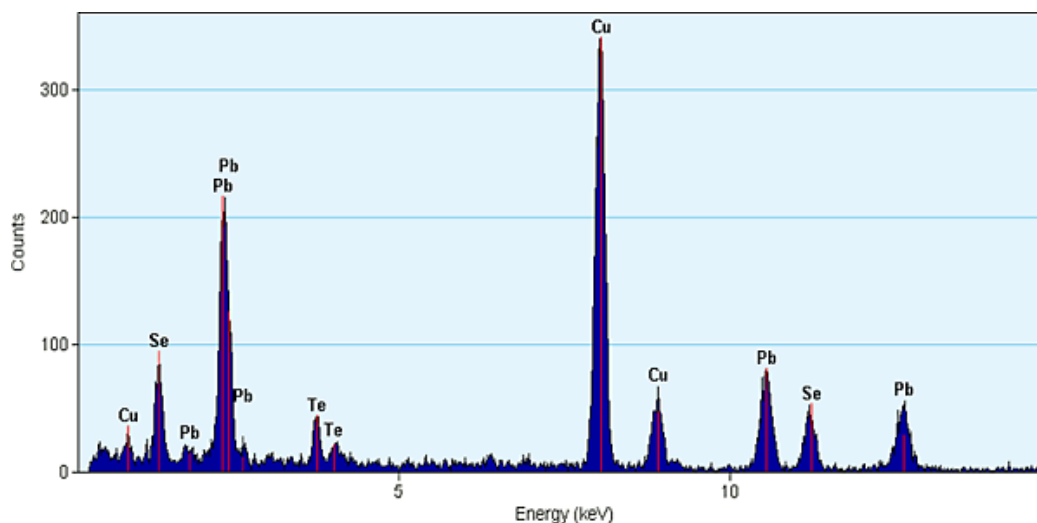


Figure 2.5: EDS Spectrum for the concentrations of chemicals on a carbon support film Cu grid

2.11.5 Electron energy loss spectroscopy (EELS)

EELS has an history of being an increasingly troublesome procedure however is on a fundamental level equipped for estimating chemical bonding, valence, atomic composition, and conduction band electronic properties, surface properties, and element-specific pair distance distribution functions (Ahn, 2004). EELS will in general work best at moderately low atomic numbers, where the excitation edges will in general be sharp, well-defined, and at experimentally accessible energy losses. An EEL tends to work best at relatively low atomic numbers, where the excitation edges tend to be sharp, well-defined, and at experimentally accessible energy losses (the signal being extremely weak past around 3 keV energy losses). EELS are maybe best created for the components ranging from carbon through the 3d transition metals (from scandium to zinc) (Ahn, 2004).

In electron energy loss spectroscopy (EELS) a material is exposed to a beam of electrons with a known, narrow range of kinetic energies.

A portion of the electrons will experience inelastic scattering, which implies that they lose and have their paths faintly and arbitrarily redirected. The amount of energy loss can be estimated by means of an electron spectrometer and translated in terms of what caused the energy loss. Inelastic interactions consist of phonon excitations, inner shell ionizations, inter- and intra-band transitions, Plasmon excitations, and Cherenkov radiation (Egerton, 2009).

The inner-shell ionizations are especially valuable for identifying the elemental parts of a material. For instance, one may find that a bigger than-anticipated number of electrons get through the material with 285 eV less energy than they had when they entered the material. This is around the measure of energy expected to expel an inner-shell electron from a carbon atom, which can be taken as proof that there is a lot of carbon present in the sample. With some consideration, and taking into account wide range of energy losses, one can define the types of atoms, and the amounts of atoms of each type, being struck by the beam.

The scattering angle (that is, the sum that the electron's path is redirected) can likewise be estimated, giving data about the dispersion relations of whatever material excitation caused the inelastic scattering (Egerton, 2009).

2.12 Conclusion

Essential for life, clean water is one of the most important natural resources on the planet. But wastewater, which is 'used water', is also a valuable resource, especially with recurring droughts and water shortages in many areas of the world. However, wastewater contains many harmful substances and cannot be released back into the environment until it is treated. Thus, the importance of wastewater treatment is twofold: to restore the water supply and to protect the planet from toxins.

Treatment of wastewater containing dyes by conventional methods is often inadequate because of its resistance to biological and chemical degradation, thereby creating the

necessity for tertiary treatment. The advanced oxidation process (AOP) constitutes as a promising treatment technology for the management of wastewater containing refractory pollutants.

So far, AOP using sulphate radicals is preferred over hydroxyl radicals because sulphate based radicals ($\text{SO}_4^{\cdot-}$) have recently been shown to be a promising alternative over hydroxyl radicals in light of the fact that $\text{SO}_4^{\cdot-}$ has higher reduction potential as compared to $\cdot\text{OH}$. PMS can be activated by various transitional metals, mainly cobalt. However, since cobalt ions are toxic, support materials must be used to inhibit cobalt leaching. This study focused on the combination of Co_3O_4 and TiO_2 using an organic binder mediated route; the $\text{Co}_3\text{O}_4/\text{TiO}_2$ heterojunction catalyst was used as a co based catalyst in PMS activation.

CHAPTER 3: EXPERIMENTAL PROCEDURE

3.1 Introduction

A detailed description of the processes and techniques used are presented in this chapter, as well as the chemicals, equipment and procedures used to prepare, characterize and evaluate the catalytic activity of the $\text{Co}_3\text{O}_4/\text{TiO}_2$.

3.2 Materials and methodology

3.2.1 Materials

Peroxymonosulfate, commercially known as Oxone (KHSO_5), ethanol 99.9%, tert-butanol as well as titanium (IV) oxide anatase (TiO_2) were obtained from Sigma Aldrich. Heynes Mathew Ltd., Bree Street, Cape Town, South Africa, supplied methyl orange (MO), golden yellow (GY) and methyl red (MR). Urea was supplied from Merck. Minema provided cobalt chloride and maleic acid. All chemicals were received without any further purification.

3.2.2 Hydrothermal preparation of cobalt oxide

In detail, cobalt oxide nanoparticles were prepared by dissolving a specific quantity of cobalt chloride in 300ml of deionized water, stirring at room temperature for four hours until the solution was completely homogenous. Then a solution of urea was added drop wise to the solution while stirring; finally, the solution was transferred into a Teflon liner, sealed in a steel autoclave (batch reactor).

The autoclave was maintained at 105°C for six hours and afterward was permitted to cool at room temperature. The subsequent precipitates were separated by centrifuging, washing several times with distilled water and absolute ethanol, and lastly, dried in a vacuum oven at 60°C for 24 hours.

3.2.3 Preparation of $\text{Co}_3\text{O}_4/\text{TiO}_2$ heterojunction catalyst

TiO_2 was used as support material to synthesize the composite material and different Co_3O_4 loadings were used.

Chemically bonded interface between TiO_2 and Co_3O_4 was created by using an organic linker, namely maleic acid. Seven different ratios (mol ratio) of $\text{Co}_3\text{O}_4/\text{TiO}_2$ composite – 98/2, 95/5, 90/10, 85/15, 80/20, 70/30, 60/40 and 50/50 – were prepared. In a typical synthesis CoOOH (A) and TiO_2 (B) were independently suspended in 30 ml of ethanol. Then 10 ml of 0.1 mol/L maleic acid was added to the ethanol - CoOOH solution; the two solutions were stirred at room temperature for about five hours. Solution A was then added to solution B and the mixture was left stirring for 16 to 18 h at room temperature.

The resulting catalyst was collected by centrifuging and washing with distilled water and absolute ethanol a few times and afterward dried in a vacuum oven at 60°C for 24 hours. Finally, the sample was calcined at various temperatures – 350, 400, 500, 600, 700, 800 and 900°C – in air for four hours, and $\text{Co}_3\text{O}_4/\text{TiO}_2$ composites were effectively created. Table 3.1 summarises the various processing conditions used in this study. The $\text{Co}_3\text{O}_4\text{-TiO}_2$ nano-crystallite interface catalyst prepared was named as $\text{XCo}_3\text{O}_4/\text{TiO}_2\text{-Y}$, where X symbolizes the Co/Ti molar ratio and Y the calcination temperature. Pictorial illustration of the synthesis procedure is presented in Figure 3.1

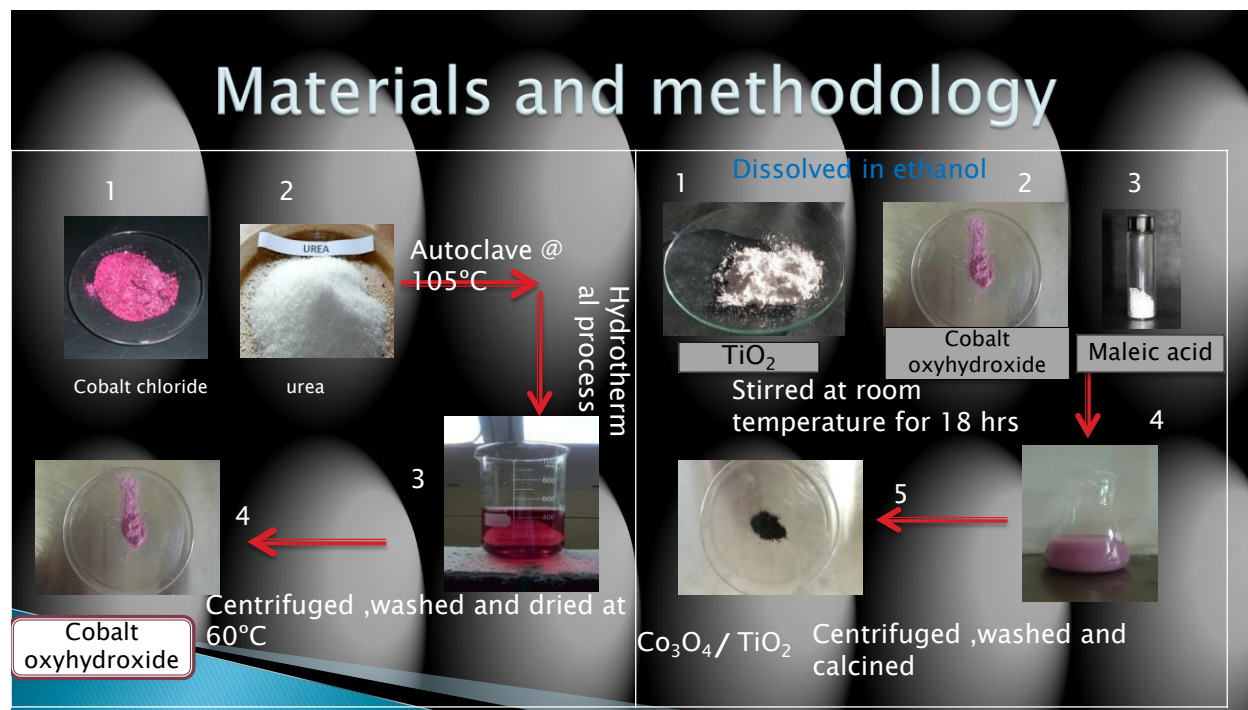


Figure 3.1: Materials and methodology of the synthesis of Co₃O₄/TiO₂ heterojunction**Table 3.1: Process variable for the synthesis of Co₃O₄/TiO₂ heterojunction**

Reaction variables	Values								Units
Co ₃ O ₄ loading	98	95	90	85	80	70	60	50	Mol%
Calcinations temperature	350	400	500	600	700	800	900		°C

3.3 Catalyst performance

Methyl orange degradation was carried out in a 250 mL glass vessel containing 200 mL of methyl orange (MO 40 mg/L). A specific amount of Oxone as the oxidant was added to the glass vessel simultaneously with certain amount of Co₃O₄/TiO₂ catalyst (Figure 3.2). Aqueous phase samples (2.0 mL) were withdrawn at different intervals, joined quickly with an equivalent volume of ethanol as a quencher and subsequently the samples collected were centrifuged to remove any trace of the catalyst. The concentration of methyl orange without catalyst was analyzed by UV–Vis spectrophotometry (SHIMADZU UV-2550) at the maximum absorption band (486 nm). A combination of three different dyes was used to prepare a synthetic dye bath effluent to evaluate the potential of the catalyst to treat real effluents, namely methyl orange (wavelength 486nm), golden yellow (wavelength 437.8nm) and methyl red (wavelength 431nm) and the composite catalyst successfully degraded all the dyes.

Co₃O₄/TiO₂, Co₃O₄ and Oxone were utilized independently and evaluated on the degradation of methyl orange. According to literature, the pH plays a significant role in the cobalt ion leaching: the higher the pH, the lower the level of metal particles leaching into the solution. An atomic absorption spectroscopy (AAS) was utilized to measure and study the cobalt leaching in the solution. For reusability of the catalyst, it was gathered by centrifugation after each application and washed with distilled water and then reused immediately without any drying or calcination. Table 3.2 summarises the experimental matrix that was conducted in this study.

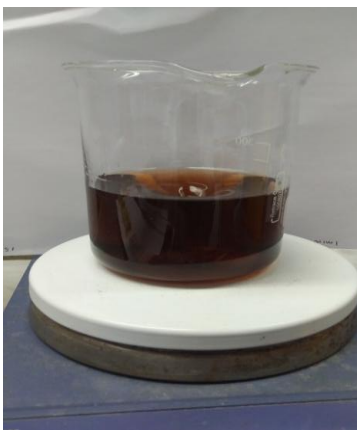


Figure 2.2: Catalyst performance in the degradation of MO

Table 2.2: Optimization of the performance parameters

Sample No	RX Temp (°C)	pH	Catalyst g/L	Dye type	Dye [con] mg/L	Co ₃ O ₄ /TiO ₂ ratio	PMS g/L
Effect of Co₃O₄ loading in the Co₃O₄/TiO₂ heterojunction							
1	20	4	0.15	MO	40	98%	0.2
2	20	4	0.15	MO	40	95%	0.2
3	20	4	0.15	MO	40	90%	0.2
4	20	4	0.15	MO	40	85%	0.2
5	20	4	0.15	MO	40	80%	0.2
6	20	4	0.15	MO	40	70%	0.2
7	20	4	0.15	MO	40	60%	0.2
8	20	4	0.15	MO	40	50%	0.2
Effect of PMS loading							
9	20	4	0.15	MO	40	70	0.1
10	20	4	0.15	MO	40	70	0.15
11	20	4	0.15	MO	40	70	0.2

12	20	4	0.15	MO	40	70	0.5
Effects of dye concentration							
13	20	4	0.15	MO	20	70	0.2
14	20	4	0.15	MO	30	70	0.2
15	20	4	0.15	MO	40	70	0.2
16	20	4	0.15	MO	60	70	0.2
17	20	4	0.15	MO	80	70	0.2
18	20	4	0.15	MO	100	70	0.2
19	20	4	0.15	MO	200	70	0.2
Effects of catalyst loading							
20	20	4	0.05	MO	40	70	0.2
21	20	4	0.1	MO	40	70	0.2
22	20	4	0.15	MO	40	70	0.2
23	20	4	0.25	MO	40	70	0.2
24	20	4	0.4	MO	40	70	0.2
Effects of reaction temperature							
25	20	4	0.15	MO	40	70	0.2
26	25	4	0.15	MO	40	70	0.2
27	30	4	0.15	MO	40	70	0.2
28	40	4	0.15	MO	40	70	0.2
Effects of mixed dyes							
	20	4	0.15	MO,MR,GY	40	70	0.2

3.4 Experimental techniques

3.4.1 Batch synthesis

The customary hydrothermal synthesis method usually occurs in an autoclave reactor (Tseng *et al.*, 2003) where an aqueous solution is gradually warmed to a specific temperature and afterwards aged for a few hours or days (Machek *et al.*, 1981).

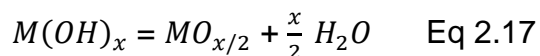
A vessel known as 'autoclave' is required for batch hydrothermal synthesis, suitable for dealing with exceptionally corrosive solvent, working under extreme temperature and pressure, as well as processing conditions with sufficient resistance. Autoclaves and pressure vessels are made from quartz cylinders or thick glass and high strength alloys, such as austenitic stainless steel, nickel, cobalt-based super alloys iron, or titanium and its alloys. Figure 2.7 illustrates a typical pressure vessel or autoclave for illustration purpose (Chowdhury, 2014).



Figure 3.3: Pressure vessel or autoclave for batch hydrothermal reactions

Batch hydrothermal synthesis, usually operated at around 373-473 K, is principally used to produce inorganic powders such as single and mixed metal oxides (Hao & Teja, 2003). Through the heat-up period, the reactions below occur to produce nuclei and, ultimately, crystals.





Materials with the desired microstructure and properties are obtained during homogeneous nucleation and grain growth processes of hydrothermal reactions. Nonetheless, it is a long process to obtain crystals of equilibrium composition by this method (Machek *et al.*, 1981).

Hydrothermal synthesis is a standout among the most commonly used procedures for the preparation of fine powders with controlled shape, crystallinity, size and composition. It is compared with other broadly utilized systems (see Table 2.3) (Darr & Poliakoff, 1999; Otsua & Oshima, 2005).

3.4.2 Metal oxide catalyst preparation

The objective of this section is to discuss the broad subject of metal oxide synthesis for heterogeneous catalysis by keeping in mind the primary preparation procedures for supported metal oxide and bulk catalyst (Le Page, 1987; Perego & Villa, 1997; Regalbuto, 2007). The three main areas are as follows:

1. production of bulk simple metal oxides;
2. production of bulk mixed oxides; and
3. Expansion of supported metal oxides.

The preparation of supported metal oxide catalysts (Lambert & Che, 2000) depends on ambient, aqueous-phase techniques (impregnation, selective adsorption and deposition–precipitation) which prevail at the industrial scale for ecological and financial reasons. The impregnation and drying steps are imperative, as well as the physical-chemical parameters that control the surface chemistry at the solid and liquid interface during active phase deposition, which in turn control the specification and distribution of the active phase in a porous support.

Surface specification of the active phase is dependent on the interfacial pH, predominantly controlled by the buffering impact of the support (density and nature of surface ionisable groups) yet weakly dependent on the initial impregnation pH (Hutchings & Védrine, 2004). By limiting the liquid convection toward the external surface, distribution of the active phase in a support material can be adjusted at both the drying and the impregnation step by using complexing or non-complexing additives. The support can also be chemically activated by attaching chemical groups such as acid or amino groups, able to bind easily with the salt to be attached (Védrine, 2017).

An inert organic binder such as maleic acid or glucose can also be added to create a chemically bonded interface between the catalyst particles and the support material. This method is cost effective and easy comparable with methods like impregnation, co precipitation and ion exchange since all reagents (namely the catalyst, the catalyst support material and the organic binder) are simply mixed in a reactor at ambient temperature and pressure.

3.5 Characterization of $\text{Co}_3\text{O}_4/\text{TiO}_2$ heterojunction catalysts

The morphology and microstructure of the interfaced $\text{Co}_3\text{O}_4/\text{TiO}_2$ catalysts were analyzed by transmission electron microscope (TEM). The crystal structure of the catalyst was characterized by X-ray diffractometry (XRD). UV–Visible diffuse reflectance spectra was collected using a Perkin Elmer lambda 35 spectrophotometer. An energy dispersive X-ray spectroscopy (EDS) was used to investigate chemical composition and the EDS spectral image (STEM-EDS SI) was collected at a pixel size of $3 \times 3 \text{ nm}^2$ using an electron beam with a nominal beam diameter of 0.3 nm. The changes in the surface chemical bonding and surface composition were characterized by Fourier transform infrared (FT-IR) spectroscopy carried out on a SHIMADZU FTIR-8400S spectrometer in the range of $4000\text{--}350 \text{ cm}^{-1}$ in a KBr matrix. A scanning electron microscope (SEM) was employed to obtain information about the sample's surface topography and composition.

An EEL was used to measure the chemical bonding, valence and conduction band electronic properties, and element-specific pair distance distribution functions.

CHAPTER 4: RESULTS AND DISCUSSION

4.1 Introduction

This chapter discusses in detail the results achieved during the experimental study of this research work, the structural analysis of the catalyst used to distinguish the difference between the pristine Co_3O_4 , TiO_2 and the $\text{Co}_3\text{O}_4/\text{TiO}_2$ composite material. The methods used were X-ray diffraction (XRD), Fourier Transform Infrared Spectroscopy (FTIR) and transmission electron microscopy (TEM).

A comparison between the created heterogeneous catalyst and the ones cited in the literature is presented in this section. The impacts of different preparing parameters – such as PMS loading, reaction temperature, dye concentration and catalyst loading – were assessed and detailed in this section.

Reusability and its application in the dye degradation sector was also assessed and discussed in this section. In conclusion, the improved catalyst leading to less cobalt leaching was determined and examined.

4.2 Structural characterization of $\text{Co}_3\text{O}_4/\text{TiO}_2$ heterojunction structure

4.2.1 X-ray diffraction analysis

XRD is an effective way to investigate the crystalline properties of the synthesized material. The XRD patterns of $\text{Co}_3\text{O}_4/\text{TiO}_2$ composites after calcination at different temperatures, as well as the spectra of pristine Co_3O_4 and TiO_2 , were obtained to identify the changes that occur after Co_3O_4 physically bonded with TiO_2 in the heterojunction catalyst.

In XRD patterns of the pure Co_3O_4 , demonstrated in Figure 4.1, the material matched the standard diffraction patterns of cubic Co_3O_4 . The TiO_2 patterns correspond with that of TiO_2 anatase tetragonal. The $\text{Co}_3\text{O}_4/\text{TiO}_2$ composite material exhibits patterns of both cubic Co_3O_4 and TiO_2 anatase tetragonal as the composite material has narrow and high intensity XRD peaks as compared to that of pure Co_3O_4 hinting towards larger

particles size than that of the later. But a narrow peak can also be due to strain effects, crystallite size and instrumental effects.

Studies reveal that the calcination temperature firmly affects the morphology of the prepared metal oxides and that results in a range of electrochemical performances. It was noticed that there was no morphology transformation between 350, 400 and 500 °C (data not shown); however, at 600 °C the morphology of the crystals change and these changes are better explained on the TEM images (Oh *et al.*, 2007).

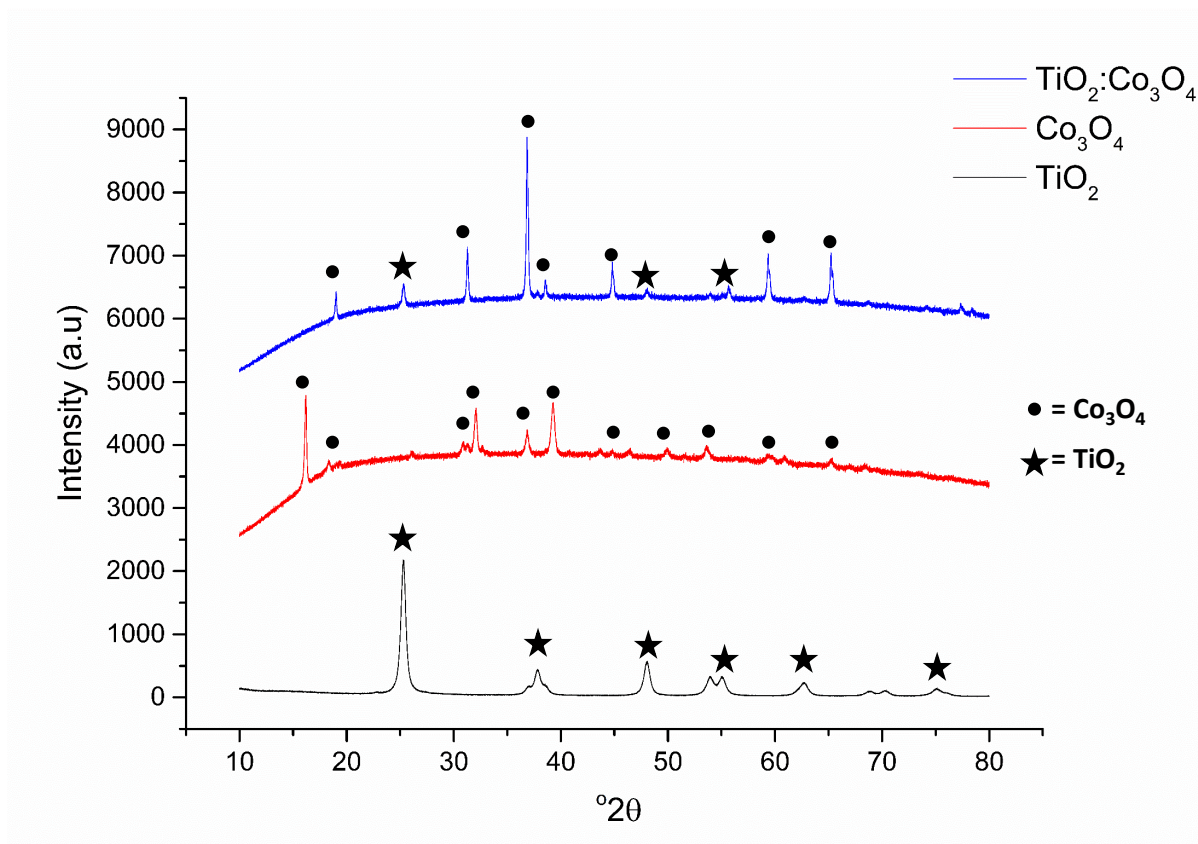


Figure 4.1: XRD patterns of different materials at different calcinations temperature

4.2.2 TEM results of TiO_2 , Co_3O_4 and $\text{Co}_3\text{O}_4/\text{TiO}_2$ heterojunction structure

TEM images were used to further evaluate the morphology of the pristine materials and the composite materials. The images clearly show the difference between the composite material and the pristine ones, and it is revealed from literature that the bigger the surface area of the particles, the better the catalytic activity.

Figure 4.2(a) shows bright-field TEM image of the $\text{TiO}_2:\text{Co}_3\text{O}_4$ sample synthesized at 350°C . As shown, the presence of TiO_2 and Co_3O_4 structures are present in the product (highlighted by square box). The high-resolution micrograph of Figure 4.2(b) shows the difference in lattice spacing between the TiO_2 and Co_3O_4 structures; whereas the EDS spectrum of Figure 4.2(c) confirms the elemental presence of Ti, Co and O in the specimen. The SAED pattern of Figure 4.2(d) shows that the specimen is polycrystalline, with the diffraction ring pattern of the cubic crystal structure of Co_3O_4 and the tetragonal crystal phase of anatase TiO_2 observed and indicated in the pattern. From the analysis of the SAED pattern of Figure 4.2(d), the average lattice constant of the face-centred cubic Co_3O_4 matrix is determined at $a=0.820\text{ nm}$, with the lattice constants of the tetragonal TiO_2 nanostructured material determined as $a=0.346\text{ nm}$ and $c=0.943\text{ nm}$.

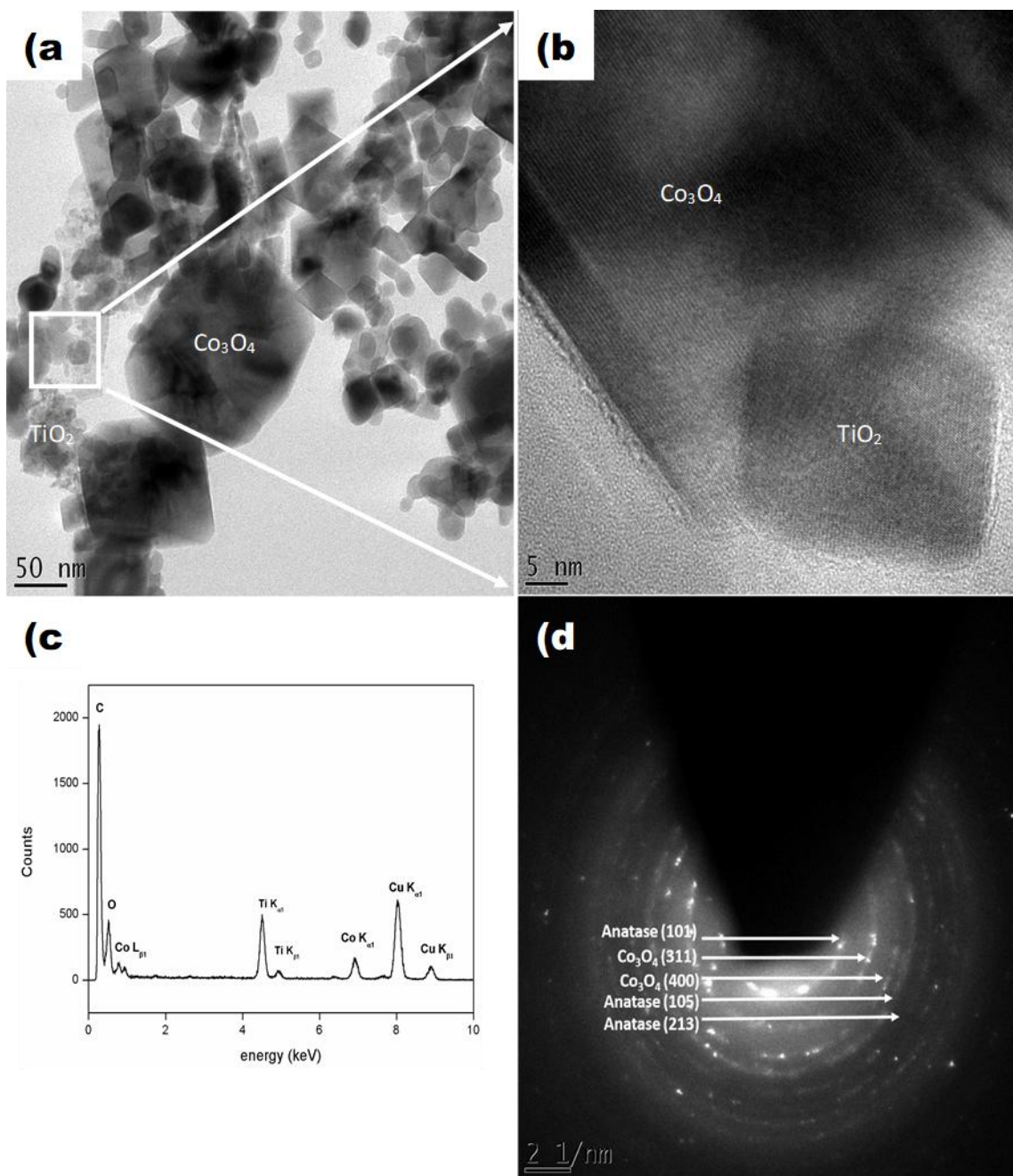


Figure 4.2: (a) and (b) TEM bright-field micrographs of $\text{TiO}_2:\text{Co}_3\text{O}_4$ at 350 °C showing the presence of both TiO_2 and Co_3O_4 nanostructures; (c) EDS spectrum; and (d) SAED pattern

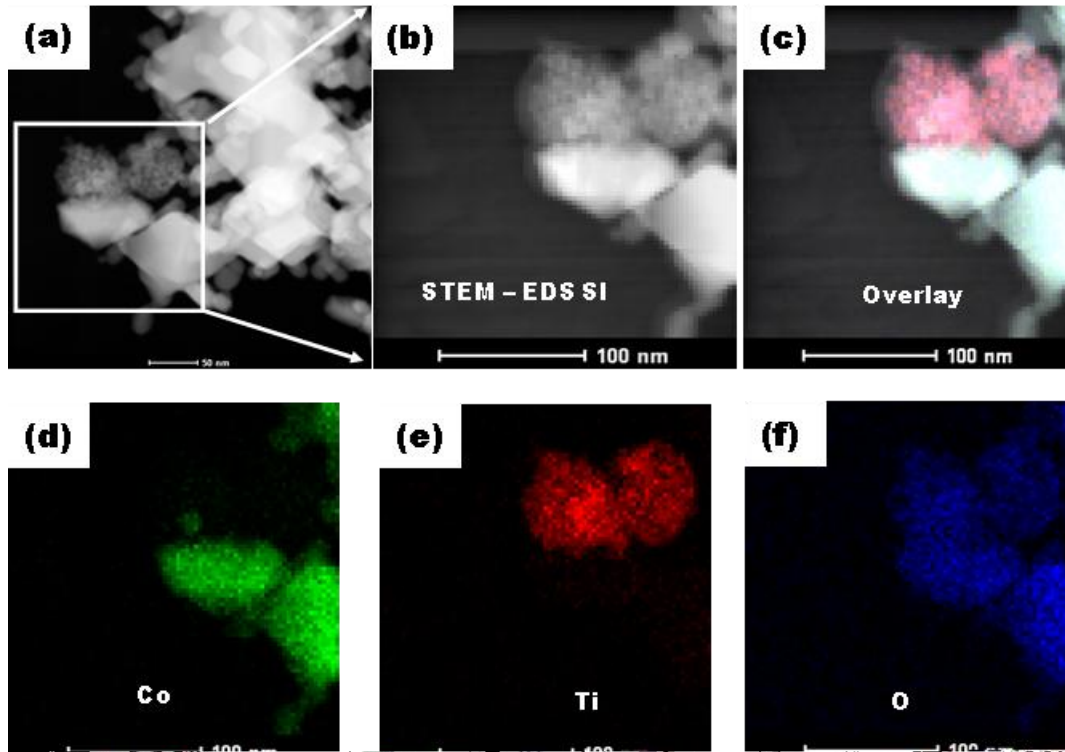
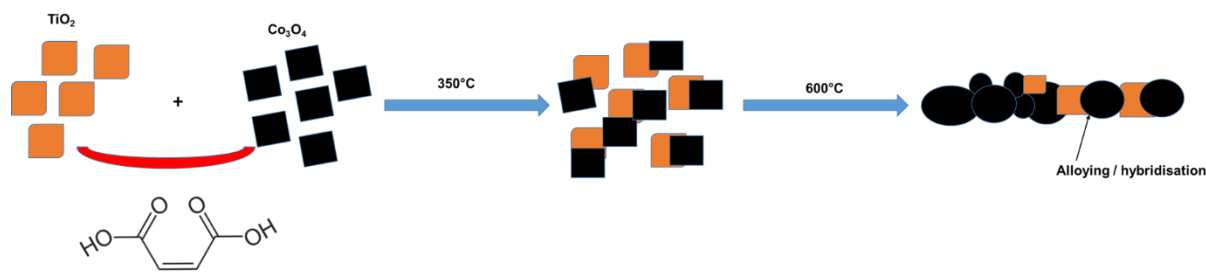


Figure 4.3: (a) HAADF STEM micrograph of the composite $\text{Co}_3\text{O}_4/\text{TiO}_2$ material at 350 °C; (b) STEM-EDS spectral image of the area indicated in (a); (c) overlaid EDS map, (d – f), Co, Ti and O maps, respectively, extracted from the STEM-EDS spectral image of (b).

Figure 4.3(a) shows a high-angular annular dark-field (HAADF) image, collected in STEM mode of the $\text{TiO}_2:\text{Co}_3\text{O}_4$ nanostructured material synthesized at 350°C. An EDS spectral image (STEM-EDS SI) was collected from the area indicated by the square in Figure 4.3(a) and is shown in Figure 4.3(b). The spectral image was collected at a pixel size of $3 \times 3 \text{ nm}^2$ using an electron beam with a nominal beam diameter of 0.3 nm. From this spectral image, the pixels representing Ti, O and Co were extracted and shown in Figures 4.3(d)–(f) respectively. These maps confirm the analysis of the bright-field and SAED results of Figure 4.2, where it was shown that the TiO_2 and Co_3O_4 exist as two separate materials, suggesting no inter-diffusion of the TiO_2 precursor material into the Co_3O_4 matrix.

Figure 4.4(a) shows the bright-field TEM image of the $\text{TiO}_2:\text{Co}_3\text{O}_4$ sample synthesized at 600°C. Unlike the case when synthesized at 350°C, the TiO_2 and Co_3O_4 do not exist

as separate materials, but instead as shown; the nanostructures form rods of individual nanoparticles. The high-resolution micrograph of Figure 4.4(b) shows a uniform lattice fringe size (d-spacing) for the individual nanoparticles constituting the nano-wires. The EDS spectrum of Figure 4.4(c), however, shows the elemental presence of Ti, Co and O in the nano-wires, suggesting that at 600°C the TiO₂ does not exist as individual nanoparticles, but rather as possible dopant in the Co₃O₄ matrix or forming a TiO₂:Co₃O₄ 'alloy' or hybrid material. Formation of rod shaped Co₃O₄/TiO₂ is illustrated in Scheme 1.



Scheme 1: Illustration of rod shaped Co₃O₄/TiO₂ formation

The SAED pattern of Figure 4.4(d) suggests the latter, as the diffraction pattern once more exhibits both the cubic crystal structure of Co₃O₄ and the tetragonal crystal phase of anatase TiO₂. From the analysis of this pattern, the lattice constant of Co₃O₄ matrix is determined as $a=0.852 \text{ nm}$, with the lattice constants of the tetragonal TiO₂ determined as $a=0.292 \text{ nm}$ and $c=923 \text{ nm}$. As can be seen, there is an increase in the lattice constant of the cubic Co₃O₄ matrix as compared to the case at 350 °C, accompanied by a decrease in the a, b and c axes of the tetragonal TiO₂ lattice. This implies that during the synthesis process at 600 °C, the TiO₂ lattice experiences a compressive stress in all three lattice axes, thereby inducing a smaller unit cell volume, which ultimately promotes the diffusion process.

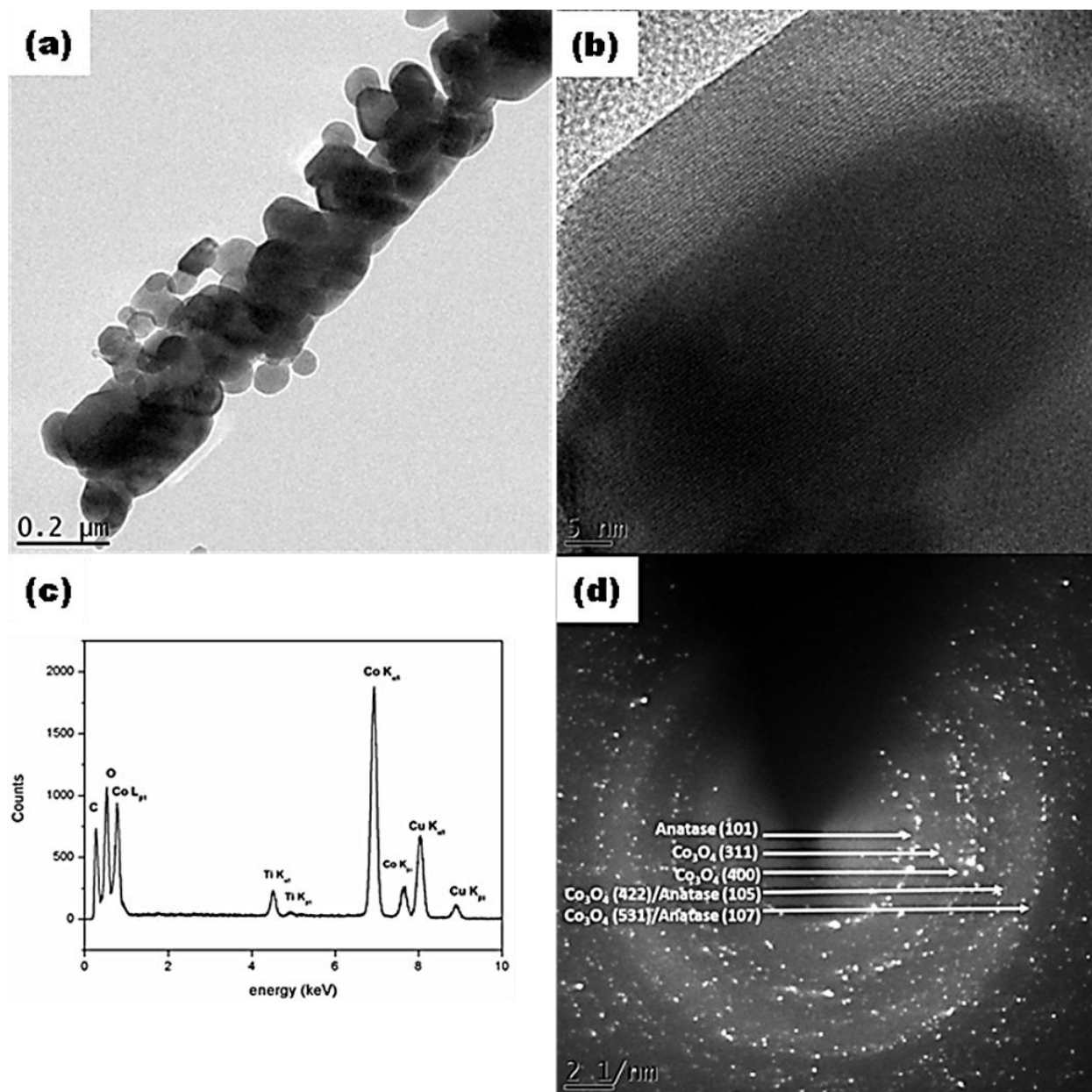


Figure 4.4: (a) and (b) TEM bright-field micrographs of sample (c) EDS spectrum and (d) SAED pattern

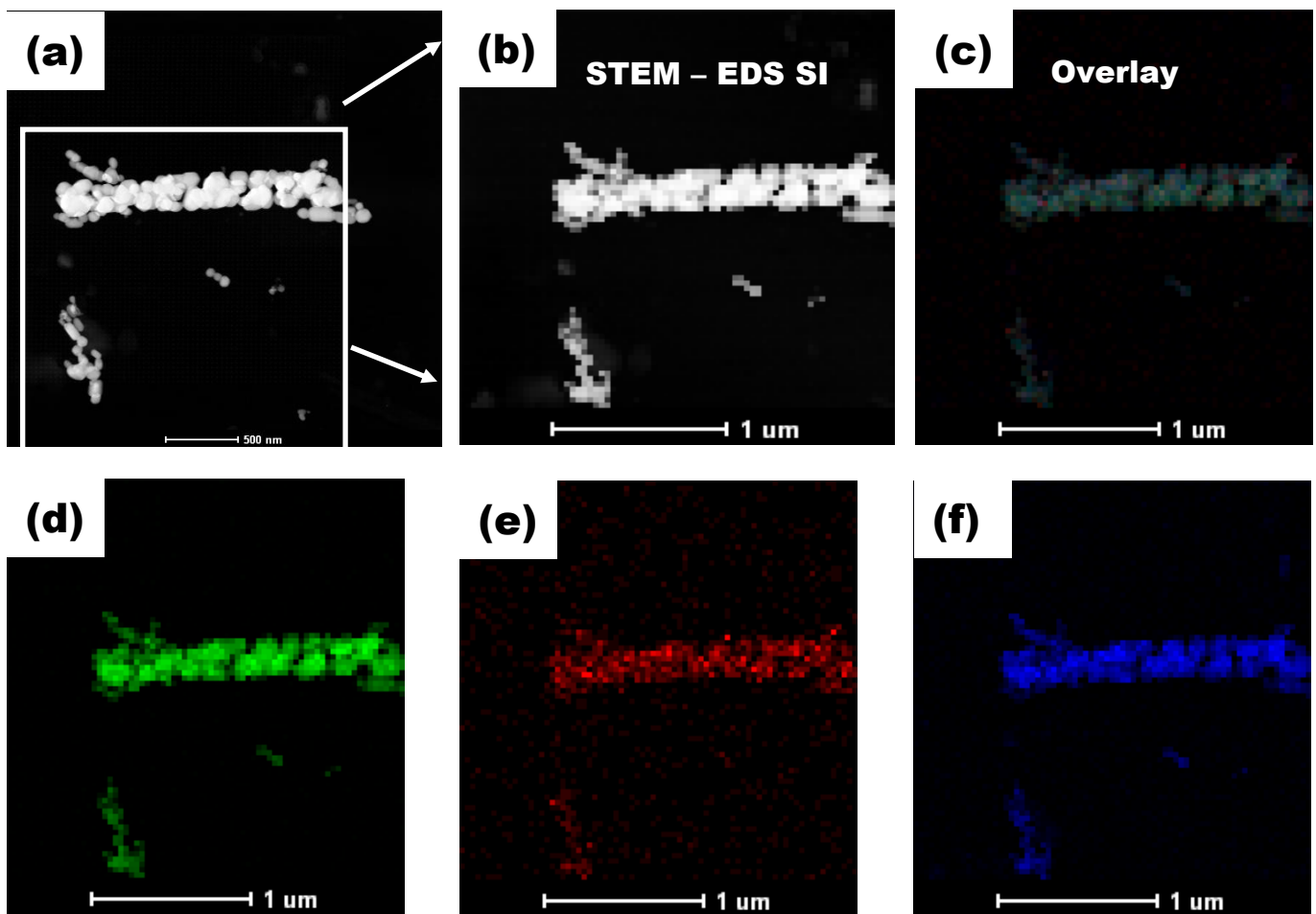


Figure 4.5: (a) HAADF STEM micrograph of the composite $\text{Co}_3\text{O}_4\text{-TiO}_2$ material; (b) STEM-EDS spectral image of the area indicated in (a); (c) overlaid EDS map, (d – f), Co, Ti and oxygen maps extracted from the STEM-EDS spectral image of (b)

The HAADF-STEM coupled with EDS analysis of Figure 4.5 confirms the above argument. The STEM-EDS spectral image of Figure 4.5(b) was collected from the boxed area indicated in Figure 4.5(a); the spectral image was collected using image pixels of $20 \times 20 \text{ nm}^2$, with each pixel containing EDS information. Figures 4.5(d) to (f) show the Ti, Co and O maps extracted from Figure 4.5(b). From these maps it is becomes evident that the TiO_2 and Co_3O_4 matrices are indeed inter-diffused, forming a hybrid material, as postulated above.

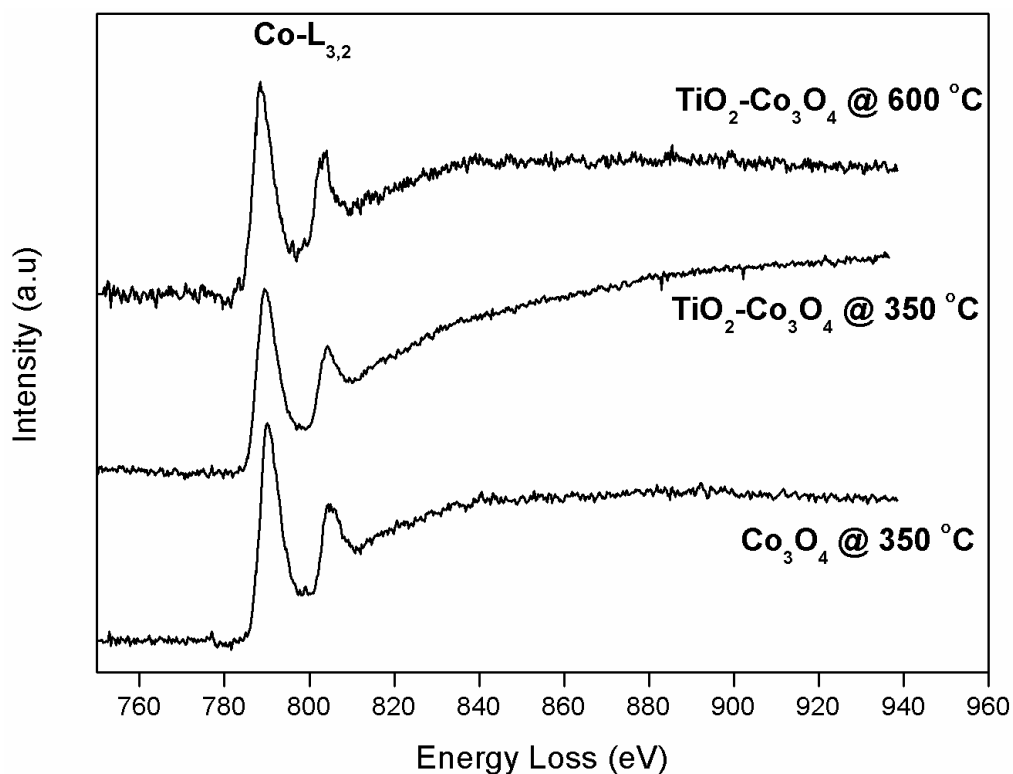


Figure 4.6: Electron energy loss spectra comparing the energy loss near edge fine structures (ELNEFS) of the Co- $L_{3,2}$ ionization edge of the structures grown at 350 and 600 °C to that of pure Co_3O_4 nanoparticles at 350 °C

Figure 4.6 compares the energy loss near edge fine structure (ELNEFS) of the Co $L_{3,2}$ edges of a pristine Co_3O_4 specimen to that of the hybrid $\text{TiO}_2:\text{Co}_3\text{O}_4$ materials synthesized at 350 and 600 °C. The Co_3O_4 spectrum shows two sharp peaks at 789 (L_3) and 804 eV (L_2), which corresponds to the Co $2p_{3/2}$ and Co $2p_{1/2}$ spin-orbit peaks of the Co_3O_4 spinel structure (Hagelin-Weaver et al., 2004). The L_3/L_2 ratio is widely considered a fingerprint method for determining the Co valence state.

From Figure 4.6, an L_3/L_2 ratio of 1.59, 1.46 and 1.49 is calculated for Co_3O_4 , $\text{TiO}_2:\text{Co}_3\text{O}_4$ at 350 °C and $\text{TiO}_2:\text{Co}_3\text{O}_4$ at 600 °C, respectively. From these values, it can be deduced that the pristine Co_3O_4 exists in the Co^{3+} oxidation state, typical of the Co_3O_4 electronic structure (Wang et al., 2000). Upon incorporation of the TiO_2 into the Co_3O_4 matrix, it can be seen that the L_3/L_2 ratio decreases for both the structures

synthesized at 350 °C and 600°C. These suggest a re-coordination of the Co valency. In the case of 350 °C sample, it was established in Figures 4.2 and 4.3 that the TiO₂ does not diffuse into the Co₃O₄ matrix due to the lower temperature. Instead, as the EELS results of Figure 4.6 suggest, hybrid bonding occurs between the Co₃O₄ and TiO₂ lattice. In the case of the 600 °C sample, the TiO₂ diffuses into the Co₃O₄ matrix, causing the re-coordination of the Co valency by the introduction of the Ti⁴⁺ ion.

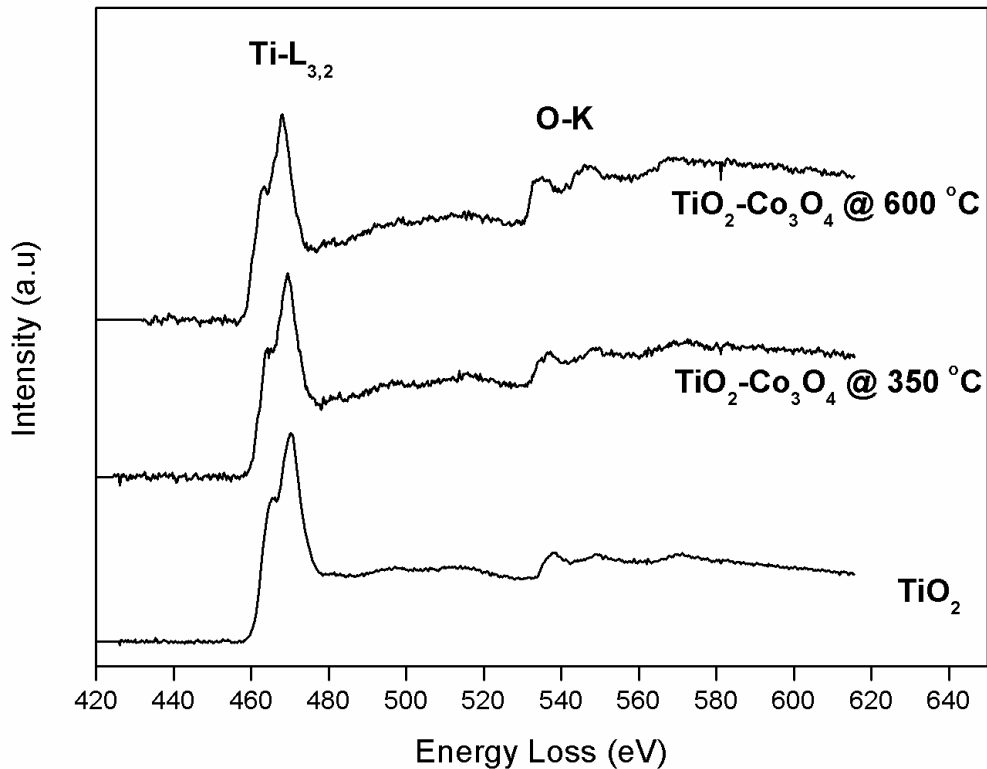


Figure 4.7: Electron energy loss spectra comparing the energy loss near edge fine structures (ELNEFS) of the Ti-L_{3,2} and O-K ionisation edges of the structures grown at 350 and 600 °C to that of pure TiO₂ nanoparticles

Figure 4.7 compares the ELNEFS of the Ti-L_{3,2} edges of pure anatase TiO₂ to that of the TiO₂:Co₃O₄ synthesized at 350°C and 600°C. Unlike the case of the Co-L_{3,2} ionization edge the L₃ and L₂ edges are separated by ~ 2.5 eV, with the L₂ edge more intense than L₃. At closer inspection, it can be seen that both the L₂ and L₃ edges exhibit shoulders on the lower energy side of the peaks. This is typical of the anatase TiO₂ crystal structure caused by crystal-field splitting of the unoccupied, anti-bonding t_{2g}

and e_g orbitals which contain mostly titanium d character (Brydson & Thomas, 1987). From these line shapes, it becomes obvious that the TiO_2 structure undergoes no discernible change in lattice at either 350 or 600°C and remains anatase. From the SAED results of Figure 4.4(d), it was shown that the TiO_2 unit cell volume decreases, increasing favourability for diffusion into the Co_3O_4 lattice. The oxygen K-edge at 532 eV exhibit three peaks, at approximately 546, 552 and 566 eV. The first peak at 538–546 is indicative of lattice oxides (Abu-Zied et al., 2015) and hence the reshaping of this peak indicates a re-coordination in the lattice of the oxides. Figure 4.7 shows that the oxygen K-edge becomes more pronounced at 600°C to the presence of the TiO_2 in the Co_3O_4 lattice, unlike the case at 300°C. This confirms, once more, the analyses of the TEM and SAED results of Figures 4.2 to 4.5.

4.2.3 FTIR results for structural analysis of TiO_2 , Co_3O_4 and $\text{Co}_3\text{O}_4/\text{TiO}_2$ heterojunction structures

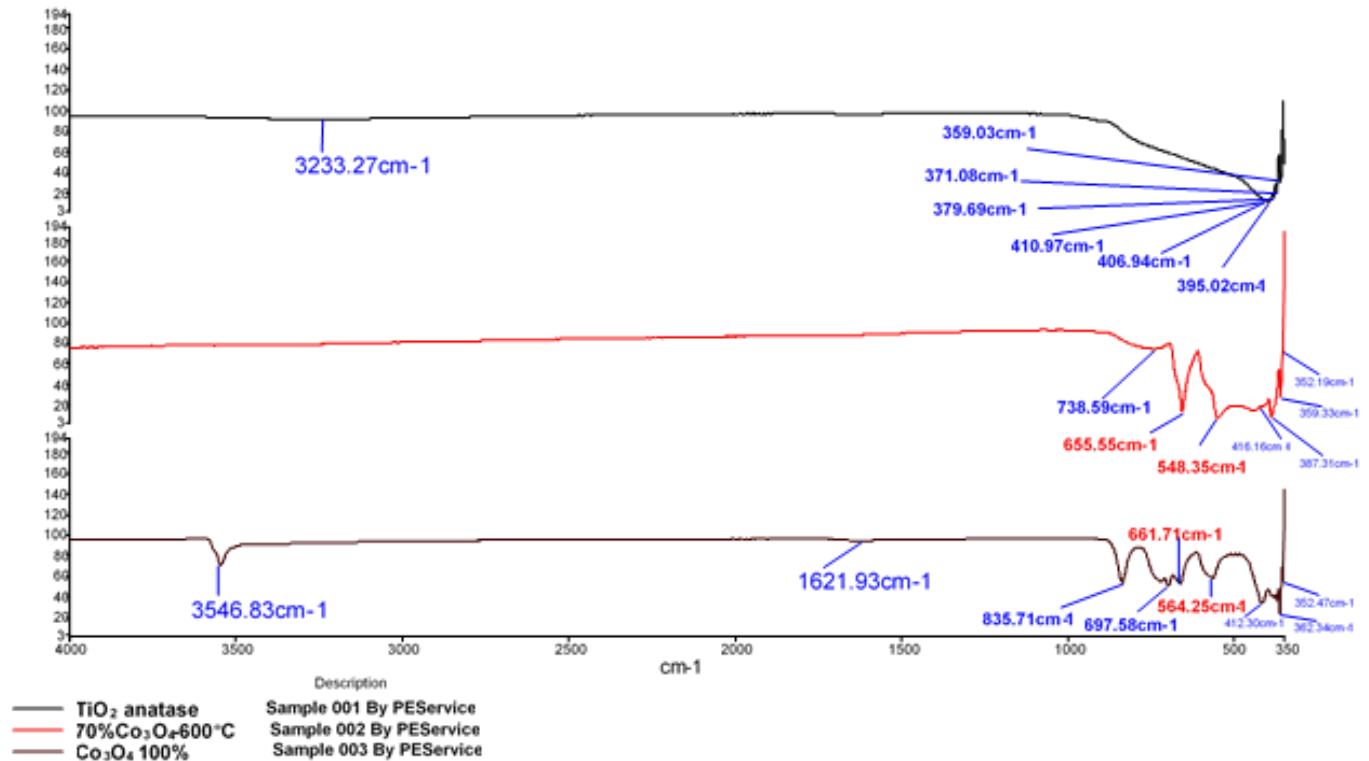


Figure 4.8: FTIR results for structural analysis of TiO_2 , Co_3O_4 and $\text{Co}_3\text{O}_4/\text{TiO}_2$ heterojunction structures

FTIR spectroscopy (Figure 4.8) were used to further evaluate the prepared $\text{Co}_3\text{O}_4/\text{TiO}_2$ composite. The FT-IR Spectrum of TiO_2 and Co_3O_4 (Figures 4.8(a) and (c)) shows two strong characteristic absorptions at 661 and 564 cm^{-1} (highlighted in red) which are attributed to the formation of Co_3O_4 and the absorption bands observed at 3548 cm^{-1} and 1621 cm^{-1} (Figure 4.8(c)) can be attributed to surface adsorbed water and hydroxyl groups.

In the FT-IR spectrum of $\text{Co}_3\text{O}_4\text{-TiO}_2$ composites (Figure 4.8(b)), the corresponding absorption peaks were shown 655cm^{-1} and 548cm^{-1} (highlighted in red) and it can be noticed that the absorption bands were diminished in the composite material. This phenomenon indicates that the TiO_2 not only covered the Co_3O_4 surface but also likely formed a strong interface with it, confirming that the composites were successfully produced. The results also indicate that the numbers of functional groups on the surface of the composite material are less than that of the pristine materials, namely Co_3O_4 and TiO_2 .

4.3 Evaluation of catalytic activity and cobalt leaching of the $\text{Co}_3\text{O}_4/\text{TiO}_2$ heterojunction

4.3.1 Effect of Co_3O_4 loading in the $\text{Co}_3\text{O}_4/\text{TiO}_2$ heterojunction structure

The catalytic activity of $\text{Co}_3\text{O}_4/\text{TiO}_2$ was evaluated on MO using a dark oxidation method; 40 mg/L MO concentration was treated in the presence of 0.2 g/L of PMS and 0.15 g/L of catalyst.

Figure 4.9(a), demonstrates the kinetic curves of heterogeneous PMS activation for the degradation of methyl orange, while using different Co_3O_4 and TiO_2 mole ratio: pristine Co_3O_4 , 98:2 $\text{Co}_3\text{O}_4\text{-TiO}_2\text{-350}$, 95:5 $\text{Co}_3\text{O}_4\text{-TiO}_2\text{-350}$, 90:10 $\text{Co}_3\text{O}_4\text{-TiO}_2\text{-350}$, 85:15 $\text{Co}_3\text{O}_4\text{-TiO}_2\text{-350}$, 70:30 $\text{Co}_3\text{O}_4\text{-TiO}_2\text{-350}$ and 60:40 $\text{Co}_3\text{O}_4\text{-TiO}_2\text{-350}$.

The degradation of MO using PMS alone was also investigated to determine the extent that PMS contributes to the degradation of the dye. It is demonstrated that pure Co_3O_4 has the highest degradation rate of ($k=0.41\text{min}^{-1}$), and degrades 98% of the dye within two minutes of reaction, while PMS on its own was less effective with the lowest degradation rate ($k=0.049\text{min}^{-1}$), only degrading 84% of the dye. This proves that the presence of the catalyst helps with the release of more sulphate radicals from PMS, leading to a faster degradation rate.

Among the composite materials, 60:40Co₃O₄/TiO₂-350 had the highest rate constant for heterogeneous PMS activation in this experimental work. Nevertheless, the difference between the rate constants of the composites materials is not significant, varying between 0.11 and 0.19 (min⁻¹). In any case, the amount of cobalt present in 60:40Co₃O₄-TiO₂-350 is 40% less than that of pristine Co₃O₄, proposing that by introducing TiO₂ as support material, the quantity of cobalt utilized could be diminished while the catalytic activity could be maintained.

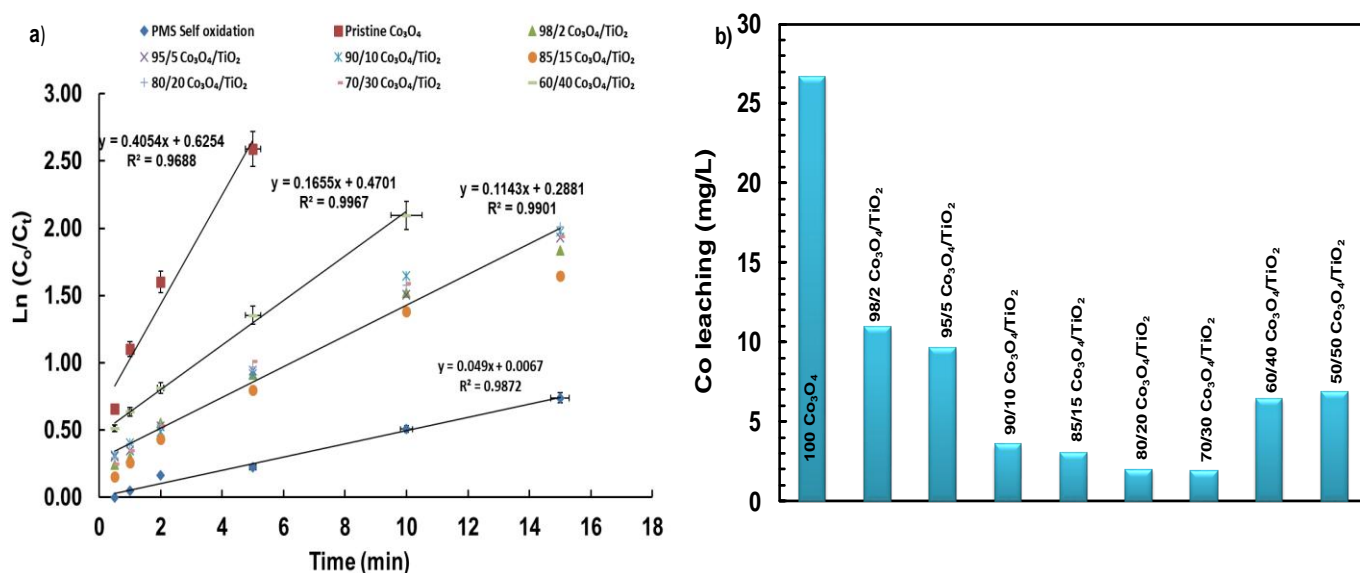


Figure 4.9: Effect of Co₃O₄/TiO₂ ratio on a) degradation kinetics of MO, b) Co leaching

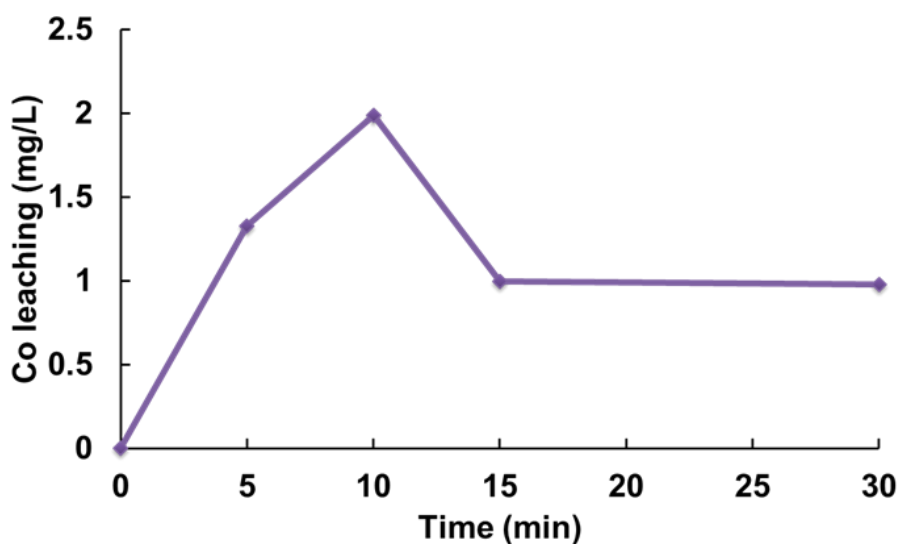
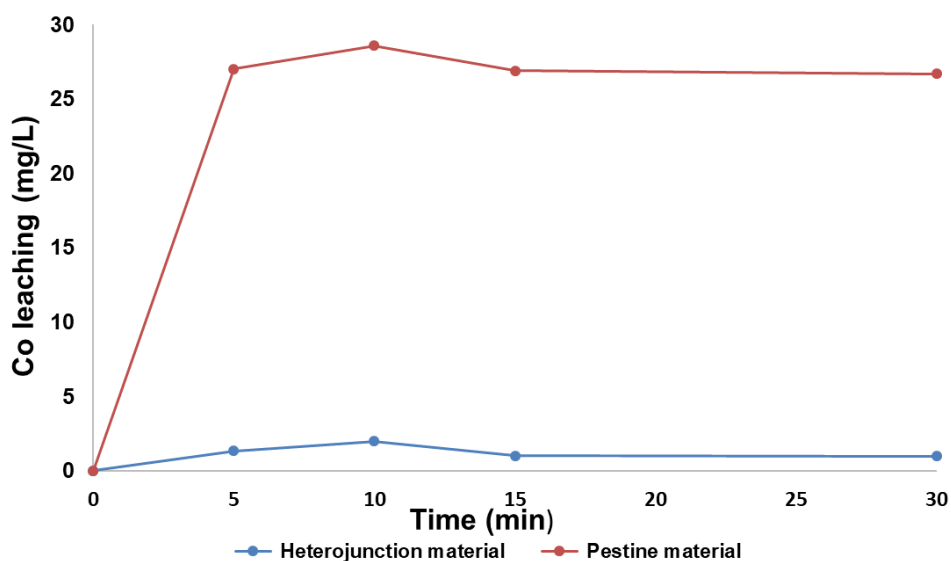


Figure 4.10: Cobalt leaching vs time during PMS activation reaction

The cobalt leaching was also highlighted in the experiments. As shown in Figure 4.9(b), the cobalt leaching for 70:30Co₃O₄-TiO₂-350 and 80:20Co₃O₄-TiO₂-350 were 1.909 mg/L and 1.982 mg/L, respectively, less than that for pure Co₃O₄ (26.7 mg/L) and the lowest amount compared to the other composite catalysts in the same reaction system. The results further confirmed that the strong Co-O-Ti bonds caused by chemically bonding Co₃O₄ on the TiO₂ surface active sites could significantly decrease the cobalt leaching and enhance the catalyst stability.

Figure 4.10 shows how the cobalt leaches into the solution with time: it can be observed that the leaching increased in the first 10 minutes, meaning that many Co ions are leached into the solution but then decreased a bit, staying constant over time, indicating that most of the cobalt ions have been consumed for the reaction.

**Figure 4.11: Comparison between pristine Co₃O₄ and the prepared composite catalyst cobalt leaching**

The effectiveness of the composite material to inhibit cobalt ion leaching as compared to the pristine material can be noticeably identified in Figure 4.11 above where the

cobalt leaching of the pristine material is 26mg/L while that of the composite material is just over 0.9mg/L.

From Figure 4.12(a) it can be seen that the reaction rate of composite material $\text{Co}_3\text{O}_4 / \text{TiO}_2$ is lower than that of the pristine Co_3O_4 but much higher than that of PMS self-oxidation. Figure 4.12(b) reveals that 57% of COD was removed following an hour of catalytic reaction as opposed to 49% of PMS self-oxidation, highlighting the potential of the prepared material in practical wastewater treatment application. Catalytic activity of the Co_3O_4 cubic particles are presented in Figure 4.12(c): control experiments were conducted to differentiate between adsorption of pristine Co_3O_4 and TiO_2 as well as PMS/ TiO_2 and PMS self-oxidation. It is evident from Figure 4.12(c) that the degradation of MO due to adsorption of both Co_3O_4 and TiO_2 is insignificant. Merely 1% MO was removed due to adsorption process. After 30 minutes of PMS/ TiO_2 and PMS self-oxidation, 78% and 76% of MO was degraded, respectively, implying that in the absence of Co_3O_4 catalyst there was not enough reactive species produced for significant MO degradation. A significant 97% of MO was degraded in two minutes of reaction Figure 4.12(d) in the presence of the synthesized pristine Co_3O_4 cubic particles and 0.18g/L of Oxone. This fast degradation of MO highlights the great catalytic PMS activation property of the synthesized Co_3O_4 particles. The MO degradation followed a first order reaction kinetics.

From the ecological perspective, conversion of any organic contaminant, for example, MO is only the initial phase in the ultimate objective, i.e. to accomplish the mineralization of the corresponding solutions. Figure 4.12(d) shows that the MO degradation rate constant for catalysis is significantly higher than the PMS self-oxidation, showing that the catalyst helps in realizing more reactive species. To inhibit cobalt leaching, a composite material was used for the degradation of MO.

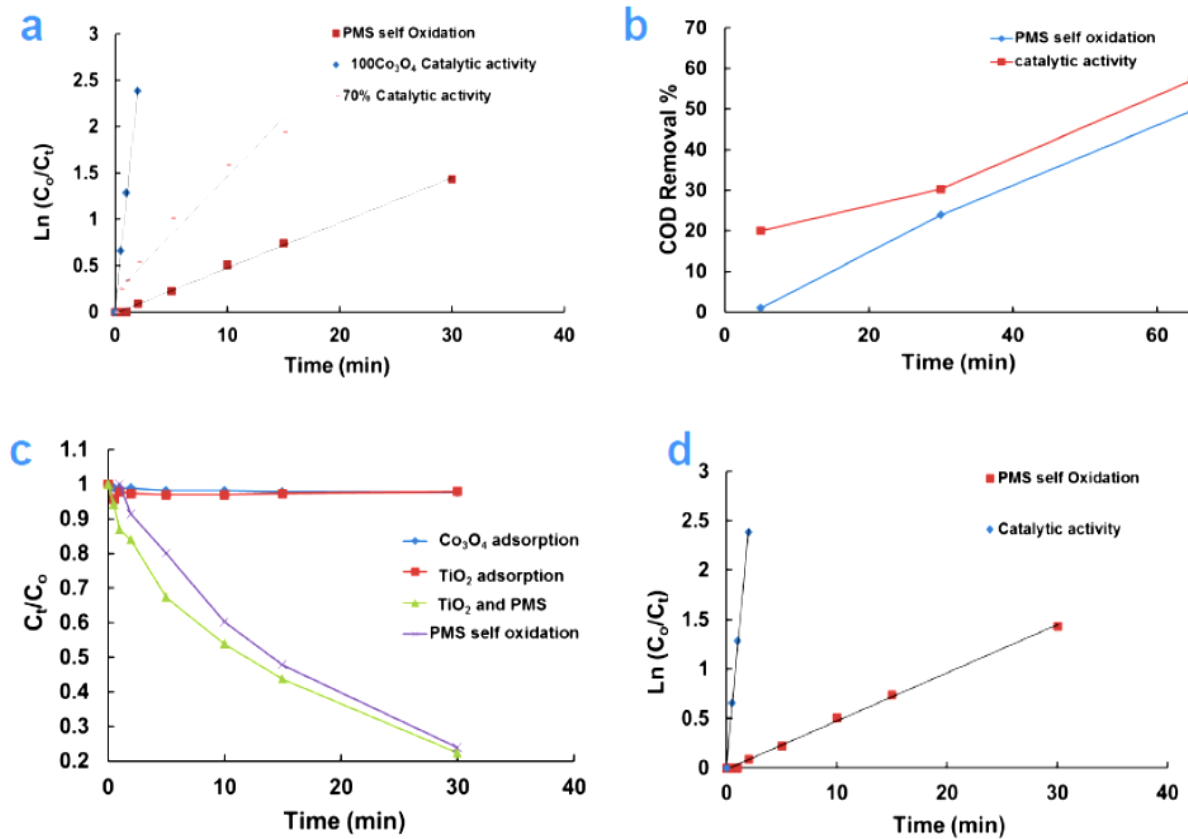


Figure 4.12: (a) MO degradation kinetics; (b) COD removal via catalysis and PMS self-oxidation; (c) MO degradation via various routes; (d) PMS self-oxidation VS catalytic activity kinetics

4.3.2 Effect of calcinations temperature

The 70:30Co₃O₄-TiO₂ composite catalyst, which gave the lowest cobalt leaching among the other heterogeneous catalysts, was calcined at various temperatures to study the effect of calcination temperature on the catalytic activity as well as the cobalt leaching, as presented in Figures 4.13(c) and (d).

It has been determined that with an increase of the calcination temperature, there is a decrease of the catalytic effectiveness of the materials (Figure 4.13(c)) while the cobalt leaching first decreased with the increase of temperature from 350-600°C but increased for the catalyst calcined at 700 °C. Hence, it can be assumed that there is a formation of strong Co-O-Ti bonds in the temperature range of 350-600°C. This is due to the

substitution of Ti^{4+} ions into Co_3O_4 host lattice as was previously confirmed from the ELNEFS study. Hence, a reduction of cobalt leaching was observed for that temperature range. The calcination temperature affects the morphology, atomic composition and crystallite structure of the catalyst, as demonstrated and explained with the TEM images; an increase in calcination temperature also results in a decrease of Co-OH, a decline resulting in a weak catalytic reaction. However, when the calcination temperature is increased above 900°C (data not shown), the CoO present in Co_3O_4 can be reduced to metallic cobalt, which releases Co^{2+} , which can activate PMS directly.

Likewise, high calcination temperature may increase the Co_3O_4 grain size, thereby reducing the contact zone to the surface of TiO_2 support. Therefore, catalysts calcined at higher temperature are susceptible to leaching. Consequently, there was an increase of cobalt leaching when the catalyst was calcined at 700°C . Catalysts (70:30 $\text{Co}_3\text{O}_4/\text{TiO}_2$) synthesized at 600°C exhibited the lowest amount of leaching (0.9 mg/L) and are not used further in this study unless otherwise stated.

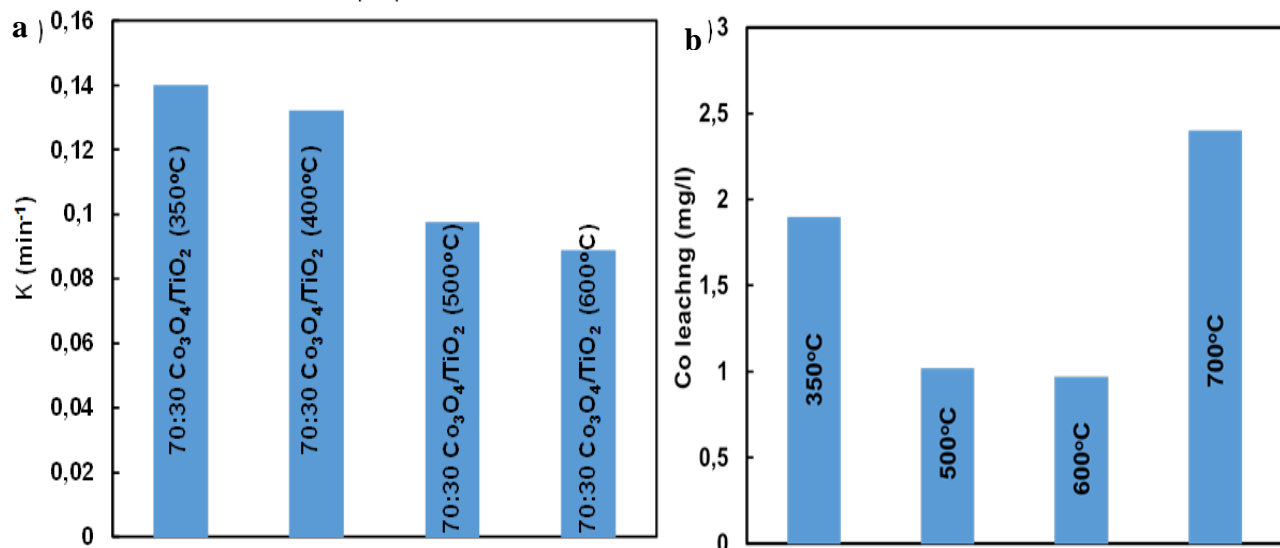


Figure 4.13: Comparison of a) degradation kinetics and b) co leaching for 70:30 $\text{Co}_3\text{O}_4/\text{TiO}_2$ catalysts synthesized at various temperatures (0.03 g/l catalyst load, 0.03 g/l oxone, 40 mg/l MO and 298 K)

4.4 The effect of operational parameters on catalytic performance

4.4.1 Effects of catalyst loading on MO

Catalyst load is a factor that influences the degradation rate of MO; it also affects the number of radical generated and therefore affects the catalytic activity.

Figure 4.14 shows the catalytic efficiency of different catalyst loading, namely, 0.05, 0.1, 0.15, 0.25 and 0.4 g/L. It was observed that the catalytic performance increased with the catalyst loading. The increase in catalyst load from 0.05 to 0.4 g/L brought a substantial increase in the catalytic performance: almost 97% of the dye was degraded in 10 minutes of reaction using 0.4 g/L of catalyst. However, there was no significant change between the catalytic efficiency of 0.05 to 0.15 g/L. Anyway, in both cases within 15 minutes of reaction almost a complete degradation of MO was achieved. As the reaction rates get higher progressively for the catalyst load of 0.05 to 0.4 g/L, it can be deduced that by increasing the catalyst load, the reaction rate also increase.

As stated in the literature, an increase in catalyst load has a positive effect on the degradation of MO: the addition of a larger number of catalysts would increase adsorption sites and provide additional catalyst sites to activate PMS, thereby resulting in a substantial increase in the reaction rate. However, too much catalyst load will result in particle aggregation leading to a reduction in catalyst surface area accessible for absorption and henceforth a drop in the catalytic degradation rate.

Additionally, 0.4 g/L was found to be the optimum catalyst load showing the highest catalytic efficiency for MO degradation. It was used in this study for the evaluation of other process parameter.

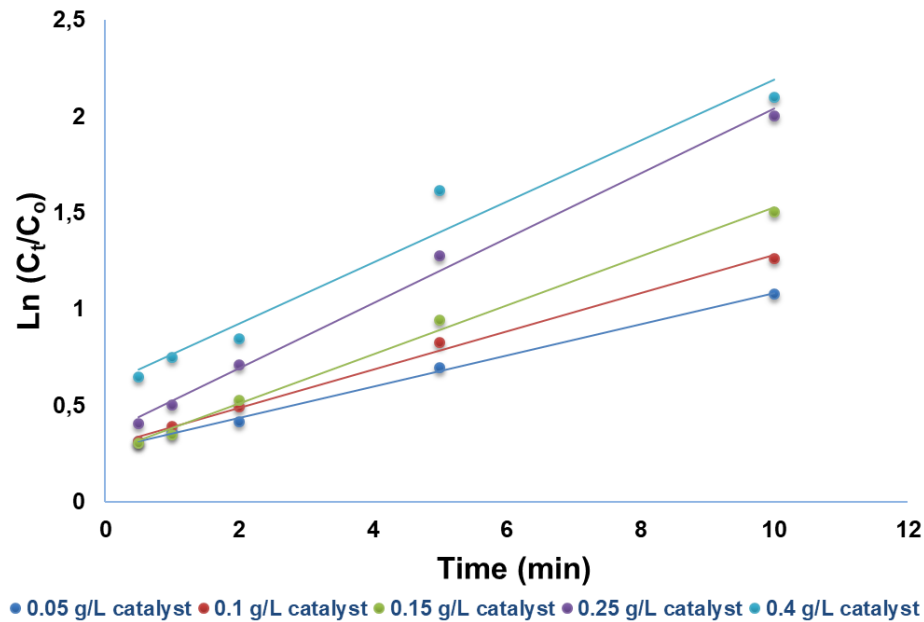


Figure 4.14: Effect of catalyst loading on MO degradation

4.4.2 Effects of PMS loading on MO degradation

MO degradation was enhanced considerably, with an increase in the initial PMS concentration. PMS enhancement of the degradation goes hand to hand with catalyst load, the latter being the factor that encouraged the production of sulphate radicals needed for the degradation of pollutants.

Figure 4.15 demonstrates the degradation performance of various PMS loading. Moreover, it can be seen that with an increase of PMS load from 0.1 to 0.5 g/L there is a significant increase in the catalytic performance and the degradation of MO.

However, an increase in PMS load without the presence of a catalyst to activate the $\text{SO}_4^{\cdot-}$ radical results in a slower degradation rate, indicating that the number of radicals released is smaller without the activation of a catalyst.

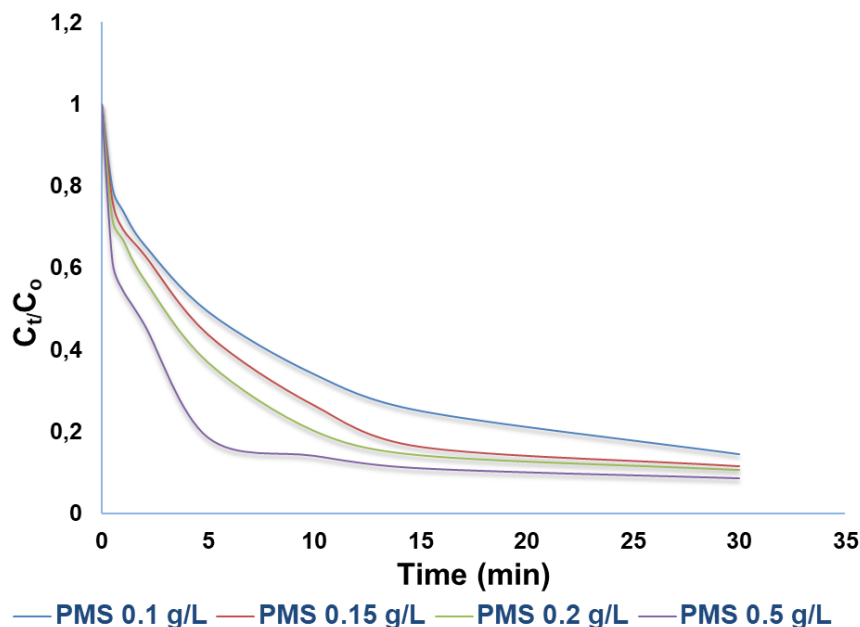


Figure 4.15: Effect of PMS loading on MO degradation

4.4.3 Effect of reaction temperature on the catalytic performance

To calculate the activation energy, the effect of reaction temperature was investigated. Reactions were carried at 20, 25, 30 and 40°C. The degradation of MO increased with increasing reaction to the temperature, a phenomenon due to the rupture of O-O bond and generation of $\text{SO}_4^{\cdot-}$ (Deng *et al.*, 2017; Shi *et al.*, 2012).

A higher reaction temperature also translates to lower activation energy barrier. The activation energy (E_a), which indicates the ease at which a reaction occurs, can be calculated with the Arrhenius equation. According to the relationship between the pseudo constants and reaction temperature in Figure 4.16, the activation energy for MO degradation was found to be $54.645 \text{ kJ mol}^{-1}$, which is in the range of chemical reactions and not adsorption. This value is not the same with the activation energy of diffusion-controlled reactions, which typically ranges from 10 to 13 kJ mol^{-1} .

In heterogeneous catalytic oxidation, when the E_a value is significantly higher than that of diffusion-controlled reaction (10– 13 kJ mol^{-1}), it is demonstrating that reaction rate of

the oxidation process is more reliant on the rate of intrinsic chemical reactions on the surface of the heterogeneous catalyst as opposed to the rate of mass transfer.

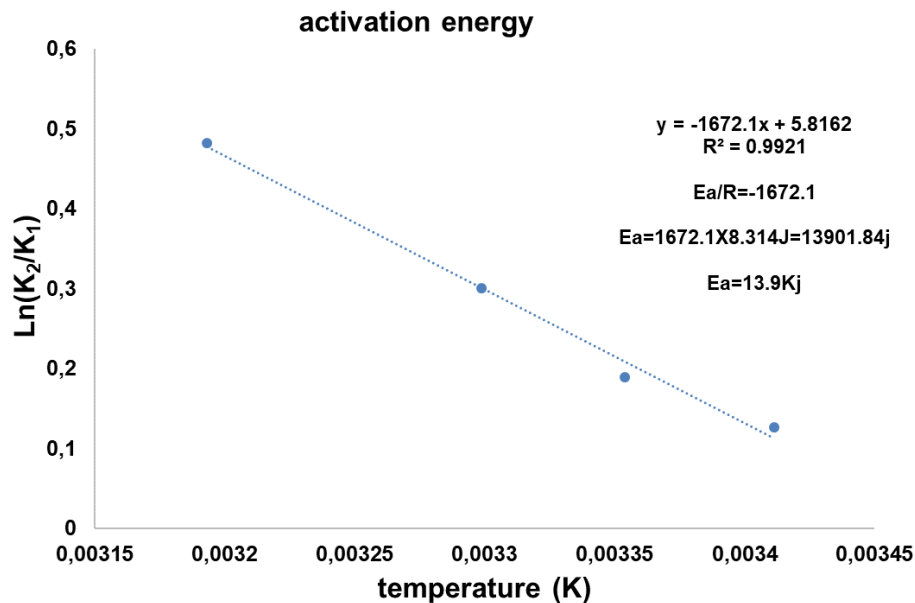


Figure 4.16: Activation energy from reaction temperature study

4.4.4 Effect of dye concentration on the degradation rate

The effect of dye concentration on the catalytic activity of the catalyst was studied. Figure 4.17 reveals that the concentration was varied from 200ppm to 20ppm. Using the catalyst and PMS loading of 0.15 g/l and 0.18g/l, respectively, the rate constant is slower with an increase in dye concentration (Figure 4.17) which means that the dye concentration is a limiting step in the $\text{Co}_3\text{O}_4/\text{TiO}_2$ -PMS oxidation; the degradation was found to follow first-order kinetics.

The decrease in catalytic activity at high dye concentrations is because as the concentration of the dye increases, the number of molecules of the dye to be adsorbed on the surface of the catalyst also increases. Consequently, the reactive species ($\text{SO}_4^{\cdot-}$) necessary for the degradation of the toxin increases as well. While the number of $\text{SO}_4^{\cdot-}$ radicals formed on the catalyst surface remains steady for a certain catalyst number and degradation time, if the dye concentration is increased for that given reaction, the available number of $\text{SO}_4^{\cdot-}$ radicals are insufficient for effective dye degradation.

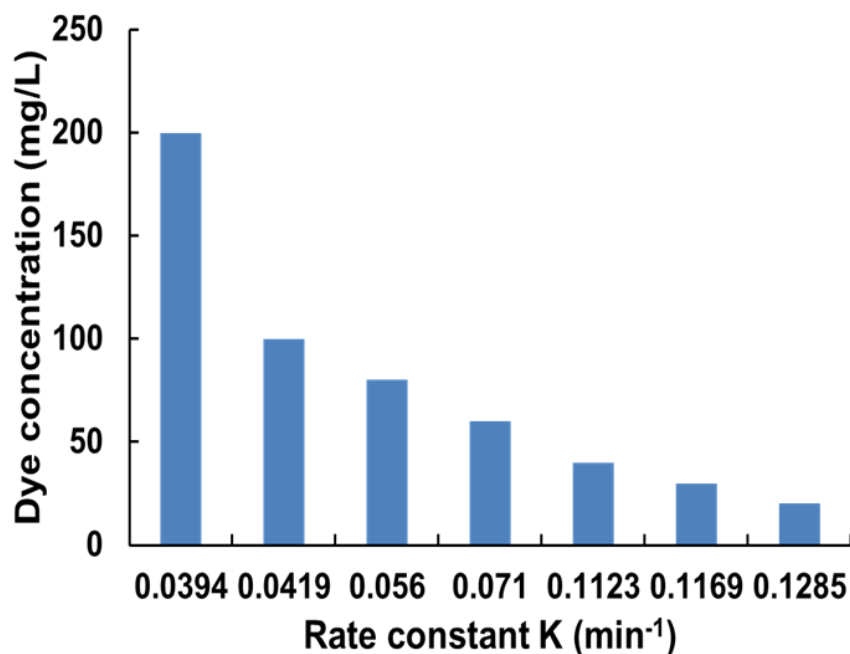


Figure 4.17: Effect of dye concentration on the rate constant

4.4.5 Comparison between $\text{Co}_3\text{O}_4/\text{TiO}_2$ heterojunction and various studies

Advantaged of the prepared catalyst

- ✓ The catalyst was synthesised using, organic binder mediated route, which is cost effective, and green method compared to the methods used in the literature.
- ✓ The cobalt leaching of the prepared catalyst was extensively studied providing more literature on the topic, which is a crucial element that is lacking in previous literature where studies mostly focused on improving the stability and the rate of reaction of the catalyst and not on the leaching.
- ✓ The cobalt leaching was reduced by 97%

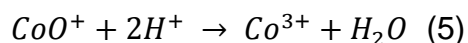
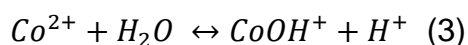
Table 4.1: Previous studies conducted on combined Co_3O_4 with various catalyst supports

Support material	Preparation method	Cobalt level,%	Degradation of organics	Performance	References
Al ₂ O ₃ , SiO ₂ , TiO ₂	Incipient wetness impregnation	9.06 wt	2,4-DCP	Interaction strength Co/TiO ₂ >Co/Al ₂ O ₃ >Co/SiO ₂ . Co leaching not mentioned	(Yang <i>et al.</i> , 2008)
Degussa P25-TiO ₂	Incipient wetness impregnation	9.06 wt	2,4-DCP	75% 2,4-DCP degradation in 2 h, with 36 µgL ⁻¹ Co leaching	(Yang <i>et al.</i> , 2007)
MgO	As above	5 wt	Methylene bleu (MB)	Complete oxidation of MB in 7 min with 0.4 mgL ⁻¹ cobalt leaching	(Zhang <i>et al.</i> , 2010)
MgO	As above	5 wt	AO7	Complete degradation of 50 mgL ⁻¹ AO7 in 10 min. Co leaching not mentioned	(Stoyanova <i>et al.</i> , 2014)
Al ₂ O ₃ , SiO ₂ , TiO ₂	Solution combustion	0.4-0.5 wt	phenol	Complete degradation of phenol on Co/TiO ₂ , Co/Al ₂ O ₃ and Co/SiO ₂ in 50, 120 and 150 min, respectively. Co leaching not mentioned	(Liang <i>et al.</i> , 2012b)
α -MnO ₂	impregnation	3 wt	Phenol	Complete oxidation of phenol on Co ₃ O ₄ /MnO ₂ , Co ²⁺ and MnO ₂ in 20, 30 and 60 min, respectively. Co leaching not mentioned	(Liang <i>et al.</i> , 2012a)
TiO ₂	hydrolysis	0.1 mol%	Red-3BS	Complete degradation of Red-3BS in 60 min with (145.8 mg L ⁻¹) cobalt leaching	(Zhu <i>et al.</i> , 2013)

Bi ₂ O ₃	Reverse co-precipitation and post-calcination	1.08:1 molar ratio	Methylene blue (MB), Rhodamine B, Phenol and 2,4-dichlorophenol	Complete degradation of MB (20 mmol L ⁻¹) with 0.36 min ⁻¹ reaction rate and 43 µg L ⁻¹ cobalt leaching	(Ding <i>et al.</i> , 2012)
Graphene sheets	Not specified	Not specified	Orange II	Complete degradation of Orange II, within 1 hour. With 0.10 mg L ⁻¹ cobalt leaching	(Yao <i>et al.</i> , 2013)
carbon microspheres	one-pot hydrothermal method		phenol	Complete degradation of phenol within 15 min Co leaching not mentioned	(Zhou <i>et al.</i> , 2015)
TiO ₂ anatase	Organic binder	70 mol%	methyl orange	Complete degradation of methyl orange within 15 min with 0.9 mg L ⁻¹ cobalt leaching	Our study

4.5 Comparison between homogeneous and heterogeneous catalytic oxidation

Homogeneous experiments using dissolved cobalt concentrations equal to that leached from $\text{Co}_3\text{O}_4/\text{TiO}_2$ heterojunction were performed with the objective of comparing the homogeneous Co/Oxone reagent with the $\text{Co}_3\text{O}_4/\text{TiO}_2/\text{Oxone}$. Homogeneous activation of PMS for MO degradation was studied, using a Co concentration of 1.9 mg L^{-1} , the same amount that was leached from the heterogeneous reaction in solution. It can be seen from Figure 4.18 that the heterogeneous catalysis is more effective than the homogeneous catalysis even though the amount of cobalt present into the solution was the same. This highlights the excellent catalytic properties of the prepared Cubic Co_3O_4 material showing that it is not the cobalt present into the solution that aids the oxidation process but it is the catalyst itself that helps release more reactive species from Oxone. The TEM analysis earlier showed that the TiO_2 does not exist as individual nanoparticles, but rather as possible dopant in the Co_3O_4 matrix or forming a $\text{TiO}_2:\text{Co}_3\text{O}_4$ 'alloy' or hybrid material. Confirmation of $\text{Co}-\text{OH}$ bonding was indicated in the FTIR analysis of the particles as discussed in previous section (Figure 4.8). Formation of surface hydroxyl groups, or $\text{Co}-\text{OH}$ bonds, are critical for the catalytic activation of PMS, as the radical generation is dependent on the CoOH^+ formation as shown in the Equations (3)–(5), thereby highlighting, once more, the potential of the composite catalyst:



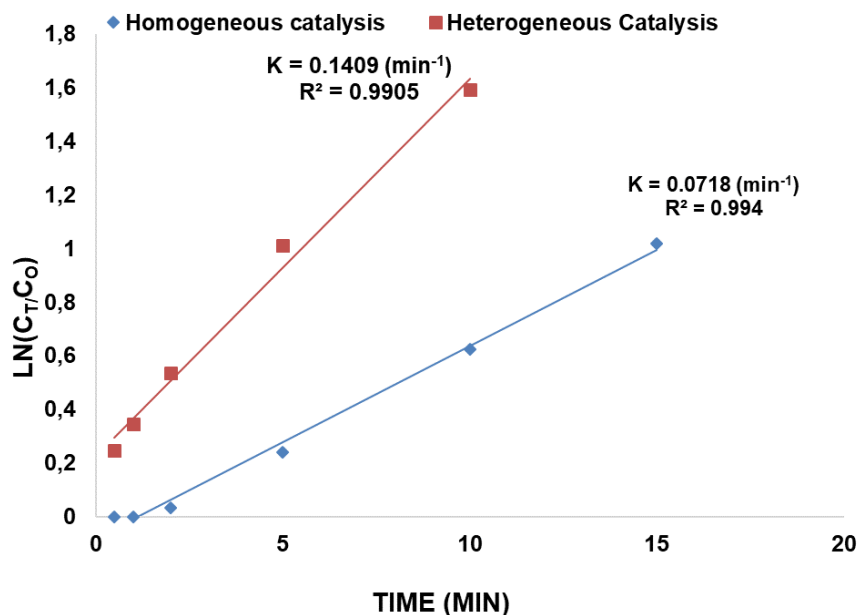


Figure 4:18: Comparison between homogeneous and heterogeneous PMS activation

4.6 Determination of reactive species (radical)

It is widely accepted in the literature that alcohols with an alpha hydrogen such as ethanol readily react with both $\bullet\text{OH}$ and $\text{SO}_4^{\bullet-}$ radicals. Alcohols without an alpha hydrogen, such as tert-butyl alcohol (TBA), are also readily reactive toward $\bullet\text{OH}$, but their reaction with $\text{SO}_4^{\bullet-}$ is over 1000-fold slower. Thus, ethanol and TBA were usually used to differentiate $\text{SO}_4^{\bullet-}$ from $\bullet\text{OH}$.

Therefore, in this study, ter-butanol (TBA) and ethanol (EtOH) were added as an SR and OH scavenger, individually, to check for the generation of both HR and SR radicals. Figure 4.19 demonstrates that the addition of TBA did not decrease the reaction rate constant significantly; on the other hand, the addition of EtOH reduced the rate constant significantly due to the quenching of generated SR. This is because TBA only quenches HR radicals and not SR, while EtOH quenches SR radicals.

Therefore, it can be concluded that in Co_3O_4 catalyzed PMS activation reaction, the generation of sulphate radicals (SR) by catalytic decomposition of PMS in

heterogeneous systems was the main reactive species for oxidation of organic contaminants, meaning SR is the dominant reactive species produced.

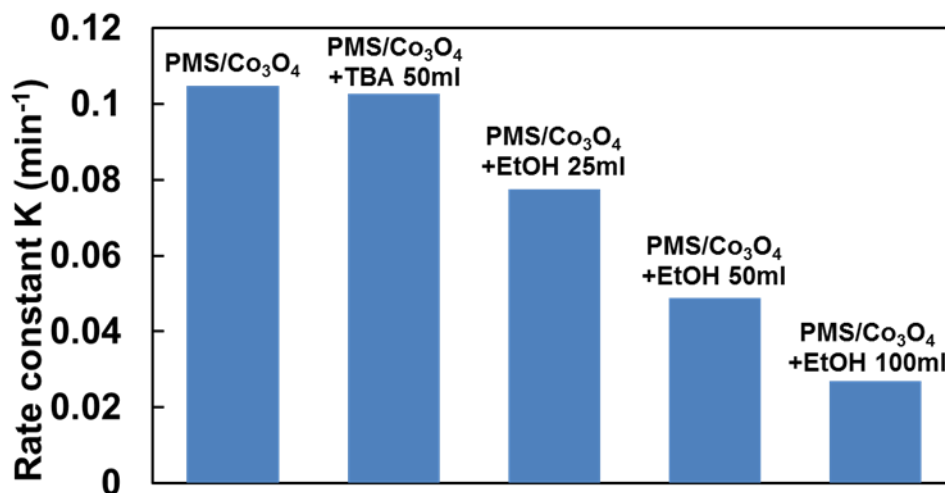


Figure 4.19: Effects of quenching reagents on MO degradation rate constants

4.7 Application of Co₃O₄/TiO₂ heterojunction for the treatment of commercial dyes

A mixture of three different dyes was prepared as a synthetic dye bath, namely methyl orange, golden yellow and methyl red. This was done to assess the potential uses of the composite material in treating real industrial effluent.

It can be seen from Figure 4.21 that the Co₃O₄/TiO₂ heterojunction catalyst effectively degraded the commercial dyes. After 30 minutes of reaction, a degradation of 95% was achieved for MO, 89% for MR and 86% for GY (inset Figure 4.20), showing the different rates of reaction. This demonstrates that the degradation of commercial complex dyes followed the first order reaction and MO has the highest rate constant, followed by MR and GY, respectively. The synthetic dye bath became colourless after 60 minutes of reaction (Figure 4.21), exhibiting Co₃O₄/TiO₂ material potential to be used as a heterogeneous catalyst for PMS activation to effectively treat industrial effluent.

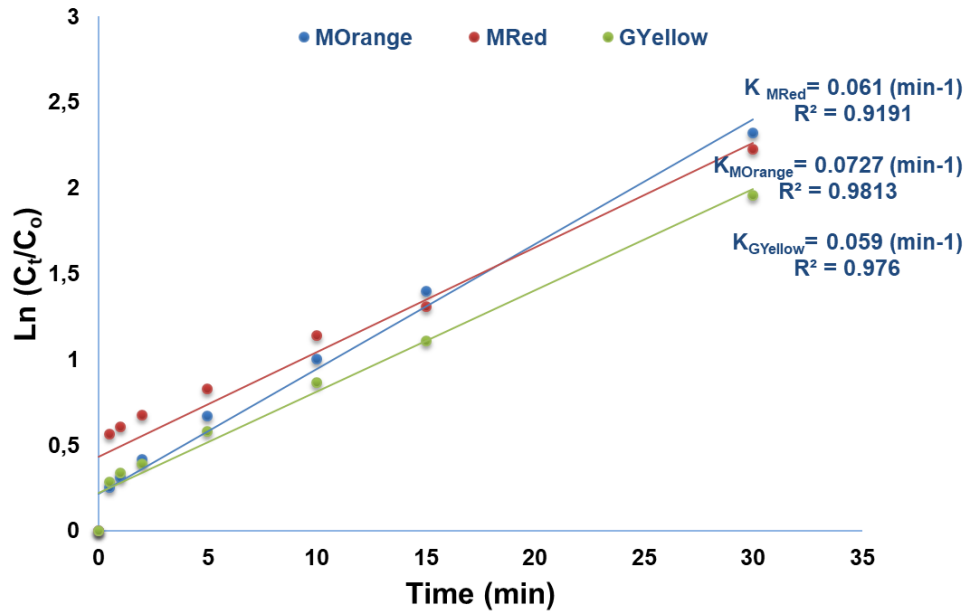


Figure 4.20: Mixed dyes study and degradation rate constant of each individual dye



Figure 4.21: Visible degradation of the mixed dyes batch over time

4.8 Catalyst recyclability and efficiency after four runs

Recyclability of a catalyst is essential both from a practical and economical perspectives. The heterojunction catalyst was promptly recycled by centrifuging from the solution, and then used in another batch for experimentation without prior drying or calcination. Figure 4.22 shows that the $\text{Co}_3\text{O}_4/\text{TiO}_2$ catalyst maintains a high catalytic

performance for all recycling stages. The catalyst was recycled up to four times without any significant loss of catalytic efficiency (Figure 4.22). After the fourth cycle, 90% degradation was attained in contrast to 95% in the first cycle after 60 minutes of reaction time. This reduction in catalytic activity can be credited to the minor loss of the material during the sample centrifugation stage.

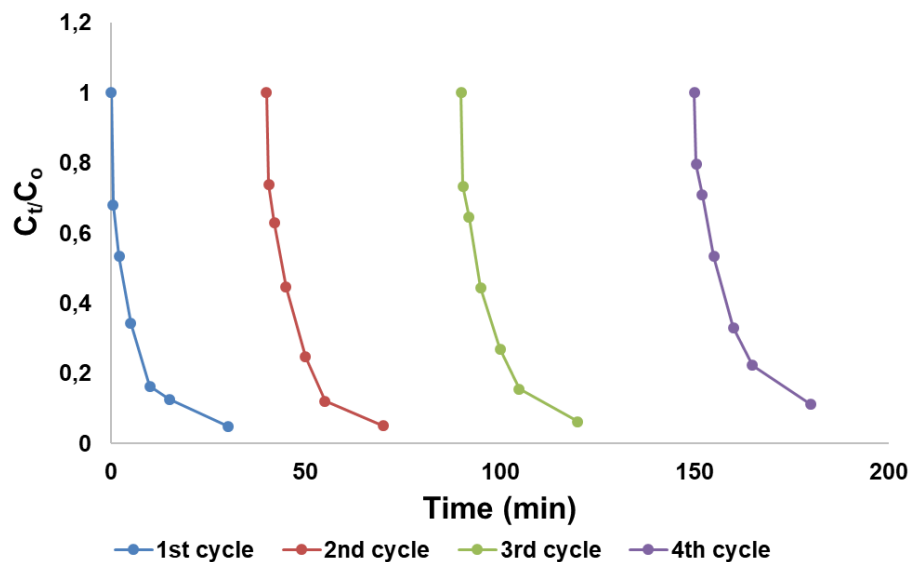


Figure 4.22: Catalyst recyclability and efficiency after four runs

4.9 Conclusion

TiO₂ nanoparticles were used as support material for Co₃O₄ to form a rod shaped Co₃O₄/TiO₂ heterojunction catalyst using an organic binder mediated route instead of wet impregnation method. This was done in order to reduce the cobalt leaching that usually results for cobalt based catalyst since the toxicity of cobalt is a major concern in wastewater treatment.

MO was utilized as a pollutant to evaluate the catalytic activity of the synthesized catalyst. Various ratios of Co₃O₄/TiO₂ were used: the 70% Co₃O₄/TiO₂ shows the lowest cobalt leaching, complete degradation just under 15 minutes of reaction of 40mg/L MO

was achieved in a solution of 200mL, containing 0.18g/l of PMS and 0.15g/L of $\text{Co}_3\text{O}_4/\text{TiO}_2$ using a dark oxidation method at ambient temperature.

As the COD removal was found to be 57% just after 60 minutes of catalytic reaction, the synthesized catalyst offers a significant reusability potential by centrifuging it back from the treated solution and using it in another experiment. For up to four recycling stages, the catalyst still showed a high catalytic performance, with only a minor decline in the fourth stage due to some particle loss during the centrifuging stage.

As the synthesized catalyst reduced the cobalt leaching up to 97% as compare to the pristine material, it can be concluded that Co_3O_4 supported TiO_2 catalyst successfully inhibited cobalt leaching while maintaining a good catalytic activity for the degradation of MO and other commercial dyes.

CHAPTER 5: SUMMARY OF RESULTS AND CONCLUSION

5.1 Introduction

This study presented a work on the degradation of an azo dye (MO) using an advanced oxidation process utilizing PMS and $\text{Co}_3\text{O}_4/\text{TiO}_2$ heterojunction as a heterogeneous catalyst. Various researchers have reported the use of Co_3O_4 on various support materials for the degradation of recalcitrant and harmful organic contaminants with the aim of decreasing cobalt ions leaching (Anipsitakis *et al.*, 2005; Chen *et al.*, 2008; Yang *et al.*, 2008; Wang *et al.*, 2014; Muhammad *et al.*, 2012; Liang *et al.*, 2012). Regardless of some encouraging results on enhancing the catalytic activity and decreasing cobalt leaching, it is yet an incredible challenge to make the heterogeneous PMS activation innovation industrially practical (Hu *et al.*, 2013).

Therefore, an organic mediated route was used to synthesize the $\text{Co}_3\text{O}_4/\text{TiO}_2$ heterojunction, reducing the costs associated with the other production methods such as impregnation, hydrothermal processes and so on.

The objectives of this study were to synthesize and evaluate the catalytic efficiency of a heterogeneous catalyst using cobalt oxide and TiO_2 as a support, used for the degradation of azo dyes and potentially used in real textile wastewater effluent, with the end goal of minimizing cobalt leaching. This is a serious issue in catalysts of this nature. Moreover, there was a point-by-point study on the major operating parameters as well as the evaluation of catalyst reusability.

5.2 Summary

A $\text{Co}_3\text{O}_4/\text{TiO}_2$ composite catalyst was successfully synthesized using Co_3O_4 nanoparticles anchored on TiO_2 via an organic binder mediated route-using maleic acid as the organic binder. The results demonstrate that the composite catalyst has a rod-like structure composed of individual nanoparticles. The EDS results showed that at 600°C the TiO_2 does not exist as individual nanoparticles, but rather as possible dopant in the Co_3O_4 matrix or forming a $\text{TiO}_2:\text{Co}_3\text{O}_4$ 'alloy' or hybrid material.

Different mol% ratio were produced – namely 98%, 95%, 90%, 85%, 80% and 70% $\text{Co}_3\text{O}_4/\text{TiO}_2$ – with the catalytic activities evaluated on the degradation of MO as well as the degree of cobalt leaching. The results showed that chemically binding Co_3O_4 with TiO_2 reduced cobalt leaching by 97% as compared to the pristine materials by ensuring strong Co-O-Ti bonds while maintaining a satisfactory catalytic activity. Moreover, 70:30 $\text{Co}_3\text{O}_4/\text{TiO}_2$ showed the lowest cobalt leaching than the rest of the composite materials prepared. In addition, $\text{Co}_3\text{O}_4/\text{TiO}_2$ activated PMS and encouraged the development of surface Co–OH complexes, enhancing the formation of both sulphate and hydroxyl radical leading to higher catalytic efficiency. The addition of the composite catalyst to the PMS showed a degradation rate of 0.1257m^{-1} , whereas the PMS has a degradation rate of 0.0487m^{-1} on its own without the addition of the composite catalyst for the same degradation time.

Different operating parameters and their effect on the catalytic activity of the $\text{Co}_3\text{O}_4/\text{TiO}_2$ were discussed, namely initial dye concentration, PMS concentration, catalyst load, reaction temperature and the dye concentration. The optimum conditions (value) were chosen for the initial dye concentration and PMS concentration as well as catalyst load. An increase in temperature showed an increase in the catalytic efficiency. Complete degradation of MO was achieved within 10 minutes of adsorption time under these optimum operating parameters.

The catalyst was also tested on a synthetic dye bath containing methyl red, methyl orange and golden yellow and was found to be effective in the degradation of these commercial dyes. In addition, complete colour removal and 95, 89 and 86% degradation for MO, MR and GY, respectively, were achieved.

Since colour removal is a crucial step from an environmental point of view, the effectiveness of the catalyst to decolourized wastewater confirmed its feasibility in treating industrial wastewater. In addition, the novel heterojunction catalyst

demonstrated a high effectiveness for the mineralization of MO. It was found that 67% of the initial COD from the MO solution was removed within 30 minutes of reaction time. The centrifugation process achieved the recycling of $\text{Co}_3\text{O}_4/\text{TiO}_2$ easily, with the material showing good recycling ability over four cycles without significant loss of its catalytic activity, suggesting that the catalyst is effective from both a practical and economic point of view.

5.3 Conclusion

A heterogeneous catalyst ($\text{Co}_3\text{O}_4/\text{TiO}_2$ heterojunction structure) has been successfully synthesized. Its catalytic activity was evaluated by MO degradation. The prepared catalyst showed enhanced catalytic performance for the degradation of MO and commercial dye bath.

5.4 Contribution

This research produced a $\text{Co}_3\text{O}_4/\text{TiO}_2$ heterojunction catalyst using a cost effective method (organic binder mediated route) as compared to the generally utilized method. Its catalytic efficiency, evaluated for various dyes, was found to be effective for complete colour removal, making it applicable in real textile wastewater treatment. The catalyst produced greatly inhibited cobalt leaching which is a great concern in PMS system using cobalt. Additionally, the study provided information on fundamental parameters for the treatment of wastewater.

5.5 Recommendations

This research focused on the development and catalytic performance of the $\text{Co}_3\text{O}_4/\text{TiO}_2$ heterojunction structure in PMS systems in order to inhibit cobalt leaching and increase the stability of Co_3O_4 . However, it is clear that additional research work is necessary:

- scaling up of the lab scale reactor to a larger volume;
- toxicity studies of the produced material and products formed after the degradation of the dyes; and
- usage of other organic binders, such as glucose.

REFERENCES

- Abu-Zied, B.M., Bawaked, S.M., Kosa, S.A. & Schwieger, W. 2015. Effect of microwave power on the thermal genesis of Co₃O₄ nanoparticles from cobalt oxalate micro-rods. *Applied Surface Science*, 351: 600–609.
- Adesina. 2004. Industrial exploitation of photocatalysis: progress, perspectives and prospects. *Catalysis Surveys from Asia*, 8(4): 265–273.
- Adschiri, T., Hakuta, Y. & Arai, K. 2000. Hydrothermal synthesis of metal oxide fine particles at supercritical conditions. *Industrial & Engineering Chemistry Research*, 39: 4901–4907.
- Adschiri, T., Hakuta, Y., Sue, K. & Arai, K. 2000a. Hydrothermal synthesis of metal oxide nanoparticles at supercritical conditions. *Journal of Nanoparticle Research*, 3: 227–235.
- Agustina, T.E., Ang, H.M. & Vareek, V.K. 2005. A review of synergistic effect of photocatalysis and ozonation on wastewater treatment. *Journal of Photochemistry and Photobiology C*, 6: 264–273.
- Ahmed, M., Barbati, S., Doumenq, P. & Chiron, S. 2012. Sulfate radical anion oxidation of diclofenac and sulfaméthoxazole for water decontamination. *Chemical Engineering Journal*, 197: 440–447.
- Ahmed, M.M., Brienza, M., Goetz, V. & Chiron, S. 2014. Solar photo-Fenton using peroxymonosulfate for organic micropollutants removal from domestic wastewater: Comparison with heterogeneous TiO₂ photocatalysis. *Chemosphere*, 117: 256–261.
- Ahmed, S., Rasul, M.G., Brown, R. & Hashib, M.A. 2011. Influence of parameters on the heterogeneous photocatalytic degradation of pesticides and phenolic contaminants in wastewater: A short review. *Journal of Environmental Management*, 92: 311–330.
- Ahn, C.C. 2004. Transmission electron energy loss spectrometry in material science and the EELS Atlas. *Wiley, Weinheim, Germany*: 4.
- Anipsitakis, G.P. & Dionysiou, D.D. 2003. Degradation of organic contaminants in water with sulfate radicals generated by the conjunction of peroxymonosulfate with cobalt. *Environmental science & technology*, 37: 4790–4797.
- Anipsitakis, G.P. & Dionysiou, D.D. 2004. Radical Generation by the Interaction of Transition Metals with Common Oxidants. *Environmental Science & Technology*, 38(13): 3705–3712.
- Anipsitakis, G.P., Stathatos, E. & Dionysiou, D.D. 2005. Heterogeneous activation of oxone using Co₃O₄. *The Journal of Physical Chemistry B*, 109(27): 13052–13055.

- Arslan, I. & Balcioglu, H.Q. 2001. Degradation of Remazol Black B Dye and Its Simulated Dyebath Wastewater by Advanced Oxidation Processes in Heterogeneous and Homogeneous Media. *Color Technology*, 117: 38.
- Arslan-Alaton, I. & Ferry, J.L. 2002. Application of polyoxotungstates as environmental catalysts: wet air oxidation of acid dye Orange II. *Dyes and Pigments*, 54(1): 25–36.
- Ashtekar, V.S., Bhandari, V.M., Shirsath, S.R., Sai Chandra, P.L.V.N., Jolhe, P.D. & Ghodke, S.A. 2013. Dye wastewater treatment: removal of reactive dyes using inorganic and organic coagulants. *Journal of Industrial Pollution Control*: 3–6.
- Atkins, P. & De Paula, J. 2006. *Atkins' physical chemistry*. Oxford University Press. Oxford.
- Austin, R. & Lim, S.F. 2008. The Sackler Colloquium on Pormoses and Perils in Nanotechnology for Medicine. *PNAS*, 45: 17217–17221.
- Aziz, H.A., Aliaz, S., Adian, M.N., Faridah, Assari, A.H. & Zahari, M.S. 2007. Color removal from land fill leachate by coagulation and flocculation processes. *Bioresource Technology*, 98: 218–220.
- Bagheri, S., Muhd Julkapli, N. & Bee Abd Hamid, S. 2014. Titanium dioxide as a catalyst support in heterogeneous catalysis. *The Scientific World Journal*, 2014. <https://www.hindawi.com/journals/tswj/2014/727496/abs/> 6 August 2017.
- Bahnemann, W., Muneer, M. & Haque, M.M. 2007. Titanium dioxide-mediated photocatalysed degradation of few selected organic pollutants in aqueous suspensions. *Catalysis Today*, 124: 133–148.
- Balandin, A.A. 1958. nature of active centers and the kinetics of catalytic dehydrogenation. *Advanced Catalysis*, 10: 96–121.
- Bamwenda, G.R., Tsubota, S., Nakamura, T. & Haruta, M. 1997. The influence of the preparation methods on the catalytic activity of platinum and gold supported on TiO₂ for CO oxidation. *Catalysis Letters*, 44(1–2): 83–87.
- Barth, A. 2007. Infrared spectroscopy of proteins. *Biochim Biophys. Acta*, 1767: 1073–1101.
- Basava Rao, V.V. & Maohan Rao, S.R. 2006. Adsorption studies on treatment of textile dyeing industrial effluent by fly ash. *Chemical Engineering Journal*, 116: 77–84.
- Baughman, G.L. & Weber, E.J. 1994. Transformation of Dyes and Related Compounds in Anoxic Sediment: Kinetics and Products. *Environmental Science & Technology*, 28(2): 267.
- Beltran, F.J. 2003. Ozone-UV Radiation-Hydrogen Peroxide Oxidation Technologies. In *Chemical Degradation Methods for Wastes and Pollutants, Environmental and Industrial Applications*. Marcel Dekker, Inc.:

- Berthomieu, C. & Hienerwadel, R. 2009. Fourier transform infrared (FTIR) spectroscopy. *Photosynthesis research*, 101(2–3): 157–170.
- Bezemer, G.L., Bitter, J.H., Kuipers, H., Oosterbeek, H., Holewijn, J.E., Xu, X.D., Kapteijn, F., Van Dillen, A.J. & de Jong, K.P. 2006. Cobalt particle size effects in the Fischer–Tropsch reaction studied with carbon nanofiber supported catalysts. *Journal of the American Chemical Society*, 128: 3956–3964.
- Bond, G.C. 1974. *Heterogeneous Catalysis: Principles and Applications*. Oxford University Press.
- Boudart, M. 1969. Catalysis by supported metals. *Advanced Catalysis*, 20: 153–167.
- Bruce, P.G., Scrosati, B. & Tarascon, J.M. 2008. Nanomaterials for rechargeable lithium batteries. *Angewandte Chemie*, 47: 2930–2946.
- Brydson, R. & Thomas, J.M. 1987. Electron energy-loss spectroscopy (EELS) and the electronic structure of titanium dioxide. *Solid State Communications*, 64: 609–612.
- Cabo, B.R., Palmeiro, I.R., Rodil, R., Rodil, E., Arce, A. & Soto, A. 2015. Synthesis of AgCl nanoparticles in ionic liquid and their application in photodegradation of Orange II. *Materials Science*, 50: 3576.
- Cai, J., Xin, W., Liu, G., Lin, D. & Zhu, D. 2016. Effect of calcination temperature on structural properties and photocatalytic activity of Mn-C-codoped TiO₂. *Materials Research*, 19(2): 401–407.
- Catillo, S., Ansart, F., Laberty-Robert, C. & Portal, J. 2002. *Journal of Power Sources*, 112: 247.
- Chan, K. & Chu, W. 2009. Degradation of atrazine by cobalt-mediated activation of peroxymonosulfate: Different cobalt counter anions in homogenous process and cobalt oxide catalysts in photolytic heterogeneous process. *Water Research Journal*, 43(8): 2513–2521.
- Chen, M.M., Sun, X., Qiao, Z.J., MA, Q. & Wang, C.Y. 2014. Anatase-TiO₂ nanocoating of Li₄Ti₅O₁₂ nanorod anode for lithium-ion batteries. *Journal of Alloys and Compounds*, 601: 38–42.
- Chen, X., Chen, J., Qiao, X., Wang, D. & Cai, X. 2008. Performance of nano-Co₃O₄/peroxymonosulfate system: kinetics and mechanism study using Acid Orange 7 as a model compound. *Applied Catalysis B: Environmental*, 80(1): 116–121.
- Cheng, W. & Cheng, H.W. 2009. Synthesis and characterization of cobalt nano-particles through microwave polyol process. *AIChE Journal*, 55: 1383–1389.
- Chowdhury, M.R. 2014. *Solvent dependent growth of one-dimensional crystalline γ -FeOOH nanorods*. PhD Thesis. Cape Peninsula University of Technology.

- Cong, P., Doolen, R.D. & Fan, Q. 1999. High-throughput synthesis and screening of combinatorial heterogeneous catalyst libraries. *Angewandte Chemie*, 38(4): 484–488.
- D'Agata, A., Fasulo, S. & Dallas, L.J. 2014. Enhanced toxicity of “bulk” titanium dioxide compared to “fresh” and “aged” nano-TiO₂ in marine mussels (*Mytilus galloprovincialis*). *Nanotoxicology*, 8(5): 549–558.
- Darr, J.A. & Poliakoff, M. 1999. New directions in inorganic and metal-organic coordination chemistry in supercritical fluids. *Chemical reviews*, 99: 495–541.
- David, B.W. & Carter, C.B. 1996. *Transmission electron microscopy*. Plenum.
- De la Peña O'Shea, V.A., de la Piscina, P., Homs, N., Aromi, G. & Fierro, J.. 2009. Development of Hexagonal Closed-Packed Cobalt Nanoparticles Stable at High Temperature. *Chemistry of Materials*, 21: 5637–5643.
- De Miguel, S.R., Vilella, J.I., Jablonski, E.L., Scelza, O.A., Salinas-Martinez de Lecea, C. & Linares-Solano, A. 2002. Preparation of Pt catalysts supported on activated carbon felts. *Applied Catalysis A: Environmental*, 32: 237–246.
- Den Breejen, J.P., Radstakee, P.B., Bezemer, G.L., Bitter, J.H., Froseth, V., Holmen, A. & De Jong, K.P. 2009. On the origin of the cobalt particle size effects in Fischer–Tropsch catalysis. *Journal of the American Chemical Society*, 131: 7197–7203.
- Deng, J., Ge, Y., Tan, C., Wang, H., Li, Q., Zhou, S. & Zhang, K. 2017. Degradation of ciprofloxacin using α -MnO₂ activated peroxymonosulfate process: Effect of water constituents, degradation intermediates and toxicity evaluation. *Chemical Engineering Journal*, 330: 1390–1400.
- Ding, Y., Zhu, L., Huang, A., Zhao, X., Zhang, X. & Tang, H. 2012. A heterogeneous Co₃O₄–Bi₂O₃ composite catalyst for oxidative degradation of organic pollutants in the presence of peroxymonosulfate. *Catalysis Science & Technology*, 2(9): 1977.
- Duarte, F., Maldonado-Hodar, F.J. & Madeira, L.. 2012. Influence of the particle size of activated carbons on their performance as Fe supports for developing fenton-like catalysts. *Industrial & Engineering Chemistry Research*, 51: 9218–9226.
- Dutta, K.P. & Ray, A.K. 2004. Experimental investigation of Taylor vortex photocatalytic reactor for water purification. *Chemical engineering Science*, 59: 5249–5259.
- Egerton, R.F. 2009. Electron energy-loss spectroscopy in the TEM". *Reports on Progress in Physics*. *Reports on progress in Physics*, 72: 1.
- Ertl, G., Knözinger, H., Schüth, F. & Weitkamp, J. 2008. *Heterogeneous Catalysis*. 2nd ed. Weinheim, Germany: Wiley-VCH.

- Fan, Y., Ma, W., He, J. & Du, Y. 2017. CoMoO₄ as a novel heterogeneous catalyst of peroxymonosulfate activation for the degradation of organic dyes. *RSC Advances*, 7(57): 36193–36200.
- Fujimoto, M., Koyama, H., Konagai, M., Hosoi, Y., Ishihara, K., Ohnishi, S. & Awaya, N. 2006. TiO₂ anatase nanolayer on TiN thin film exhibiting high-speed bipolar resistive switching. *Applied Physics Letters*, 89(22).
- Furman, O.S., Teel, A.L. & Watts, R.J. 2010. Mechanism of base activation of persulfate. *Environmental science & technology*, 44(16): 6423–6428.
- Galkin, A.A., Kostyuk, B.G. & Kuznetsova, N.N. 2001. Unusual approach to the preparation of heterogeneous catalysts and supports using water in subcritical and supercritical states. *Kinetics and Catalysis*, 42: 154–162.
- Gao, Y., Zhang, Z., Li, S., Liu, J., Yao, L., Li, Y. & Zhang, H. 2016. Insights into the mechanism of heterogeneous activation of persulfate with a clay/iron-based catalyst under visible LED light irradiation. *Applied Catalysis B: Environmental*, 185: 22–30.
- Goldstein, J.I. 2003. *Scanning Electron Microscopy and X-ray Microanalysis*. 3rd ed. New York: Plenum Press.
- Grasselli, R.K. 2014. Site isolation and phase cooperation: Two important concepts in selective oxidation catalysis: A retrospective. *Catalysis Today*, 238: 10–27.
- Grosso, D., Soler-Illia, G.J. de . A., Crepaldi, E.L., Cagnol, F., Sinturel, C., Bourgeois, A., Albouy, P.A. & Sanchez, C. 2003. Highly Porous TiO₂ Anatase Optical Thin Films with Cubic Mesostructure Stabilized at 700°C. *Chemistry of Materials*, 15(24): 4562–4570.
- Guan, Y.H., Ma, J., Ren, Y.M., Liu, Y.L., Xiao, J.Y., Lin, L.Q. & Zhang, C. 2013. *Water Research journal*, 47: 5431–5438.
- Guo, Y.G., Hu, J.S. & Wan, L.J. 2008. Nanostructured materials for electrochemical energy conversion and storage devices. *Advanced Materials*, 20: 2878–2887.
- Guo, Y.G., Hu, Y.S., Sigle, W. & Maier, J. 2007. Superior electrode performance of nanostructured mesoporous TiO₂ (Anatase) through efficient hierarchical mixed conducting networks. *Advanced Materials*, 19(16): 2087–2091.
- Haber, J. 1989. The concept of structure sensitivity in catalysis by oxides. *Studies in Surface Sciences and Catalysis*, 48: 447–467.
- Hagelin-Weaver, H.A.E., Hoflund, G.B., Minahan, D.M. & Salait, G.N. 2004. Electron energy loss spectroscopic investigation of Co metal, CoO, and Co₃O₄ before and after Ar⁺ bombardment. *Applied Surface Science*, 235: 420–448.

- Hao, Y. & Teja, A.S. 2003. Continuous hydrothermal crystallization of α -Fe₂O₃ and Co₃O₄ nanoparticles. *Journal of Materials Research*, 18: 415–422.
- Haque, M.M. & Muneer, M. 2003. Heterogeneous photocatalysed degradation of a herbicide derivative, isoproturon in aqueous suspension of titanium dioxide. *Journal of Environmental Management*, 69: 169–176.
- Hävecker, M., Trunschke, A., Wrabetz, S., Kröhnert, J., Csepei, L.I., d'Alnoncourt, R.N. & Kolen'ko, Y.V. 2012. A Surface chemistry of phase-pure M1 MoVTenb oxide during operation in selective oxidation of propane to acrylic acid. *Journal of Catalysis*, 285: 48–60.
- Hayashi, H. & Hakuta, Y. 2010. National R&D Institute for Nonferrous and Rare Metals. *Materials*, 3: 3794–3817.
- Hinshelwood, C.N. 1940. *The Kinetics of Chemical Change*. Oxford. UK.
- Hirsch, P. 1965. Electron microscopy of thin crystals. *Butterworths*.
- Ho, W.H., Li, C.F. & Lui, H.C. 2008. Electrochemical performance of In₂O₃ thin film electrode in lithium cell. *Journal of Power Sources*, 175: 897–902.
- Hou, L., Zhang, L. & Wang, L. 2013. *Chemical Engineering Journal*, 229: 577–584.
- Hu, C.G., Mou, Z.Y., Lu, G., Chen, N., Dong, Z., Hu, M. & Qu, L. 2013. 3D graphene–Fe₃O₄ nanocomposites with high-performance microwave absorption. *Chemical Physics Journal*, 15: 13038.
- Hu, P. & Long, M. 2016a. Cobalt-catalyzed sulfate radical-based advanced oxidation: a review on heterogeneous catalysts and applications. *Applied Catalysis B: Environmental*, 181: 103–117.
- Hu, P. & Long, M. 2016b. Cobalt-catalyzed sulfate radical-based advanced oxidation: A review on heterogeneous catalysts and applications. *Applied Catalysis B: Environmental*, 181: 103–117.
- Hui, W., Jianbo, Z., Chuanxin, M., Xiangyang, D., Ning, T., Jiang, P. & Deren, Y. 2008. From cobalt nitrate carbonate hydroxide hydrate nanowires to porous Co₃O₄ nanorods for high performance lithium-ion battery electrodes. *Nanotechnology*, 19.
- Hutchings, G.J. & Védrine, J.C. 2004. *Catalyst preparation. In Basic Principles in Applied Catalysis*. Baerns, M. Berlin, Germany: Springer.
- Julkapli, N.M., Bagheri, S. & Abd Hamid, S.B. 2014. Recent advances in heterogeneous photocatalytic decolorization of synthetic dyes. *The Scientific World Journal*: 25.
- Kanamori, T., Matsuda, M. & Miyake, M. 2009. *Journal of Hazardous Materials*, 169: 240.

- Katsoyiannis, I.A., Canonica, S. & Von Gunten, U. 2011. Efficiency and energy requirements for the transformation of organic micropollutants by ozone, O₃/H₂O₂ and UV/H₂O₂. *Water Research Journal*, 45: 3811–3822.
- Kim, T.H., Park, C., Yang, J. & Kima, S. 2004. Comparison of disperse and reactive dye removals by chemical coagulation and Fenton oxidation. *Journal of Hazardous Materials*, 122: 95–103.
- Kim, T.S., Stiehl, J.D., Reeves, C.T., Meyer, R.J. & Mullins, C.B. 2003. Cryogenic CO oxidation on TiO₂-supported gold nanoclusters precovered with atomic oxygen. *Journal of the American Chemical Society*, 125(8): 2018–2019.
- Klimuik, E., Filipkowska, U. & Korzeniowska, A. 1999. Effects of pH and coagulant dosage on effectiveness of coagulation of reactive dyes from model wastewater by polyaluminium chloride. *Polish Journal of Environmental Studies*, 8(2): 73–79.
- Krishnan, S., Rawindran, H., Sinnathambi, C.M. & Lim, J.W. 2017. Comparison of various advanced oxidation processes used in remediation of industrial wastewater laden with recalcitrant pollutants. In *IOP Conference Series: Materials Science and Engineering*. IOP Publishing: 012089.
- Lambert, J.F. & Che, M. 2000. The molecular approach to supported catalysts synthesis: State of the art and future challenges. *Journal of Molecular Catalysis A: Chemical*, 162: 5–18.
- Lathasree, S., Rao, A.N., Siva Samlor, V. & Rengaraj, K. 2004. Heterogeneous photocatalytic mineralization of phenols in aqueous solutions. *Journal of Molecular Catalysis A: Chemical*, 223: 101–105.
- Le Page, J.F. 1987. *Applied Heterogeneous Catalysis: Design-Manufacture-Use of Solid Catalysts*. Paris, France: Technip.
- Leng, Y. 2013. *Materials Characterization: Introduction to Microscopic and Spectroscopic Methods*. Wiley.
- Leng, Y., Lui, J., Jiang, P. & Wang, J. 2014. Organometallic polyoxometalate hybrid based on V-Schiff base and phosphovanadomolybdate as a highly effective heterogenous catalyst for hydroxylation of benzene. *Chemical Engineering Journal*, 239: 1–7.
- Li, W., Wu, P., Zhu, Y., Huang, Z., Lu, Y., Li, Y., Dang, Z. & Zhu, N. 2015. Catalytic degradation of bisphenol A by CoMnAl mixed metal oxides catalyzed peroxy monosulfate: Performance and mechanism. *Chemical Engineering Journal*, 279: 93–102.
- Liang, H., Sun, H., Patel, A., Shukla, P., Zhu, Z.H. & Wang, S.B. 2012a. *Applied Catalysis B: Environmental*, 127: 330–335.

- Liang, H.W., Ting, Y.Y., Sun, H.Q., Ang, H.M., Tadé, M.O. & Wang, S.B. 2012b. *Journal of Colloid and Interface Science*, 58: 372.
- Lietti, L., Forzatti, P. & Bregani, F. 1996. Steady-state and transient reactivity study of TiO₂-supported V₂O₅-WO₃ De-NO_x catalysts: relevance of the vanadium-tungsten interaction on the catalytic activity. *Industrial & Engineering Chemistry Research*, 35(11): 3884–3892.
- Lin, S.D., Bollinger, M. & Vannice, M.A. 1993. Low temperature CO oxidation over Au/TiO₂ and Au/SiO₂ catalysts. *Catalysis Letters*, 17(3–4): 245–262.
- Liu, H., Bruton, T.A., Li, W., Buren, J.V., Prasse, C., Doyle, F.M. & Sedlak, D.L. 2016. Oxidation of Benzene by Persulfate in the Presence of Fe(III)- and Mn(IV)-Containing Oxides: Stoichiometric Efficiency and Transformation Products. *Environmental Science & Technology*, 50(2): 890–898.
- Liu, R., Jin, R., An, J., Zhao, Q., Chen, T. & Lui, G. 2014. Hollowshell- structured nanospheres: a recoverable heterogeneous catalyst for rhodium-catalyzed tandem reduction/lactonization of ethyl 2-acylarylcarboxylates to chiral phthalides. *Chemistry : An Asian Journal*, 9(5): 1388–1394.
- Lundblad, A. & Bergman, B. 1997. *Solid State Ionics*, 96: 183.
- Luo, F., Yang, D., Chen, Z.L., Megharaj, M. & Naidu, R. 2015. The mechanism for degrading Orange II based on adsorption and reduction by ion-based nanoparticles synthesized by grape leaf extract. *Journal of Hazardous Materials*, 296: 37.
- Luo, Q., Beller, M. & Jiao, H. 2013. Formic acid dehydrogenation on surfaces : a review of computational aspect. *Journal of Theoretical and Computational Chemistry*, 12(7).
- Lutze, H. 2013. *Microsoft Word-Dissertation Holger Lutze 28.7. 2013 final ohne Lebenslauf für Bib.* Germany: University Duisburg-Essen. https://duepublico.uni-duisburg-essen.de/servlets/DerivateServlet/Derivate-35021/Lutze_Diss.pdf 6 August 2017.
- Ma, J.F., Wang, K., Li, L.Y., Zhang, T.L., Kong, Y. & Komarneni, S. 2015. • Visible-light photocatalytic decolorization of Orange II on Cu₂O/ZnO nanocomposites. *Ceramics International*, 41: 2050.
- Machek, V., Hanika, J., Sporka, K., Ruzicka, V. & Kunz, J. 1981. Relation between the distribution of platinum, its dispersion, and activity of catalysts prepared by impregnation of activated carbon with chloroplatinic acid solutions. *Search Results Web result with site links Collection of Czechoslovak Chemical Communications*, 46: 3270–3377.
- Manigandan, R., Giribu, K., Suresh, R., Vijayalakshmi, L., Stepen, A. & Narayanan, V. 2013. Cobalt Oxide Nanoparticles: Characterization and its Electrocatalytic Activity towards Nitrobenzene. *Chemical Science Transactions*, 2(S1). <http://www.e-journals.in/abstract.asp?Totarticle=10> 16 August 2018.

- Mathews, R.W. 1988. Kinetics of photocatalytic oxidation of organic solutes over titanium dioxide catalysis. *Journal of Catalysis*, 111: 264–272.
- Mathews, R.W. 1986. Photooxidation of organic material in aqueous suspensions of titanium dioxide. *Water Research Journal*, 20(5): 569–578.
- Matta, R., Tlili, S. & Barbati, S. 2011. Removal of carbamazepine from urban wastewater by sulfate radical oxidation. *Environmental Chemistry Letters*, 9: 347–353.
- Mehlomakulu, B., Nguyen, T.T.N., Delichère, P., van Teen, E. & Millet, J.M.M. 2012. Identification of the active species in oxidation reactions on mixed oxide catalysts: Supra-surface or bulk-surface species. *Journal of Catalysis*, 289: 1–10.
- Mills, A. & Morris, S. 1993. Photo-mineralization of 4-chlororphenol sensitized by titanium dioxide: a study of the initial kinetics of carbon dioxide photogeneration. *Journal of Photochemistry and Photobiology A: Chemistry*, 71: 75–83.
- Monteagudo, J.M., Durán, A., Latorre, J. & Expósito, A.J. 2016. Application of activated persulfate for removal of intermediates from antipyrine wastewater degradation refractory towards hydroxyl radical. *Journal of hazardous materials*, 306: 77–86.
- Muhammad, S., Saputra, E., Sun, H.Q., Izidoro, J.C., Fungaro, D., Ang, H.M., Tadé, M.O. & Wang, S.B. 2012. Coal fly ash supported Co₃O₄ catalysts for phenol degradation using peroxymonosulfate. *RSC Advances*, 2: 5645.
- Muneer, M. & Bahnemann, D. 2002. Semiconductor-mediated photocatalysed degradation of two selected pesticide derivatives, terbacil and 2,4,5-tribromoimidazole, in aqueous suspension. *Applied Catalysis B: Environmental*, 36: 95–111.
- Nawaz, M.S. & Ahsan, M. 2014. Comparison of physico-chemical, advanced oxidation and biological techniques for the textile wastewater treatment. *Alexandria Engineering Journal*, 53(3): 717–722.
- Neamtu, M., Yediler, A., Siminiceanu, I., Macoveanu, M. & Kettrup, A. 2004. Decolorization of Disperse Red 354 Azo Dye in Water by Several Oxidation Processes? A Comparative Study. *Dyes and pigments*, 60: 61.
- Neta, P., Huie, R.E. & Ross, A.B. 1988. Rate constants for reactions of inorganic radicals in aqueous solution. *The Journal of Physical Chemistry B*, 17(3): 1027–1284.
- Nillson, R., Nordlinder, R. & Wass, U. 1993. Asthma, Rhinitis and Dermatitis in Workers Exposed to Reactive Dyes. *British Journal of Industrial Medicine*, 50: 65.
- Nolan, M. 2013. Modifying ceria (111) with a TiO₂ nanocluster for enhanced reactivity. *Journal of Chemical Physics*, 139(18).

- Oh, S.W., Bang, H.J., Bae, Y.C. & Sun, Y.-K. 2007. Effect of calcination temperature on morphology, crystallinity and electrochemical properties of nano-crystalline metal oxides (Co₃O₄, CuO, and NiO) prepared via ultrasonic spray pyrolysis. *Journal of Power Sources*, 173(1): 502–509.
- Oputu, O.U. 2016. *Advanced oxidation process using ozone/heterogeneous catalysis for the degradation of phenolic compounds (chlorophenols) in aqueous system*. PhD Thesis. Cape Peninsula University of Technology.
- Ostrovski, V.E. 2012. Oscillation theory of heterogeneous catalysis and its use for identification of the reaction scheme and kinetics: Catalytic liquid-phase benzene-ring hydrogenation as an example. *Journal of Scientific and Israel Technology Advanced*, 14: 57–79.
- Otsua, J. & Oshima, Y. 2005. New approaches to the preparation of metal or metal oxide particles on the surface of porous materials using supercritical water: Development of supercritical water impregnation method. *Journal of Supercritical Fluids*, 33: 61–67.
- Papić, S., Koprivanac, N., Božić, A.L., Vujević, D., Dragičević, S.K., Kušić, H. & Peternel, I. 2006. Advanced oxidation processes in azo dye wastewater treatment. *Water environment research*, 78(6): 572–579.
- Parent, Y., Blake, D., Magrini, B.K., Lyons, C., Turchi, C.S., Watt, A., Wolfrum, E. & Prairie, M. 1996. Solar photocatalytic process for the purification of water: state of development and barriers to commercialization. *Solar Energy*, 56: 429–437.
- Park, K.W. & Seol, K.S. 2007. Nb-TiO₂ supported Pt cathode catalyst for polymer electrolyte membrane fuel cells. *Electrochemistry Communications*, 9(9): 2256–2260.
- Perego, C. & Villa, P. 1997. Catalyst preparation methods. *Catalysis Today*, 34: 281–305.
- Pinheiro, H.M., Touraud, E. & Thomas, O. 2004. Aromatic amines from azo dye reduction: status review with emphasis on direct UV spectrophotometric detection in textile industry wastewaters. *Dyes and Pigments*, 61(2): 121–139.
- Piticescu, R.M., Piticescu, R.R. & Vasile, E. 2012. Hydrothermal procedures: a challenge in the environmental production of nanomaterials. *National R&D Institute for Nonferrous and Rare Metals*.
- Plichta, F. & Salomon, M. 1987. *Journal of Power Sources*, 21: 25.
- Qamar, M. & Muneer, M. 2005. Comparative photocatalytic study of two selected pesticide derivatives, indole-3-acetic acid and indole-3-butyric acid in aqueous suspensions of titanium dioxide. *Journal of Hazardous Materials*, 120: 219–227.
- Rahman, M.A. & Muneer, M. 2005a. Heterogeneous photocatalytic degradation of picloram, dicamba, and floumeturon in aqueous suspensions of titanium dioxide. *Journal of Environmental Science and Health*, 40: 247–267.

- Rahman, M.A. & Muneer, M. 2005b. Photocatalysed degradation of two selected pesticide derivatives, dichlorvos and phosphamidon, in aqueous suspensions of titanium dioxide. *Desalination and Water Treatment*, 181: 161–172.
- Ramakrishnan, V., Kim, H., Park, J. & Yang, B. 2016. Cobalt oxide nanoparticles on TiO₂ nanorod/FTO as a photoanode with enhanced visible light sensitization. *RSC Advances*, 6(12): 9789–9795.
- Rastogi, A., Ai-Abed, S.R. & Dionysiou, D.D. 2009. Sulfate radical-based ferrous-peroxymonosulfate oxidative system for PCBs degradation in aqueous and sediment systems. *Applied Catalysis B: Environmental*, 85: 171–179.
- Regalbuto, J.R. 2007. *Catalyst Preparation Science and Engineering*. Boca Raton, FL, USA: CRC Press.
- Ren, X., Zhang, H. & Cui, Z. 2007. Acetylene decomposition to helical carbon nanofibers over supported copper catalysts. *Materials Research Bulletin*, 42(12): 2202–2210.
- Riman, R.E. 2002. *Ann. Journal of materials science*, 27(6): 16–36.
- Salari, D., Daneshvar, N., Aghazadeh, F. & Khataee, A.R. 2005. Application of artificial neural networks for modeling of the treatment of wastewater contaminated with methyl tert-butyl ether (MTBE) by UV/H₂O₂ process. *Journal of Hazardous Materials*, 125(1–3): 205–210.
- Saputra, E., Muhammad, S., Sun, H.Q., Ang, H.M., Tadó, M.O. & Wang, S.B. 2013. Manganese oxides at different oxidation states for heterogeneous activation of peroxymonosulfate for phenol degradation in aqueous solutions. *Journal of Colloid and Interface Science*, 407: 467–473.
- Selvabharathi, G., Adishkumar, S., Jenefa, S., Ginni, G., Rajesh Banu, J. & Tae Yeom, I. 2016. Combined homogeneous and heterogeneous advanced oxidation process for the treatment of tannery wastewaters. *Journal of Water Reuse and Desalination*, 6(1): 59–71.
- Sharma, J., Mishra, I.M., Dionysiou, D.D. & Kumar, V. 2015. Oxidative removal of Bisphenol A by UV-C/peroxymonosulfate (PMS): Kinetics, influence of co-existing chemicals and degradation pathway. *Chemical Engineering Journal*, 276: 193–204.
- Shi, P., Su, R., Zhu, S., Li, D. & Xu, S. 2012. Supported cobalt oxide on graphene oxide: Highly efficient catalysts for the removal of Orange II from water. *Journal of Hazardous Materials*, 299–330: 331–339.
- Shibasaki-Kitakawa, N., Honda, H., Kuribayashi, H., Toda, T., Fukumura, T. & Yonemoto, T. 2007. Biodiesel production using anionic ion-exchange resin as heterogeneous catalyst. *Bioresource Technology*, 98(2): 416–421.

- Shifu, C. & Gengyu, C. 2005. Photocatalytic degradation of pesticides using floating photocatalyst TiO₂/SiO₂ beads by sunlight. *Solar Energy*, 79: 1–9.
- Shukla, P., Wang, S., Singh, K., Ang, H.M. & Tade, M.O. 2010a. Cobalt exchanged zeolites for heterogeneous catalytic oxidation of phenol in the presence of peroxymonosulphate. *Applied Catalysis B: Environmental*, 99: 163–169.
- Shukla, P.R., Wang, S.B., Sun, H.Q., Ang, H.M. & Tade, M.O. 2010b. Activated carbon supported cobalt catalysts for advanced oxidation of organic contaminants in aqueous solution. *Applied Catalysis B: Environmental*, 100: 529–534.
- Si, L., Huang, Z., Tang, L.D. & Yang, C. 2014. Facile preparation of Ti³⁺ self-doped TiO₂ nanosheets with dominant 001 facets using zinc powder as reductant. *Journal of Alloys and Compounds*, 601: 88–93.
- Singh, H.K., Haque, M.M., Saquib, M. & Muneer, M. 2007c. Heterogeneous photocatalysed degradation of 4-chlorophenoxyacetic acid in aqueous suspensions. *Journal of Hazardous Materials*, 142: 374–380.
- Singh, H.K., Saquib, M., Haque, M.M. & Muneer, M. 2007b. Heterogeneous photocatalyzed degradation of uracil and 5-bromouracil in aqueous suspensions of titanium dioxide. *Journal of Hazardous Materials*, 142: 425–430.
- Singh, H.K., Saquib, M., Haque, M.M., Muneera, M. & Bahnemann, D. 2007a. Titanium dioxide mediated photocatalysed degradation of phenoxyacetic acid and 2,4,5-trichlorophenoxyacetic acid, in aqueous suspensions. *Journal of Molecular Catalysis A: Chemical*, 264: 66–72.
- Slokar, Y.M. & Le Marechal, A.M. 1998. Methods of decoloration of textile wastewaters. *Dyes and pigments*, 37(4): 335–356.
- Soofivand, F. & Salavati-Niasari, M. 2015. Co₃O₄/graphene nanocomposite: pre-graphenization synthesis and photocatalytic investigation of various magnetic nanostructures. *RSC Advances*, 5(79): 64346–64353.
- Stoyanova, M., Slavova, I., Christoskova, S. & Ivanova, V. 2014. *Applied Catalysis A: Environmental*, 476: 121.
- Sui, L.X., Wang, Z.B., Yang, M., Huo, L., Gu, D.M. & Yin, G.P. 2014. Investigation on C-TiO₂ nanotubes composite as Pt catalyst support for methanol electrooxidation. *Journal of Power Sources*, 255: 43–51.
- Sun, H., Liu, S., Zhou, G., Ang, H.M., Tade, M.O. & Wang, S. 2012. *ACS Applied Materials & Interfaces*, 4: 5466–5471.

- Tan, Y., Gao, Z., Li, Z., Tian, W., Qian, W., Yang, C. & Zhang, H. 2016. Unique 1D Co₃O₄ crystallized nanofibers with (220) oriented facets as high-performance lithium ion battery anode material. *Scientific Reports*, 6.
- Tarascon, J.M. & Armand, M. 2001. *Nature*, 414: 359.
- Tauster, S.J., Fung, S.C., Baker, R.T.K. & Horsley, J.A. 1981. Strong interactions in supported-metal catalysts. *Science*, 211(4487).
- Thomas, J.M. 2012. The societal significance of catalysis and the growing practical importance of single-site heterogeneous catalysts. *proceeding of the Royal Society A*, 468: 1884–1903.
- Thomas, J.M. & Thomas, W.J. 2014. Principles and Practice of Heterogeneous Catalysis. Wiley-VCH.
- Tseng, H.H., Wey, M.Y. & Fu, C.H. 2003. Carbon materials as catalyst supports for SO₂ oxidation: catalytic activity of CuO-AC, Carbon, , 41: 139–149.
- Turchi, C.S. & Ollis, D.F. 1990. Photocatalytic degradation of organic water contaminant mechanisms involving hydroxyl radical attack. *Journal of Catalysis*, 122: 178–192.
- Uysal, B. & Oksal, B.S. 2013. New heterogeneous B(OEt)₃- MCM-41 catalyst for preparation of α,β -unsaturated alcohols. *Research on Chemical Intermediates*.
- Védrine, J.C. 2017. Heterogeneous Catalysis on Metal Oxides. *Catalysis Letters*.
- Védrine, J.C. 2014. Revisiting active sites in heterogeneous catalysis: Their structure and dynamical behaviour. *Applied Catalysis A: Environmental*, 474: 45–50.
- Volta, J.C. & Portefaix, J.L. 1985. Structure sensitivity of mild oxidation reactions on oxide catalysts: A review. *Applied Catalysis*, 18: 1–32.
- Waldemer, R.H., Tratnyek, P.G., Johnson, R.L. & Nurmi, J.T. 2007. Oxidation of Chlorinated Ethenes by Heat-Activated Persulfate: Kinetics and Products. *Environmental science & technology*, 41: 1010–1015.
- Wan, K.T. & Davis, M.E. 1994. Design and synthesis of a heterogeneous asymmetric catalyst. *Nature*, 370(6489): 449–450.
- Wang, H.L., Lui, L.F. & Yang, Y. 2010. Mn₃O₄-graphene hybrid as a high-capacity anode material for lithium ion batteries. *132*: 13978–13980.
- Wang, Y.X., Sun, H.Q., Ang, H.M., Tadé, M.O. & Wang, S.B. 2014. Ferric carbide nanocrystals encapsulated in nitrogen-doped carbon nanotubes as an outstanding environmental catalyst. *Chemical Engineering Journal*, 245(2).

- Wang, Z., Du, Y., Lui, Y., Zou, B., Xiao, J.Y. & Ma, J. 2013. Degradation of organic pollutants by NiFe₂O₄/peroxymonosulfate: Efficiency, influential factors and catalytic mechanism. *RSC Advances*, 00: 1–3.
- Wang, Z.L., Yin, J.S. & Jiang, Y.D. 2000. EELS analysis of cation valence states and oxygen vacancies in magnetic oxides. *Micron*, 31: 571–580.
- Wei, G., Liang, X., He, Z., Liao, Y., Xie, Z., Liu, P., Ji, S., He, H., Li, D. & Zhang, J. 2015. Heterogeneous activation of Oxone by substituted magnetites Fe_{3-x}M_xO₄ (Cr, Mn, Co, Ni) for degradation of Acid Orange II at neutral pH. *Journal of Molecular Catalysis A: Chemical*, 398: 86–94.
- Winter, M., Besenhard, J.O. & Spahr, M.E. 1998. Insertion electrode materials for rechargeable lithium batteries. *Advanced Materials*, 10: 3115–3141.
- Woodley, S. & Catlow, C. 2009. Structure prediction of titania phases: Implementation of Darwinian versus Lamarckian concepts in an Evolutionary Algorithm. *Materials Science*, 45(1): 84–95.
- Wu, C.Z., Yin, P. & Zhu, X. 2006. Synthesis of hematite (α-Fe₂O₃) nanorods: diameter-size and shape effects on their applications in magnetism, lithium ion battery, and gas sensors. *Journal of Physical Chemistry: B*, 110: 17806–17812.
- Xu, J., Li, K., Shi, W., Li, R. & Peng, T. 2014. Rice-like brookite titania as an efficient scattering layer for nanosized anatase titania film-based dye-sensitized solar cells. *Journal of Power Sources*, 260: 233–242.
- Xu, L. & Wang, J. 2012. *Environmental Science & Technology*, 46: 10145–10153.
- Yamaguchi, K., Yoshida, C., Uchida, S. & Mizuno, N. 2005. Peroxotungstate immobilized on ionic liquid-modified silica as a heterogeneous epoxidation catalyst with hydrogen peroxide. *Journal of the American Chemical Society*, 127(2): 530–531.
- Yan, W., Mahurin, S.M., Pan, Z., Overbury, S.H. & Dai, S. 2005. Ultrastable Au nanocatalyst supported on surface-modified TiO₂ nanocrystals. *Journal of the American Chemical Society*, 127(30): 10480–10481.
- Yang, B., Tian, Z., Wang, B., Sun, Z., Zhang, L., Guo, Y.G., Li, H. & Yan, S. 2015. *RSC Advances*, 5: 20674–20683.
- Yang, H.X. & Li, L. 2014. Tin-indium/graphene with enhanced initial Coulombic efficiency and rate performance for lithium ion batteries. *Journal of Alloys and Compounds*, 584: 76–80.
- Yang, Q., Choi, H., Al-Abed, S.R. & Dionysiou, D.D. 2009. Iron–cobalt mixed oxide nanocatalysts: heterogeneous peroxymonosulfate activation, cobalt leaching, and

- ferromagnetic properties for environmental applications. *Applied Catalysis B: Environmental*, 88: 462–469.
- Yang, Q., Choi, H., Chen, Y. & Dionysiou, D.D. 2008. Heterogeneous activation of peroxymonosulfate by supported cobalt catalysts for the degradation of 2,4-dichlorophenol in water: The effect of support, cobalt precursor, and UV radiation. *Applied Catalysis B: Environmental*, 77(3–4): 300–307.
- Yang, Q., Choi, H. & Dionysiou, D.D. 2007. Nanocrystalline cobalt oxide immobilized on titanium dioxide nanoparticles for the heterogeneous activation of peroxymonosulfate. *Applied Catalysis B: Environmental*, 74(1–2): 170–178.
- Yao, J., Shen, X.P. & Wang, B. 2009. In situ chemical synthesis of SnO₂-graphene nanocomposite as anode materials for lithium-ion batteries. *Electrochemistry Communications*, 11: 1849–1852.
- Yao, X.Y., Kong, J.H. & Tang, X.S. 2014. Facile synthesis of porous CoFe₂O₄ nanosheets for lithium-ion battery anodes with enhanced rate capability and cycling stability. *RSC Advances*, 4: 27488–27492.
- Yao, Yunjin, Xu, C., Yu, S., Zhang, D. & Wang, S. 2013. Facile Synthesis of Mn₃O₄ – Reduced Graphene Oxide Hybrids for Catalytic Decomposition of Aqueous Organics. *Industrial & Engineering Chemistry Research*, 52: 3637–3645.
- Yao, Y., Xu, M., Qin, J., Wei, F., Rao, M. & Wang, S. 2013. Synthesis of magnetic cobalt nanoparticles anchored on graphene nanosheets and catalytic decomposition of Orange II. *Industrial & Engineering Chemistry Research*, 52(49): 17341–17350.
- Yoshimura, M. & Suchanek, W. 1997. *Solid State Ionics*, 98: 197–208.
- Zhang, J.J., Huang, T. & Yu, A.S. 2015. Synthesis and effect of electrode heat-treatment on the superior lithium storage performance of Co₃O₄ nanoparticles. *Journal of Power Sources*, 273: 894–903.
- Zhang, P.W., Yokoyama, T., Itabashi, O., Suzuki, T.M. & Inoue, K. 1998. *Hydrometallurgy*, 47: 259.
- Zhang, S., Fan, Q., Gao, H., Huang, Y., Liu, X., Li, J., Xu, X. & Wang, J. 2016. *Journal of Materials Chemistry A*, 4: 1414–1422.
- Zhang, T., Zhu, H. & Croue, J.. 2013. *Environmental Science & Technology*, 47: 2784–2791.
- Zhang, W., Tay, H.L., Lim, S.S., Wang, Y.S., Zhong, Z.Y. & Xu, R. 2010. *Applied Catalysis B: Environmental*, 95: 93.

- Zhao, J.Z., Tao, Z.L. & Liang, J. 2008. Facile synthesis of nanoporous γ -MnO₂ structures and their application in rechargeable Li-ion batteries. *Crystal Growth & Design*, 8: 2799–2805.
- Zhou, G., Zhou, L., Sun, H., Ang, H.M., Tadé, M.O. & Wang, S. 2015. Carbon microspheres supported cobalt catalysts for phenol oxidation with peroxymonosulfate. *Chemical Engineering Research and Design*, 101: 15–21.
- Zhu, X.J., Zhu, Y.W. & Murali, S. 2011. Nanostructured reduced graphene oxide/Fe₂O₃ composite as a highperformance anode material for lithium ion batteries. *Acs Nano*, 5: 3333–3338.
- Zhu, Y., Chen, S., Quan, X. & Zhang, Y. 2013. Cobalt implanted TiO₂ nanocatalyst for heterogeneous activation of peroxymonosulfate. *RSC Advances*, 3(2): 520–525.
- Ziółkowski, J., Bordes, E. & Courtine, P. 1993. Dynamic description of the oxidation of n-butane on various faces of (VO)₂P₂O₇ in terms of the crystallochemical model of active sites. *Journal of Molecular Catalysis A: Chemical*, 84: 307–326.

APPENDICES

Appendix A

Table A.2: Experimental conditions for catalytic performance on MO

Material	MO (Ppm)	PMS (g/L)	Catalyst (g/L)
Co ₃ O ₄	40	0.2	0.15
TiO ₂	40	0.2	0.15
98% Co ₃ O ₄ /TiO ₂	40	0.2	0.15
95% Co ₃ O ₄ /TiO ₂	40	0.2	0.15
90% Co ₃ O ₄ /TiO ₂	40	0.2	0.15
85% Co ₃ O ₄ /TiO ₂	40	0.2	0.15
80% Co ₃ O ₄ /TiO ₂	40	0.2	0.15
70% Co ₃ O ₄ /TiO ₂	40	0.2	0.15
60 % Co ₃ O ₄ /TiO ₂	40	0.2	0.15
50% Co ₃ O ₄ /TiO ₂	40	0.2	0.15

Table A.3: Raw data and real concentration calculation for catalytic performance of Co₃O₄ using various ratios on methyl orange

concentrations										
Time (min)	100% Co ₃ O ₄	PMS	98% Co ₃ O ₄ /TiO ₂	95% Co ₃ O ₄ /TiO ₂	90% Co ₃ O ₄ /TiO ₂	85% Co ₃ O ₄ /TiO ₂	80% Co ₃ O ₄ /TiO ₂	70% Co ₃ O ₄ /TiO ₂	60% Co ₃ O ₄ /TiO ₂	50% Co ₃ O ₄ /TiO ₂
0	40	40	40	40	40	40	40	40	40	40
0.5	20.728	40	31.368	29.482	29.22	29.33	34.26	31.232	23.932	25.268
1	11.06	40	29.672	28.178	26.698	26.876	30.928	28.28	21.182	24.907
2	3.69	36.546	23.042	23.634	24.524	23.39	25.878	23.446	17.746	23.778
5	2.956	31.994	16.072	15.608	16.016	12.578	18.022	14.554	10.332	9.7694
10	2.83	24.106	8.75	8.882	7.696	5.386	10.038	8.14	4.912	5.3928
15	2.754	19.112	6.376	5.812	5.546	5.352	7.714	5.73	4.67	4.2382
30	2.68	9.578	4.534	4.414	4.598	3.98	5.888	4.158	3.298	3.273

C _t /C _o										
Time (min)	100% Co ₃ O ₄	PMS	98% Co ₃ O ₄ /TiO ₂	95% Co ₃ O ₄ /TiO ₂	90% Co ₃ O ₄ /TiO ₂	85% Co ₃ O ₄ /TiO ₂	80% Co ₃ O ₄ /TiO ₂	70% Co ₃ O ₄ /TiO ₂	60% Co ₃ O ₄ /TiO ₂	50% Co ₃ O ₄ /TiO ₂

0	1	1	1	1	1	1	1	1	1	1
0.5	0.5182	1	0.7842	0.73705	0.7305	0.8565	0.7464	0.7808	0.5983	0.6317
1	0.2765	1	0.7418	0.70445	0.66745	0.773225	0.6719	0.707	0.52955	0.622674
2	0.09225	0.91365	0.57605	0.59085	0.6131	0.64695	0.58475	0.58615	0.44365	0.59445
5	0.0739	0.79985	0.4018	0.3902	0.4004	0.45055	0.380385	0.36385	0.2583	0.244235
10	0.07075	0.60265	0.21875	0.22205	0.1924	0.25095	0.20642	0.2035	0.1228	0.13482
15	0.06885	0.4778	0.1594	0.1453	0.13865	0.19285	0.1338	0.14325	0.11675	0.105955
30	0.067	0.23945	0.11335	0.11035	0.11495	0.1472	0.0995	0.10395	0.08245	0.081825

Ln (C_o/C_i)

Time (min)	100% Co ₃ O ₄	PMS	98% Co ₃ O ₄ /TiO ₂	95% Co ₃ O ₄ /TiO ₂	90% Co ₃ O ₄ /TiO ₂	85% Co ₃ O ₄ /TiO ₂	80% Co ₃ O ₄ /TiO ₂	70% Co ₃ O ₄ /TiO ₂	60% Co ₃ O ₄ /TiO ₂	50% Co ₃ O ₄ /TiO ₂
0	0	0	0	0	0	0	0	0	0	0
0.5	0.657394011	0	0.243091189	0.305099546	0.314026048	0.154900961	0.292493629	0.247436244	0.513662979	0.459340681
1	1.285544458	0	0.298675614	0.350337922	0.404290798	0.257185199	0.397645759	0.346724613	0.63572769	0.47373057
2	2.383252996	0.090307713	0.551560816	0.526193101	0.489227224	0.435486267	0.536570874	0.534179549	0.812719316	0.52011867
5	2.605042451	0.223331069	0.911800827	0.941095851	0.915291232	0.79728622	0.966571381	1.011013584	1.353633579	1.409624402
10	2.648602742	0.506418682	1.519825754	1.504852697	1.648178741	1.382501563	1.577842351	1.592089274	2.097198263	2.003814724
15	2.675825054	0.738563044	1.836338513	1.928954708	1.975802507	1.645842594	2.011409131	1.943163923	2.147720382	2.244740803
30	2.70306266	1.429410652	2.177274902	2.204098146	2.163258028	1.915963073	2.307597635	2.263845265	2.49556323	2.503172459
Rate	1.1864	0.0487	0.1088	0.1213	0.1269	0.1095	0.1268	0.1257	0.1853	0.1888

constant (k)										
-----------------	--	--	--	--	--	--	--	--	--	--

Table A.4: raw data of the catalytic performance of 70% at various calcinations temperatures

Concentration at various calcinations temperatures							
time	350°C	400°C	500°C	600°C	700°C	800°C	900°C
0	40	40	40	40	40	40	40
0.5	31.232	26.7554	34.1934	33.109	38.1966	32.1326	28.586
1	28.28	24.3214	32.4636	31.9326	38.0072	31.3916	28.125
2	23.446	20.0724	29.3104	27.8414	34.3812	28.3918	27.1656
5	14.554	14.4222	20.2056	20.5394	28.6888	24.8874	21.9196
10	8.14	7.3856	12.3252	13.4876	21.26	18.4674	15.9594
15	5.73	4.3152	8.5798	9.0442	15.8726	14.4558	12.3918
30	4.158	2.9558	4.3936	4.028	7.2692	6.5608	5.4578
C_t/C_o							
	1	1	1	1	1	1	1
	0.7808	0.668885	0.854835	0.827725	0.954915	0.803315	0.71465

0.707	0.608035	0.81159	0.798315	0.95018	0.78479	0.703125
0.58615	0.50181	0.73276	0.696035	0.85953	0.709795	0.67914
0.36385	0.360555	0.50514	0.513485	0.71722	0.622185	0.54799
0.2035	0.18464	0.30813	0.33719	0.5315	0.461685	0.398985
0.14325	0.10788	0.214495	0.226105	0.396815	0.361395	0.309795
0.10395	0.073895	0.10984	0.1007	0.18173	0.16402	0.136445

Ln C _t /C ₀						
0	0	0	0	0	0	0
0.24743624	0.40214313	0.15684681	0.18907431	0.04613295	0.21900836	0.3359624
0.34672461	0.49752283	0.20875999	0.22525202	0.05110384	0.24233911	0.3522206
0.53417955	0.68953372	0.31093705	0.36235533	0.15136955	0.34277908	0.386928
1.01101358	1.02011077	0.68291966	0.66653446	0.33237265	0.4745178	0.6014982
1.59208927	1.6893473	1.17723351	1.08710871	0.63205208	0.77287244	0.9188315
1.94316392	2.22673578	1.53946885	1.48675579	0.9242851	1.01778374	1.1718445
2.26384526	2.60511011	2.20873052	2.29560948	1.70523321	1.80776691	1.9918337

Table A.5 : raw data cobalt leaching for various cobalt loading and effect of calcinations temperatures on cobalt ions leaching

calcination temperature °C	cobalt leaching (mg/L)	cobalt ratio mol%	cobalt leaching (mg/L)
350	1.909	100%	26.7
500	1.0211	98%	10.95
600	0.978	95%	9.668
700	2.415	90%	3.56
800	4.048	85%	3.07
900	7.161	80%	1.982
		70%	1.909
		60%	6.446
		50%	6.862

Table A.6: Raw data and real concentration calculation for the effect of dye concentration on the degradation of MO of 70%

Co₃O₄/TiO₂

Concentration					Ln C _t /C _o						
(40ppm)	(60ppm)	(80ppm)	(100ppm)	(200ppm)	(40ppm)	(60ppm)	(80ppm)	(100ppm)	(200ppm)	(40ppm)	(60ppm)
40	60	80	100	200	0	0	0	0	0	0	0

29.22	48.766	51.421	80.28	158.849	0.231428	0.361161	0.314026	0.207311	0.44198	0.21965	0.230363
26.698	37.524	49.033	78.096	152.087	0.451771	0.504071	0.404291	0.469364	0.489533	0.247231	0.273865
24.524	33.789	44.76	75.685	144.884	0.69555	0.525826	0.489227	0.574209	0.580712	0.27859	0.322384
16.016	25.092	35.745	66.419	120.591	1.260896	1.039212	0.915291	0.871795	0.805616	0.409187	0.505913
7.696	18.147	27.799	53.475	103.431	1.779041	1.640241	1.648179	1.195839	1.057027	0.625956	0.659413
5.546	13.679	22	43.806	89.3882	2.148149	2.023944	1.975803	1.478483	1.290984	0.825399	0.805329
4.598	7.817	12.25	30.628	65.105	2.230264	2.328929	2.163258	2.038044	1.876501	1.183256	1.122316

Table A.7: data and real concentration calculation for the effect of catalyst load on the degradation of MO of 70% Co₃O₄/TiO₂

Concentration (mg/L)					Ln C _t /C ₀					
0.01	0.02	0.03	0.05	0.08	time	ln 0.01	ln 0.02	ln 0.03	ln 0.05	ln 0.08
40	40	40	40	40	0	0	0	0	0	0
29.172	29.234	29.482	26.674	20.902	0.5	0.31567	0.313547	0.3051	0.40519	0.649035
27.854	27.058	28.178	24.152	18.942	1	0.361903	0.390897	0.350338	0.504512	0.747498
26.332	24.38	23.634	19.658	17.166	2	0.418095	0.495116	0.526193	0.710395	0.845949

19.896	17.494	15.608	11.1558	7.954	5	0.698361	0.827021	0.941096	1.27692	1.615205
13.638	11.342	8.882	5.416	4.914	10	1.076019	1.260367	1.504853	1.999522	2.096791
9.556	6.63	5.812	4.446	4.262	15	1.43171	1.797275	1.928955	2.196875	2.239141
4.166	4.066	4.414	3.656	3.49	30	2.261923	2.28622	2.204098	2.39251	2.438978

Table A.8: data and real concentration calculation for the effect of PMS load on the degradation of MO of 70% $\text{Co}_3\text{O}_4/\text{TiO}_2$

time	Concentration (g/L)				C_t/C_0				
	0.02	0.03	0.035	0.04	0.10	0.02	0.03	0.04	0.10
0	40	40	40	40	40	1	1	1	1
0.5	31.824	30.536	29.856	28.724	24.616	0.7956	0.7634	0.7181	0.6154
1	29.594	27.766	26.876	26.742	21.802	0.73985	0.69415	0.66855	0.54505
2	26.288	25.294	23.39	22.864	18.5	0.6572	0.63235	0.5716	0.4625
5	19.75	17.474	15.2154	14.738	7.444	0.49375	0.43685	0.36845	0.1861
10	13.624	10.536	8.2568	8.038	5.666	0.3406	0.2634	0.20095	0.14165
15	10.046	6.492	5.352	5.66	4.448	0.25115	0.1623	0.1415	0.1112
30	5.814	4.586	3.98	4.22	3.466	0.14535	0.11465	0.1055	0.08665